

# Oxygen transport membranes fabricated with a modified phase-inversion casting method

**Citation for published version (APA):**

Liu, Y. (2021). *Oxygen transport membranes fabricated with a modified phase-inversion casting method*. [Phd Thesis 1 (Research TU/e / Graduation TU/e), Chemical Engineering and Chemistry]. Technische Universiteit Eindhoven.

**Document status and date:**

Published: 05/02/2021

**Document Version:**

Publisher's PDF, also known as Version of Record (includes final page, issue and volume numbers)

**Please check the document version of this publication:**

- A submitted manuscript is the version of the article upon submission and before peer-review. There can be important differences between the submitted version and the official published version of record. People interested in the research are advised to contact the author for the final version of the publication, or visit the DOI to the publisher's website.
- The final author version and the galley proof are versions of the publication after peer review.
- The final published version features the final layout of the paper including the volume, issue and page numbers.

[Link to publication](#)

**General rights**

Copyright and moral rights for the publications made accessible in the public portal are retained by the authors and/or other copyright owners and it is a condition of accessing publications that users recognise and abide by the legal requirements associated with these rights.

- Users may download and print one copy of any publication from the public portal for the purpose of private study or research.
- You may not further distribute the material or use it for any profit-making activity or commercial gain
- You may freely distribute the URL identifying the publication in the public portal.

If the publication is distributed under the terms of Article 25fa of the Dutch Copyright Act, indicated by the "Taverne" license above, please follow below link for the End User Agreement:

[www.tue.nl/taverne](http://www.tue.nl/taverne)

**Take down policy**

If you believe that this document breaches copyright please contact us at:

[openaccess@tue.nl](mailto:openaccess@tue.nl)

providing details and we will investigate your claim.

# Oxygen transport membranes fabricated with a modified phase-inversion casting method

## PROEFSCHRIFT

ter verkrijging van de graad van doctor aan de Technische Universiteit  
Eindhoven, op gezag van de rector magnificus prof.dr.ir. F.P.T. Baaijens, voor  
een commissie aangewezen door het College voor Promoties, in het openbaar te  
verdedigen op vrijdag 05 februari 2021 om 16:00 uur

door

Yuliang Liu

geboren te Shandong, China

Dit proefschrift is goedgekeurd door de promotoren en de samenstelling van de promotiecommissie is als volgt:

voorzitter: prof.dr.ir. D. C. Nijmeijer

1<sup>e</sup> promotor: prof.dr.eng. F. Gallucci

2<sup>e</sup> promotor: prof.dr.ir. M. van Sint Annaland

leden: prof.dr. J. Serra (Universitat Politècnica de Valencia)

prof.dr. E. Curcio (University of Calabria)

dr. Z. Borneman

prof.dr. T. Noël (Universiteit van Amsterdam)

dr. A. Arratibel (Tecnalia)

*Het onderzoek of ontwerp dat in dit proefschrift wordt beschreven is uitgevoerd in overeenstemming met de TU/e Gedragscode Wetenschapsbeoefening.*

This dissertation was approved by  
the 1<sup>o</sup> promotor:

prof.dr.eng. F. Gallucci

and 2<sup>o</sup> promotor:

prof.dr.ir. M. van Sint Annaland

A catalogue record is available from the Eindhoven University of Technology  
Library

ISBN: 978-90-386-5209-2

The work described in this thesis has been carried out within the Inorganic Membranes and Membrane Reactors group and the Chemical Process Intensification group, Eindhoven University of Technology, The Netherlands. We acknowledge the financial support from China Scholarship Council (CSC).



**Inorganic Membranes  
& Membrane Reactors**



**Multiphase  
Reactors  
Group**

Department of  
Chemical Engineering & Chemistry



Copyright © 2021, Yuliang Liu

Cover design: Yuliang Liu

*To my family*

献给我的家人

# Summary

As an alternative to some mature techniques for pure oxygen production, such as cryogenic distillation or pressure swing adsorption, dense ceramic membranes can offer great potential because of their unlimited selectivity, low energy cost and possibility of integration inside oxygen consuming reactors. The operating conditions of the oxygen transport membranes include ultra-high temperature, large oxygen partial pressure gradient, as well as exposure to strongly reactive (both reducing and oxidising) atmospheres. These conditions bring formidable challenges to the membrane material and geometry selection, and sealing of the membranes to gas-tight permeation cells or reactors.

Application of a suitable membrane geometry is important for the successful design of an oxygen separation unit. Membrane tubes, planar disks as well as hollow fibres are the most often used geometries for oxygen transport membranes. The comparatively easy fabrication process has made the planar disks widely applied at lab scale to investigate the membrane performance. However, in a membrane reactor, a large amount of reactant may by-pass the planar membrane and may remain un-reacted because of the low effective membrane area and insufficient gas mixing. Hollow fibres and tubular membranes have larger surface areas than planar disks, but the insufficient mechanical strength of hollow fibres hampers their application. Tubular membranes exhibit similar characteristics as hollow fibres (high area/volume ratio) while assuring high mechanical strength and ease of handling in membrane reactors. Therefore, tubular membranes are preferred for industrial processes. For industrial applications, it is necessary to seal the tubular membrane with a gas-tight connection to the permeation cell. A smaller sealing area can reduce the probability of leakage from the joining parts. To simplify the sealing process and to reduce the stress caused by the thermal expansion difference between the connection part and the membrane, it is

preferred to seal only one side of the membrane tube. An overview of the research on mixed ionic-electronic conducting membranes for oxygen separation and their application in membrane reactors is given in Chapter 2, whereas several dead-end tubular membranes are prepared in Chapter 3 with a modified phase inversion casting method. The phase inversion process in the water bath result in finger-like channels inside the membrane, thereby reducing the mass transfer resistance for oxygen permeation.

The harsh operating conditions of ceramic membranes require special membrane materials to provide simultaneously a high permeation flux and a good mechanical and chemical stability. However, most of the materials provide good permeability, e.g. several perovskites, show insufficient stability in the chemical process. Dual-phase membranes, which can combine a sufficient permeability with good stability are developed to overcome the dilemma of single-phase membranes. In Chapter 4, several different combinations of materials were used for the preparation of dual-phase membranes, and their permeability and chemical stability have been compared. Based on the performance of the dual-phase membranes, some triple-phase membranes with good stability have also been developed in this chapter. Element substitution was considered to be another way to improve the chemical stability of some highly permeable membrane materials. To compare the strategies of phase combination and element substitution, a Sb doped  $\text{SrFeO}_{3-\delta}$  membrane was fabricated and tested in Chapter 5.

The increased wall thickness of the tubular membranes compared to the hollow fibre membranes results in better strength but at the same time lower their permeability. To solve this problem, an asymmetric membrane was developed, where a thin membrane layer was coated onto a porous support. With this structure, combined high mechanical strength and good permeability can be

realised in a membrane tube. The porous support tubes were usually produced with an extrusion process, which results in a sponge-like microstructure. The highly tortuous channels in this structure cause large mass-transfer resistance. In Chapter 6, the modified phase-inversion casting method is used for the fabrication of the porous support. Finger-like channels can be obtained in the support during the phase inversion process, which decrease the mass transfer resistance for oxygen transfer. The selective layer material is mixed in the slurry for the preparation of membrane support with the purpose to achieve a compatible shrinkage behaviour of the two layers during sintering at ultra-high temperature.

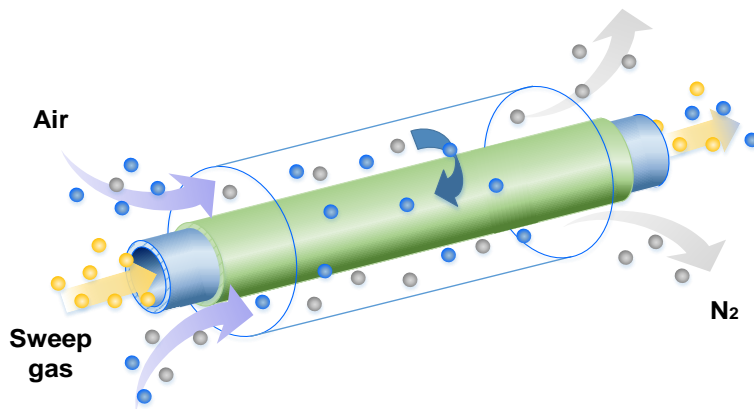
The modified phase-inversion casting method is a low-cost method with high versatility. It can be applied for the production of dead-end membranes and porous membrane supports from different materials. Membranes of different thickness and length can also be produced by adjusting the size of the casting tools. With this method suitable membranes for oxygen separation can be prepared, bringing their application in membrane reactors a step closer.



# Table of contents

<i>Chapter 1 Introduction.....</i>	<i>1</i>
<i>Chapter 2 Mixed ionic-electronic conducting membranes for oxygen separation..</i>	<i>13</i>
<i>Chapter 3 Dead-end CGO-BSCF membranes fabricated with modified phase-inversion casting method.....</i>	<i>57</i>
<i>Chapter 4 Dual-phase and triple-phase membranes with high CO<sub>2</sub>-tolerance .....</i>	<i>89</i>
<i>Chapter 5 Co-free SrFe<sub>0.8</sub>Sb<sub>0.2</sub>O<sub>3-δ</sub>-based membranes.....</i>	<i>113</i>
<i>Chapter 6 Supported membranes fabricated with a combined phase-inversion and dip-coating process .....</i>	<i>135</i>
<i>Chapter 7 Conclusions and outlook.....</i>	<i>167</i>
<i>List of Publications .....</i>	<i>173</i>
<i>Acknowledgements .....</i>	<i>177</i>
<i>Curriculum Vitae.....</i>	<i>181</i>

# Chapter 1 Introduction



*In this chapter, current challenges related to the production of robust oxygen transport membranes for industrial applications, strategies to solve the problems, as well as the outline of this thesis is presented.*

## 1.1 Problem definition

Great attention is paid to global warming driven by anthropogenic greenhouse gas emissions in these years. Reduction of anthropogenic emissions to the atmosphere can be realized by carbon capture from fossil-fuel power plants and from other energy intensive plants, like steel, iron or cement facilities. Oxyfuel combustion, i.e. using clean oxygen instead of air to combust the fuels, represents an efficient way for carbon capture, as it enables the production of highly CO<sub>2</sub> enriched exhaust gas due to the absence of N<sub>2</sub> in the combustion process, which allows a more direct and cheaper CO<sub>2</sub> separation process. Oxygen is generally produced by cryogenic distillation or pressure swing adsorption (PSA) systems, which both require high investments and operating costs [1,2]. Cryogenic distillation technology provides high-purity oxygen (>99%), while, generally, the purity is lower for PSA at around 95% [3]. Recent international policies about energy security and greenhouse gas emissions are challenging the conventional oxygen production systems.

Air separation using ceramic membranes with mixed electronic and oxygen-ionic conductivity is a clean technology with high energy efficiency, which makes it a potential cheaper alternative to conventional methods for oxygen production [4]. Continuous supply of oxygen and infinite perm-selectivity can be achieved at elevated temperatures with an oxygen chemical-potential driving force across the membranes. Additionally, the mixed-conductive membranes can be coupled with some high temperature oxygen-consuming reactions resulting in even higher benefits due to the process integration [5]. The integration of membranes into membrane reactors has been one of the main applications for oxygen transport membranes because of the high operating temperatures required by both the separation and reaction processes. Oxidative coupling of methane, partial oxidation of methane, and oxidative dehydrogenation of ethane are the reaction

systems where the application of these membranes attracted the most interest in the literature. Actually, companies among which Air Products and Praxair are currently doing big efforts in this field, developing novel oxygen membrane units for both air separation and their integration into reaction processes. Looking at the different reaction systems, oxidative coupling of methane is a high-temperature reaction, which is commonly performed between 750 and 950 °C. This process directly produces olefins from natural gas as feedstock, which mainly consists of three primary reactions and many consecutive reactions (for instance, Stansch et al. [6] used 10 reactions to describe the OCM kinetics), making this process rather complex. The main problem with this reaction system is that consecutive oxidation reactions make it difficult to achieve both high conversion and high yields. Generally, the C<sub>2</sub> yields in conventional reactors are restricted to less than 20%, while yields higher than 30% are required to make the systems economically viable [7]. The use of membrane reactors allows obtaining high yields by distributively feeding the oxygen along the reactor, thus preventing the complete oxidation reactions [8].

Another application of the oxygen transport membranes in the oxyfuel power plants, for electricity production with CO<sub>2</sub> capture.

The exposure to complex strongly reducing and strongly oxidizing gas mixtures during operation inside the reactor requires the membrane to have good chemical stability. In particular, exposure to CO<sub>2</sub>-containing gas mixtures generates the demand for a CO<sub>2</sub>-tolerant membrane material.

The mixed ionic and electronic conduction (MIEC) of solid oxide material was initially described by Takahashi et al. [9] in 1976. Afterward, Cales and Baumard [10,11] introduced the mixed conducting oxide concept to oxygen transport membranes. However, favourable oxygen permeability was not achieved until

Teraoka et al. [12] made a breakthrough on oxygen separation membranes in 1985 by introducing perovskite membranes. One of the drawbacks of many perovskite membranes with good permeability has always been the thermal instability at the high temperatures required for achieving appreciable oxygen fluxes, and the chemical instability in acid gases. Attempts of increasing the stability include doping the perovskite (and MIEC) with different elements, which clearly improved the thermal and chemical stability while resulting in a decrease in the oxygen permeation rate [13,14]. It is generally accepted that materials with superior oxygen ionic conductivity usually have correspondingly lower stability when exposed to reducing atmospheres. This is easily explained by the fact that weak chemical bonding of metal and oxygen could be favourable for the fast oxygen mobility in membranes, but it also increases the chances for metals to be reduced at a high temperature in reducing atmosphere [15].

***Till now the trade-off between the oxygen permeability and membrane (chemical, thermal or mechanical) stabilities, and the problems associated with the sealing and handling of the membranes in the reactors are all the factors that hamper industrial application of oxygen transport membranes.***

## 1.2 Purpose of this study

The performance of the membranes can be influenced by the partial pressure difference across the membranes, the operating temperatures, the surrounding atmospheres, and the membrane materials, geometric configuration and thicknesses. Since the development of the oxygen transport membranes, great effort has been devoted to improve the permeability, stability and compatibility of the membranes to the reactors.

The oxygen permeation rate in MIEC membranes is controlled by two different mechanisms, namely ionic transport within the membrane and surface membrane exchange. When the permeation process is controlled by bulk diffusion, the oxygen permeate flux will increase when decreasing the thickness of the membrane [16,17]. Membranes with a thickness in the order of 400 to 500  $\mu\text{m}$  are, however, sufficiently thin, because the surface exchange rate becomes the limiting factor for smaller membrane thicknesses, as shown in Figure 1.1 [18].

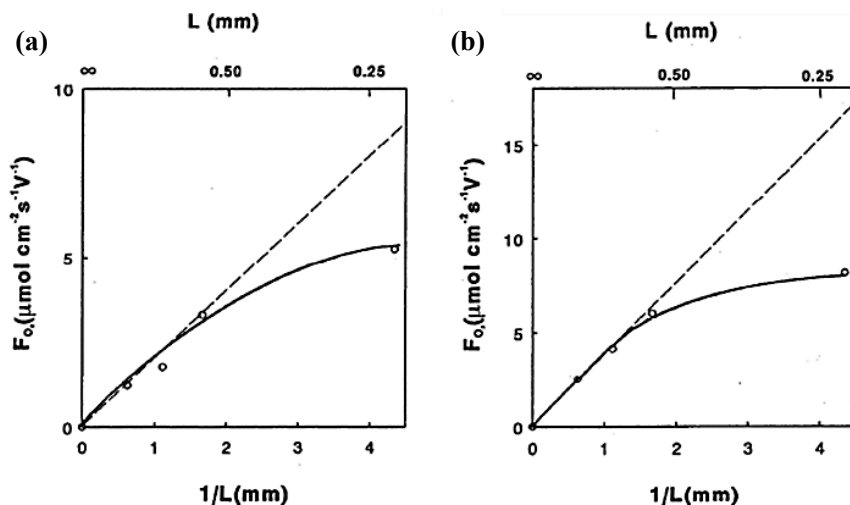
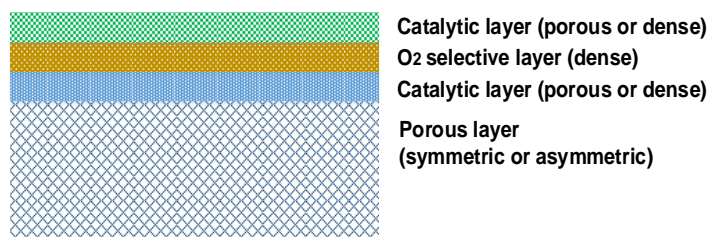


Figure 1.1. Thickness dependence of oxygen permeation of self-supported  $(\text{Bi}_2\text{O}_3)\text{-}(\text{Er}_2\text{O}_3)\text{-Ag}$

membranes at 750 °C (a) and 850 °C (b) [18].

However, thin film membranes of these thicknesses are typically not sufficiently mechanically stable. To develop more stable membranes, research is ongoing to produce asymmetric MIEC membranes with a thin dense layer coated on a thicker porous support, as proposed by Teraoka et al. [19] in 1989. With supported membranes, a high oxygen permeation flux can be achieved without sacrificing the mechanical stability of the membrane. Meanwhile, thinner membranes usually maintain their chemical stability better, because elevated bulk diffusion rates of oxygen can help reduce unwanted chemical reduction on the surface of the membrane [20].



**Figure 1.2.** Schematic representation of an asymmetric membrane with several functional layers.

An oxygen selective layer supported onto a porous substrate is the simplest example of an asymmetric membrane structure. Additional layers with specific functions can be added, for example a surface activation layer and/or a catalytic layer, to improve and extend the performance of the membranes, which also increases the complexity of the membrane structure (see Figure 1.2) [17,21]. While many articles have been published on self-supported MIEC oxygen transport membranes, only a limited number of articles were published on the production and testing of asymmetric membranes. Since the preparation of ceramic membranes includes a sintering process at ultra-high temperatures and

the high-temperature sintering normally leads to a large shrinkage of the material, compatible shrinkage behaviour for the materials of different layers is critical for obtaining leakage free supported membranes. Moreover, each layer of the membrane should have good chemical stability and no reaction should take place between layers. All of these requirements bring challenges for the material selection for supported membranes.

*This work aims at making a step forward to the industrial application of ceramic membranes for oxygen separation by application of robust membrane materials, reduction of the membrane thickness and formation of membrane geometries that are suitable for their integration inside membrane reactors. Membranes of different materials or composites are prepared and compared, and also triple-phase membranes are developed to obtain membranes with high chemical stability. A modified phase-inversion method is applied for the membrane fabrication process to obtain ceramic membranes with low gas transfer resistance due to the formation of microchannels inside the membrane. Porous supported membranes are prepared with the purpose to improve the membrane permeability without sacrificing the mechanical strength, and sealing and handling of the membranes in the reactor was simplified with the formation of a dead-end membrane geometry.*



### 1.3 Outline of the thesis

In Chapter 2, we report the mechanism for oxygen transport through MIEC membranes, and summarize recent advances on self-supported and supported oxygen membranes. We also give a comparison between single-phase and dual-phase membranes, and discuss factors that affect the oxygen permeation and membrane stability. Possible strategies that can be pursued to increase the oxygen permeation rate are also indicated in this chapter.

A modified phase inversion casting method for the formation of a dead-end tubular membrane shape in a single step is introduced in Chapter 3. Considering the difficulties to achieve combined good permeability and chemical stability in a single-phase material, dual-phase composites are applied for the membrane fabrication. In this chapter,  $\text{Ce}_{0.9}\text{Gd}_{0.1}\text{O}_{1.95-\delta}$  (CGO)- $\text{Ba}_{0.5}\text{Sr}_{0.5}\text{Co}_{0.8}\text{Fe}_{0.2}\text{O}_{3-\delta}$  (BSCF) composites are used as the membrane material. The performance of the membrane is optimised by adjusting the process conditions in the fabrication process. Long finger-like channels, which are found to promote the oxygen permeation flux without decreasing the membrane mechanical strength, are obtained in the dead-end tubes by adjusting the ceramic loadings of the casting slurries. The performance of the dual-phase membranes with varied CGO:BSCF ratios are compared. The membranes containing more BSCF showed higher oxygen permeation fluxes with helium as sweep gas. It will also be shown that the CGO content plays an important role in enhancing the mechanical strength of the CGO-BSCF membranes.

In Chapter 4, except for the CGO-BSCF membrane, the oxygen ionic conductor  $\text{Ce}_{0.9}\text{Gd}_{0.1}\text{O}_{2-\delta}$  is paired with two other electronic oxides, including  $\text{NiFe}_2\text{O}_4$  (NFO) and  $\text{La}_2\text{NiO}_{4+\delta}$  (LNO), forming different kinds of dual-phase membranes. The performance of the membranes is compared in terms of oxygen flux and  $\text{CO}_2$

tolerance. The CGO/BSCF provides the highest permeation flux among the three composites with either helium or CO<sub>2</sub> fed as sweep gas, although a sharp decrease in the permeation rate is observed for the CGO/BSCF when CO<sub>2</sub> was in contact with the membrane. Based on the results for the dual-phase membranes, some CGO/BSCF/NFO triple-phase membranes are developed. The triple-phase membranes are found to be less sensitive to the presence of CO<sub>2</sub> in the sweep gas than CGO/BSCF, and the application of the two triple-phase composites instead of the dual-phase ones promotes the oxygen permeation fluxes when the membranes are swept with 100 % CO<sub>2</sub>. The results provide valuable information for the material selection and performance optimization of the CGO-based multi-phase membranes for oxygen permeation. Some Sb doped SrFeO<sub>3-δ</sub> membranes are fabricated and tested in Chapter 5, the permeability, activation energy and operation stability of which will be compared with that of the CGO/BSCF with pure helium or CO<sub>2</sub> as sweep gas.

Thin-film membrane layers coated onto porous supports is widely considered as an efficient way to obtain high-performance oxygen transport membranes with both good permeability and high mechanical strength. However, conventional preparation methods of membrane support usually result in highly tortuous channels with high mass transfer resistance. In Chapter 6, tubular porous MgO and MgO/CGO supports are fabricated with a simple phase inversion casting method. Long finger-like channels are obtained inside the dual-phase supports by adjusting the ceramic loading, polymer concentration and particle surface area, as well as by introducing ethanol inside the casting slurries. These supports are used to produce thin supported CGO membranes. The shrinkage of the support tube at high temperatures was greatly affected by the polymer/ceramic ratio in the slurry. Compatible shrinkage behaviour of the two layers will be realized and gas-tight membrane will be obtained by adjusting the slurry composition for membrane preparation.

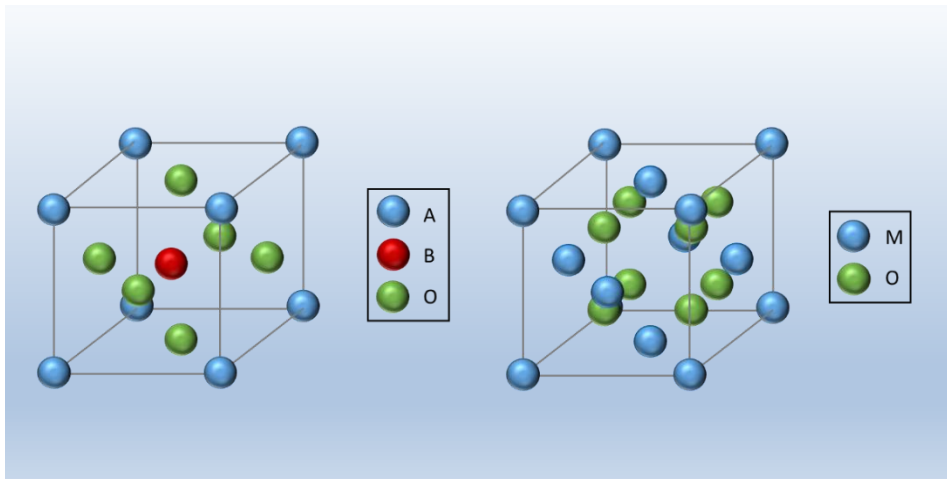
The main results obtained from the experiments in Chapter 1-6 as well as the outlook for the future research are summarised in Chapter 7.

## References

- [1] R.W. Baker, Future directions of membrane gas separation technology, *Ind. Eng. Chem. Res.* 41 (2002) 1393–1411.
- [2] A. Leo, S. Liu, J. C. D. da Costa, Development of mixed conducting membranes for clean coal energy delivery, *Int. J. Greenh. Gas Control.* 3 (2009) 357–367.
- [3] B. Belaisaoui, Y. Le Moullec, H. Hagi, E. Favre, Energy efficiency of oxygen enriched air production technologies: Cryogeny vs membranes, *Sep. Purif. Technol.* 125 (2014) 142–150.
- [4] J. Sunarso, S. Baumann, J. M. Serra, W. A. Meulenber, S. Liu, Y. S. Lin, J. C. Diniz da Costa, Mixed ionic-electronic conducting (MIEC) ceramic-based membranes for oxygen separation, *J. Memb. Sci.* 320 (2008) 13–41.
- [5] H. J. M. Bouwmeester, Dense ceramic membranes for methane conversion, *Catal. Today.* 82 (2003) 141–150.
- [6] Z. Stansch, L. Mleczko M, Baerns, Comprehensive kinetics of oxidative coupling of methane over the  $\text{La}_2\text{O}_3/\text{CaO}$  catalyst, *Ind. Eng. Chem. Res.* 36 (1997) 2568–2579.
- [7] A. Cruellas, J. J. Bakker, M. van Sint Annaland, J. A. Medrano, F. Gallucci, Techno-economic analysis of oxidative coupling of methane: Current state of the art and future perspectives, *Energy Convers. Manag.* 198 (2019) 111789.
- [8] A. Cruellas, T. Melchiori, F. Gallucci, M. van Sint Annaland, Oxidative Coupling of Methane: A Comparison of Different Reactor Configurations, *Energy Technol.* 8 (2020) 1–15.
- [9] T. Takahashi, T. Esaka, H. Iwahara, Electrical conduction in the sintered oxides of the system  $\text{Bi}_2\text{O}_3/\text{BaO}$ , *J. Solid State Chem.* 16 (1976) 317–323.
- [10] B. Calès, Mixed conduction and defect structure of  $\text{ZrO}_2\text{-CeO}_2\text{-Y}_2\text{O}_3$  solid solutions, *J. Electrochem. Soc.* 131 (1984) 2407.
- [11] B. Cales, J. F. Baumard, Oxygen semipermeability and electronic conductivity in calcia-stabilized zirconia, *J. Mater. Sci.* 17 (1982) 3243–3248.
- [12] Y. Teraoka, H. M. Zhang, S. Furukawa, N. Yamazoe, Oxygen permeation through perovskite-type oxides, *Chem. Lett.* 14 (1985) 1743–1746.

- [13] S.P.S. Badwal, F.T. Ciacchi, Ceramic membrane technologies for oxygen separation, *Adv. Mater.* 13 (2001) 993–996.
- [14] J. C. Boivin, G. Mairesse, Recent material developments in fast oxide ion conductors, *Chem. Mater.* 10 (1998) 2870–2888.
- [15] X. Yin, C. Choong, L. Hong, Z. Liu, Crafting  $\text{La}_{0.2}\text{Sr}_{0.8}\text{MnO}_{3-\delta}$  membrane with dense surface from porous YSZ tube, *J. Solid State Electrochem.* 10 (2006) 643–650.
- [16] X. Meng, W. Ding, R. Jin, H. Wang, Y. Gai, F. Ji, Y. Ge, D. Xie, Two-step fabrication of  $\text{BaCo}_{0.7}\text{Fe}_{0.2}\text{Nb}_{0.1}\text{O}_{3-\delta}$  asymmetric oxygen permeable membrane by dip coating, *J. Memb. Sci.* 450 (2014) 291–298.
- [17] D. K. Ramachandran, M. Sjøgaard, F. Clemens, J. Gurauskis, A. Kaiser, Fabrication and performance of a tubular ceria based oxygen transport membrane on a low cost MgO support, *Sep. Purif. Technol.* 147 (2015) 422–430.
- [18] C. S. Chen, H. Kruidhof, H. J. M. Bouwmeester, H. Verweij, A. J. Burggraaf, Thickness dependence of oxygen permeation through erbiastabilized bismuth oxide-silver composites, *Solid State Ionics.* 99 (1997) 215–219.
- [19] Y. Teraoka, T. Fukuda, N. Miura, N. Yamazoe, Development of oxygen semipermeable membrane using mixed conductive perovskite-type oxides (part 2), *J. Ceram. Soc. Japan.* 97 (1989) 533–538.
- [20] B. J. Mitchell, R. C. Rogan, J. W. Richardson, B. Ma, U. Balachandran, Stability of the cubic perovskite  $\text{SrFe}_{0.8}\text{Co}_{0.2}\text{O}_{3-\delta}$ , *Solid State Ionics.* 146 (2002) 313–321.
- [21] V. Sadykov, V. Zarubina, S. Pavlova, T. Krieger, G. Alikina, A. Lukashevich, V. Muzykantov, E. Sadvokaya, N. Mezentseva, E. Zevak, V. Belyaev, O. Smorygo, Design of asymmetric multilayer membranes based on mixed ionic-electronic conducting composites supported on Ni-Al foam substrate, *Catal. Today.* 156 (2010) 173–180.

# Chapter 2 Mixed ionic-electronic conducting membranes for oxygen separation



*In this chapter, the mechanism for oxygen transport through MIEC membranes, popular membrane materials and configurations, and factors that affect the oxygen permeation and membrane stability are presented. Possible ways that can be pursued to increase the oxygen permeation rate are also indicated.*

***This chapter is based on the paper: Mixed ionic-electronic conducting membranes (MIEC) for their application in membrane reactors: a review. Processes, 2019, 7(3): 128.***

## 2.1. Mechanism for the oxygen transport through MIEC membranes

In general, the driving force for oxygen permeation through the mixed ionic-electronic conducting (MIEC) membranes is the oxygen chemical potential difference between the feed and permeate side of the membrane. A schematic representation of oxygen separation is shown in Figure 2.1.

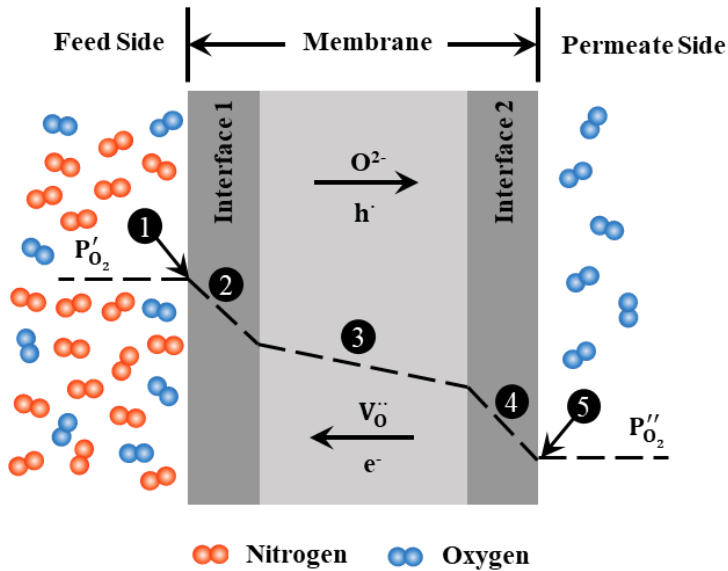


**Figure 2.1.** Schematic representation of oxygen permeation through dense ceramic membranes when air is employed as feedstock stream [1].

The oxygen diffusion mechanism involves five steps [2]:

1. Bulk-to-surface mass transfer of gaseous oxygen.
2. Dissociation (surface exchange): The oxygen molecule is adsorbed on the membrane surface and dissociates catalytically in oxygen ions ( $O^{2-}$ ). On the high oxygen partial pressure side, this can be expressed using the Kröger-Vink

notation below.



where  $V_O^{\bullet}$  refers to oxygen vacancies in the ceramic and  $O_O^x$  to oxygen ions ( $O^{2-}$ ) occupying the oxygen lattice.

3. Bulk diffusion: under a pressure gradient between the feed and permeate side, the oxygen ions diffuse through the ceramic crystal lattice (mainly oxygen vacancies, but also other defects). To maintain electric neutrality, electrons are transported at the same time in the opposite direction.

4. Association (surface exchange): The oxygen ions recombine to form oxygen molecules and desorb from the surface of the membrane. The reaction involved in this step can be represented by the following formula.



5. Surface-to-bulk mass transfer of gaseous oxygen (permeate side): Gas transport in the permeate side alone or helped by a sweep gas (helium,  $CO_2$ , etc.).

Membranes of different thickness and varied materials were found to have different controlling steps among the five.



## 2.2. Materials for MIEC oxygen membranes

### 2.2.1. Single-phase ionic transport materials

Oxygen transport membranes can be composed of different structures, such as perovskite, fluorite, spinel and Ruddlesden–Popper-type oxides. Among all materials, the perovskite and fluorite-type materials are the most studied as oxygen membranes. Both types of structures have been well investigated with different doping strategies, and both as self-supported membranes and supported selective layers with different thicknesses.

#### 2.2.1.1. Perovskites

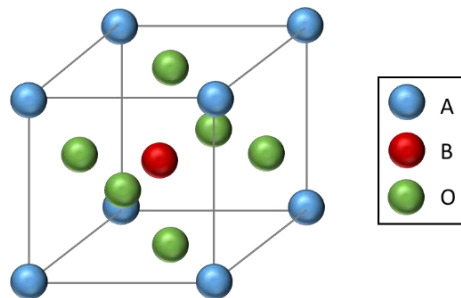


**Figure 2.2.** Crystalline structure of perovskite (ABO<sub>3</sub>) [3].

Perovskite-type ceramics represent one of the most attractive oxygen transport membrane materials because of their high electronic conductivity as well as good ionic conductivity. The perovskite structure can be expressed as ABO<sub>3</sub>. As Figure 2.2 shows, the unit cell is an FCC (face-centered cubic) crystal, where A cations are located on the corners of the cubic lattice and the smaller B cation is located in the body-centered position. Oxygen anions are located at the face-centered positions. Alkaline earth metal ions (Ca<sup>2+</sup>, Ba<sup>2+</sup>, Sr<sup>2+</sup>, etc.) and/or lanthanide metal

ions ( $\text{La}^{3+}$ ,  $\text{Ga}^{3+}$ ,  $\text{Sm}^{3+}$ , etc.) are usually located at the A-sites [4], while the B-sites are mostly transition metal ions [5]. When cations with lower oxidation states partially substitute the original A-site ions, oxygen vacancies, which can facilitate the oxygen ion movement in the membranes, would develop to sustain the electrical neutrality. Besides, the oxidation state of the B-site cations can also increase to compensate for the effective negative charge which allows the electrons transporting through the membranes by hopping between the valence-variable metal ions.

The oxygen transport rate in a perovskite is governed by an Arrhenius expression (positive activation energy) and is higher when the temperature is increased. The activation energy depends mainly on the bond energy of metal-oxygen in the lattice and the parameter  $r_{\text{critical}}$ , which corresponds to the radius of the opening between the two A site cations and the one B site cation through which the mobile anion must pass [6]. During the last three decades, there have been several series of perovskite oxides that attracted a great deal of attention of researchers.

$\text{SrCoO}_{3-\delta}$  based perovskite materials have excellent conductive properties of oxygen. A high oxygen permeation flux of  $2.1 \cdot 10^{-6}$  mol/cm<sup>2</sup>·s for self-supported  $\text{SrCo}_{0.8}\text{Fe}_{0.2}\text{O}_{3-\delta}$  (SCF) membrane was reported by Teraoka et al. [7] However lower chemical and thermal stabilities of SCF oxides were observed in their application processes. A big effort has been devoted to improve the stability of this kind of membranes by doping A-site ions with La, Ba, Ca etc. and/or doping the B-sites with some stable cations, for example Mn, Nb, Ti, Ta, Cr, Al and Zr.

The  $\text{La}_{1-x}\text{M}_x\text{Co}_{1-y}\text{Fe}_y\text{O}_{3-\delta}$  (M = Ba, Sr, and Ca) membranes are a type of perovskite, which have been widely studied. Stevenson et al. [8] investigated the oxygen permeability and the lattice weight loss at a high temperature for A-site substitution of this type of membranes. They observed a weight loss of the

membranes when the temperature increases, which was attributed to lattice oxygen release. This effect would contribute toward increasing the concentration of oxygen vacancies and the ionic conductivity in the membrane, resulting in an increase in the oxygen permeation flux. In particular, Stevenson's group found that, as the Sr content is increased in the oxide, the oxygen permeation flux increased significantly, and this was consistent with the thermogravimetric (TGA) results showing a greater oxygen deficiency at higher temperatures. The oxygen permeability of  $\text{La}_{0.2}\text{M}_{0.8}\text{Co}_{0.2}\text{Fe}_{0.8}\text{O}_{3-\delta}$  (M = Ba, Sr and Ca) perovskite membranes has also been tested by Li et al. [9]. Sr substituted membranes showed the best oxygen permeability. However, the thermal stability is lower than the Ba-substituted oxides, which is attributed to the low average bond energy and high free volume of the Sr substitution compounds.

Since Shao et al. [10] improved the phase stability of SCF materials by partially substituting Sr in the perovskite compounds with Ba, lots of studies have been conducted on the  $\text{Ba}_x\text{Sr}_{1-x}\text{Co}_{0.8}\text{Fe}_{0.2}\text{O}_{3-\delta}$  (BSCF) compounds. Different Ba content BSCF composite oxides were synthesized by Babakhani et al. [11], and the phase stability and oxygen permeability were studied. They found that  $\text{Ba}_{0.5}\text{Sr}_{0.5}\text{Fe}_{0.2}\text{Co}_{0.8}\text{O}_{3-\delta}$  has the highest oxygen permeation flux among the  $\text{Ba}_x\text{Sr}_{1-x}\text{Co}_{0.8}\text{Fe}_{0.2}\text{O}_{3-\delta}$  ( $x = 0.3, 0.5, 0.7$  and  $0.9$ ) oxides over the entire temperature region because of its combined high free state of oxygen vacancies and high oxygen-vacancy gradient. Afterward, Babakhani [12] and his colleagues exploited the  $\text{Ba}_{0.5}\text{Sr}_{0.5}\text{Co}_{0.8}\text{Fe}_{0.1}\text{R}_{0.1}\text{O}_{3-\delta}$  (R= Mn, Co, Fe, Ce, Ni, Cr, Al) membrane materials by doping Fe ions in the B-site of  $\text{Ba}_{0.5}\text{Sr}_{0.5}\text{Fe}_{0.2}\text{Co}_{0.8}\text{O}_{3-\delta}$  and found that introducing Al, Ce and Ni cations can help to increase the oxygen transport capability of BSCF oxides, but doping Fe with Al, Ce and Cr can impair the structural stability of the BSCF membranes. Several researchers have tried to fabricate asymmetric oxygen transport membranes with a selective layer of BSCF, and due to the shrinkage mismatch problem, similar material is usually chosen to

prepare the porous support. For instance, Li et al.[13] produced a supported membrane with the BSCF powders for both the selective layer and the support, and an improved oxygen permeability was observed when comparing with self-supported BSCF membranes.

Additionally, the full substitution of Sr in the A site of BSCF oxides with Ba has also been investigated with different substitutions in the B site. For instance the  $\text{BaCo}_{0.7}\text{Fe}_{0.2}\text{M}_{0.1}\text{O}_{3-\delta}$  ( $\text{M} = \text{Ta}, \text{Nb}, \text{Zr}$ ) membranes were successfully prepared by Cheng et al. [14], and the research group reported that among the three kinds of membranes,  $\text{BaCo}_{0.7}\text{Fe}_{0.2}\text{Zr}_{0.1}\text{O}_{3-\delta}$  showed the highest oxygen permeability while  $\text{BaCo}_{0.7}\text{Fe}_{0.2}\text{Ta}_{0.1}\text{O}_{3-\delta}$  gave the best structural stability. After that a series of perovskite oxides,  $\text{BaCo}_{0.7}\text{Fe}_{0.3-x}\text{Ta}_x\text{O}_{3-\delta}$  (BCFT,  $x=0-0.15$ ) were synthesized by Liu et al. [15] and the oxygen permeability in the BCFT membranes is observed to first increase and then decrease with increasing Ta content in the symmetric membranes. Finally, a similar influence of the Zr content on the oxygen permeation flux of the  $\text{BaCo}_{0.7}\text{Fe}_{0.3-x}\text{Zr}_x\text{O}_{3-\delta}$  (BCFZ,  $x=0-0.12$ ) oxide membranes was reported by Yao et al [16].

#### 2.2.1.2. Fluorite-type material

Fluorite oxide structures, are represented by  $\text{MO}_2$ , where M is the large four valent cations, such as  $\text{Zr}^{4+}$  or  $\text{Ce}^{4+}$  [17]. The crystal structure of a fluorite is shown in Figure 2.3, where the cations are in the FCC (face-centred cubic) structure, while the oxygen anions are positioned in the interstitial holes forming a simple cubic structure inside the FCC structure of the cations. These structures exhibit a very poor electronic conductivity. Thus, an external electronic conduction is required to apply fluorites as oxygen transport membranes.

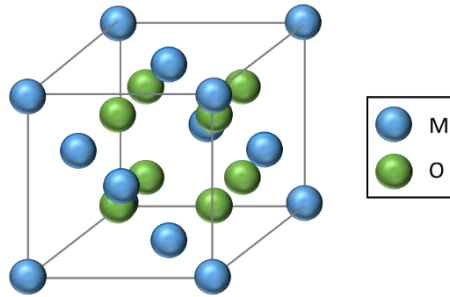


**Figure 2.3.** Fluorite-type structure [18].

Typical fluorite oxides used are  $\text{ZrO}_2$ ,  $\text{CeO}_2$ , and  $\text{Bi}_2\text{O}_3$ . Several oxides such as yttria-stabilized zirconia (YSZ), gadolinium-doped ceria (CGO), or samarium-doped ceria (CSO) present high oxygen ion conduction as well. Employing Gd as a dopant in cerium oxide, the best conductivity was obtained in concentrations of around 10% to 20% [19]. Doped ceria with trivalent elements shows a stable crystal lattice due to the similar size of the host and dopant ions [20]. In case of doping with Pr, the ambipolar conductivity is enhanced [21].

Bismuth oxide-based materials provide a comparatively high level of oxygen permeability. However, the oxygen flux is too low compared with some perovskites since the fluorite oxides have a low electronic conductivity [4].

Zirconium oxide is one of the most studied fluorite type materials. Bulk zirconia is a polymorphic ceramic material, which may exist at different ranges of temperatures and atmospheric pressures: monoclinic ( $<1000\text{ }^\circ\text{C}$ ), tetragonal ( $1100\text{--}2370\text{ }^\circ\text{C}$ ), and cubic ( $>2370\text{ }^\circ\text{C}$ ) [22]. The cubic structure is stable at temperatures above  $2300\text{ }^\circ\text{C}$  with a high oxygen ionic conductivity. This phase can be stabilized by doping with rare earth oxides like  $\text{Y}_2\text{O}_3$ , which is the most employed metal oxide for that purpose.

The main benefit of these fluorite-type materials is their small chemical expansion and their phase stability under CO<sub>2</sub> and reducing environments in comparison to perovskite materials [23].

### ***2.2.2. Dual-phase composites***

Due to the difficulties in identifying a single material that exhibits both high permeation flux and good stability, dual-phase membranes are attracting increasing interest by several research groups. In a dual-phase membrane, one phase can act as the oxygen-ionic conductor while the other one as the electronic conductive phase. An infinitely continuous or percolative network is required to enhance both processes (ionic transport through a ceramic conductive phase and electron conduction through an electronic conductive metallic or ceramic phase) [18]. To maintain electroneutrality in the membrane, a balance between oxygen ions and electrons is required. At the same time, the electronic conductive phase can also promote the association/dissociation of oxygen molecules at the surface, compared with the single-phase materials with only oxygen-ionic conductivity [24].

A precise control on the preparation process is necessary to avoid the formation of defects and cracks, since the expansion coefficients between the materials would cause leaks and jeopardize complete gas separation for the dual-phase membrane [25].

#### ***2.2.2.1. Dual-phase composites based on ceramic-metallic mixtures***

In the early stage of the development of dual-phase membranes, noble metals were applied as the electronic conduction phase, while ceramics like fluorite-based materials were generally selected as the ionic conductive phase.

Mazanec [26] produced and tested the first dual-phase composite membranes consisting of YSZ with Pd, Pt,  $\text{In}_{90}\text{Pr}_{10}$ , and  $\text{In}_{95}\text{Pr}_{2.5}\text{Zr}_{2.5}$ . The oxygen permeation flux was improved when the volume percentage of metal was above the critical value for obtaining a percolative composite, while the best results were obtained with a 50 vol.% of  $\text{In}_{95}\text{Pr}_{2.5}\text{Zr}_{2.5}$ . It was observed that 30 vol.% of metal is required in the mixture to obtain a percolated network [27].

Chen et al. [24] worked extensively on YSZ/Pd. In their first study, they compare a YSZ fluorite with a dual-phase YSZ/Pd with different volume ratios. When the volume percentage of palladium is around 40%, the oxygen flux through the membrane increases three orders of magnitude compared with YSZ alone. Kim and co-workers [28] prepared a 10  $\mu\text{m}$  thick layer of YSZ/Pd onto a porous alumina support by dip-coating with an extra YSZ thin layer on top of that to reduce the leakage of the composite. The oxygen permeation rate through the asymmetric membrane was lower than expected at 1050 °C when using either air or pure oxygen as feed gas. The authors attributed the observed low membrane flux to the YSZ submicron layer deposited on top of the YSZ/Pd, which led to a decrease in electron conductivity.

In another study by Chen et al. [29], an erbium-stabilized bismuth oxide-noble metal (Ag and Au) membrane was prepared and compared with a YSZ/Pd membrane. A higher oxygen permeation rate ( $1.19 \cdot 10^{-7} \text{ mol/cm}^2 \cdot \text{s}$ ) was observed for the self-supported 1.6 mm thick  $(\text{Bi}_2\text{O}_3)(\text{Er}_2\text{O}_3)\text{-Ag}$  (40% in volume) membrane at 800 °C, which is one order of magnitude higher compared with the permeation rate through the 1.72 mm thick membrane of YSZ/Pd. The thickness dependency of the erbium-stabilized bismuth oxide-silver composites were studied at different temperatures, which have the best result with self-supported membranes of 230  $\mu\text{m}$  thick at 852 °C ( $3.08 \cdot 10^{-7} \text{ mol/cm}^2 \cdot \text{s}$ ) [30]. A thicker membrane (1 mm) was tested at a lower temperature (680 °C) and exhibited an

O<sub>2</sub> flux of one order of magnitude lower [31].

Capoen et al. [32] observed that when CaO replaces erbium oxide, there is no improvement in the oxygen permeability. The authors also found that addition of Au instead of Ag does not improve the oxygen flux due to the low activity of Au for oxygen dissociation. A higher permeation flux ( $1.79 \cdot 10^{-7}$  mol/cm<sup>2</sup>·s) was measured at 680 °C for a composite (Bi<sub>2</sub>O<sub>3</sub>)<sub>0.75</sub>-(Er<sub>2</sub>O<sub>3</sub>)<sub>0.25</sub> with 40 vol.% of silver. Kim et al. prepared a fluorite type Bi<sub>1.5</sub>Y<sub>0.3</sub>Sm<sub>0.2</sub>O<sub>3</sub> (BYS) mixed with 40 vol.% silver [33], which showed a larger O<sub>2</sub> flux ( $5.8 \cdot 10^{-7}$  mol/cm<sup>2</sup>·s) at a higher temperature (850 °C) for a membrane with a thickness of 1.3 mm. From a practical and industrial application perspective, employment of noble metals is restricted due to their high price [29], unless thinner yet stably-supported membranes can be produced. In Table 2, some physical properties and prices of the metals used in the dual-phase oxygen membranes are summarized.

**Table 2.1.** Physical properties and price of some metals used as the electronic conductive phase in dual-phase membranes [34]. TEC: thermal expansion coefficient. Tm: melting point.

Element	Tm (°C)	TEC 10 <sup>6</sup> (°C <sup>-1</sup> )	Cp at 25 °C (J/g·K)	Electrical Resistivity			Price (€/kg)
				10 <sup>-8</sup> (Ω·m)			
				700 °C	800 °C	900 °C	
Pd	1555	11.8	0.246	24.2	27.1	29.4	60000
Ag	962	18.9	0.235	4.21	4.91	5.64	700
Pt	1768	8.8	0.133	25.4	28.7	32	24000
Au	1064	14.2	0.129	5.82	6.81	7.86	52000

#### 2.2.2.2. Dual-phase composites based on mixed ceramics

Another option to enhance the electronic conductivity without increasing the



price as much as with noble metals, is to mix the ionic conducting phase with another ceramic phase that can conduct electrons, such as perovskites and spinel materials. For the case of ceramic-ceramic systems, some other aspects need to be considered, including the stability of both phases (temperature and CO<sub>2</sub> tolerance, etc.) and the thermal-chemical expansion compatibility between both phases, and this is discussed in the next section.

Perovskite and spinel structures show a higher electronic conductivity than other ceramic materials, and, therefore, they are employed as the electronic phase, whereas structures of the fluorite type are used as the oxygen conductive phase. Furthermore, fluorite structured materials present good phase stability under CO<sub>2</sub> and reducing atmospheres and have low thermal expansion coefficients when compared with perovskites [23].

A dual-phase oxygen membrane based on 40 wt.% of Pr<sub>0.6</sub>Sr<sub>0.4</sub>Fe<sub>2</sub>O<sub>3- $\delta$</sub>  (PSFO) and 60 wt.% of Ce<sub>0.9</sub>Pr<sub>0.1</sub>O<sub>2- $\delta$</sub>  (CPO) was found to be chemically stable under a reducing atmosphere and provided an oxygen flux of  $1.34 \cdot 10^{-7}$  mol/cm<sup>2</sup>·s and  $1.93 \cdot 10^{-7}$  mol/cm<sup>2</sup>·s at 950 °C when CO<sub>2</sub> and helium was employed as sweep gas, respectively [35]. In another study [36], the Pr was replaced with La in the electronic conducting phase (La<sub>0.9</sub>Sr<sub>0.1</sub>FeO<sub>3- $\delta$</sub> ) and Sm was used instead of Pr for the fluorite type oxygen ion conducting phase (Ce<sub>0.8</sub>Sm<sub>0.2</sub>O<sub>2- $\delta$</sub> , CSO). The highest oxygen permeation flux was obtained for (CSO)<sub>0.7</sub>-(LSFO)<sub>0.3</sub> at 950 °C, which is  $1.59 \cdot 10^{-7}$  mol/cm<sup>2</sup>·s for a 1.1 mm thick membrane swept with either helium or CO<sub>2</sub>. In case of CO as sweep gas, the oxygen partial pressure difference became larger leading to an increase in the oxygen permeation flux ( $8.92 \cdot 10^{-7}$  mol/cm<sup>2</sup>·s) and, at the same time, the activation energy decreased to 96.2 kJ/mol compared to 115 kJ/mol obtained when CO<sub>2</sub> or He was employed as sweep gas. In order to accelerate surface reactions for the CGO-LSCF membrane, Pt was deposited as a catalyst in the surface [37]. The oxygen flux was enhanced with the addition of

Pt. A thinner membrane (600  $\mu\text{m}$  thick) made by CSO mixed with a 40 vol.% of  $\text{LaBaCo}_2\text{O}_{5+\delta}$  (LBCO) exhibited an oxygen flux of  $4.59 \cdot 10^{-7}$   $\text{mol}/\text{cm}^2 \cdot \text{s}$  at 950  $^\circ\text{C}$  [38].

Yoon et al. [39] reported on a highly permeable and stable membrane under an  $\text{H}_2\text{-CO}_2$  atmosphere, composed by Ca-doped and Co-doped yttrium chromite,  $\text{Y}_{0.8}\text{Ca}_{0.2}\text{Cr}_{0.8}\text{Co}_{0.2}\text{O}_{3-\delta}$  (YCCC) and samaria-doped ceria,  $\text{Sm}_{0.2}\text{Ce}_{0.8}\text{O}_{1.9}$  (SDC). An oxygen flux of  $2.1 \cdot 10^{-6}$   $\text{mol}/\text{cm}^2 \cdot \text{s}$  was measured for a 1.3-mm thick membrane at 950  $^\circ\text{C}$ . A long-term test was performed at 950  $^\circ\text{C}$  with air at the feed side and 50%  $\text{CO}_2$  + 50% forming gas (3%  $\text{H}_2$  + 97%  $\text{N}_2$ ) at the permeate side. The initial flux decreased less than 2% after 350 h.

A 1-mm thick CGO-LSM membrane showed no degradation after 100 h of operation at 950  $^\circ\text{C}$ , which showed an oxygen flux of  $\sim 8 \cdot 10^{-8}$   $\text{mol}/\text{cm}^2 \cdot \text{s}$  [40]. However, after 500 h of operation, the oxygen flux decreased to  $\sim 2.2 \cdot 10^{-9}$   $\text{mol}/\text{cm}^2 \cdot \text{s}$ . No phase transformation was found according to XRD analysis. The authors attributed the decay to the possible formation of a new phase between CGO grains due to the diffusion of elements from the perovskite phase, which blocked the ionic conductivity. Employing CGO and replacing LSM with BSCF [41], higher oxygen fluxes were achieved of  $8.04 \cdot 10^{-7}$  and  $1.33 \cdot 10^{-6}$   $\text{mol}/\text{cm}^2 \cdot \text{s}$  at 875 and 950  $^\circ\text{C}$ , respectively, using helium as sweep gas.

An YSZ mixed with  $\text{La}_{0.8}\text{Sr}_{0.2}\text{MnO}_{3-\delta}$  (LSM) membrane showed a lower permeation rate at 900  $^\circ\text{C}$ , when it was prepared by two-step sequential tape casting ( $3.31 \cdot 10^{-8}$   $\text{mol}/\text{cm}^2 \cdot \text{s}$ ) compared to a membrane obtained via phase-inversion casting ( $1.90 \cdot 10^{-7}$   $\text{mol}/\text{cm}^2 \cdot \text{s}$ ) [42]. In both cases, the thickness of the selective layer was around 150  $\mu\text{m}$ . In the case that LSM was replaced by BSCF, the oxygen fluxes were observed to be 1 to 2 orders of magnitude higher in the temperature range of 875-950  $^\circ\text{C}$ , despite the thicker membrane (500  $\mu\text{m}$ ) [41].

## **2.3. Performance loss of the membranes under different conditions**

As has already been amply discussed, the operation conditions of the oxygen transport membranes include ultra-high temperature, large oxygen partial pressure difference and the exposure to different gaseous components, like H<sub>2</sub>S and CO<sub>2</sub>. The selection of the membrane materials is a very critical point since the high permeability and good operation stability need to be fulfilled at the same time. The chemical and thermal expansion, cation diffusion and creep, phase transformation, and gas poisoning under different operation conditions are all factors that may cause performance loss of the membranes.

### ***2.3.1. Chemical and thermal expansion***

Chemical and thermal expansion is one of the key factors that may influence the performance of MIEC membranes, especially during the sealing process and co-sintering of different layers for asymmetric membranes. In engineering, the thermal expansion behaviour is usually considered to be linear. However, for some MIEC oxides such as the Fe-containing or Co-containing perovskites, two factors may cause dilatometric behaviour. When the membrane is operated in the low temperature range, the lattice atomic vibrations with temperature would lead to the intrinsic thermal expansion and this expansion behaviour is almost linear, while at higher temperatures, apart from the thermal expansion, the creation of oxygen vacancies resulting from the loss of lattice oxygen could be another factor that contribute to the dilatometric behaviour which is the chemical-included expansion (even if most of the reported expansion coefficients are specified as thermal). As a result, those membranes usually exhibit higher thermal expansion coefficients at higher temperatures.

The undesired chemical expansion is the result of high temperatures and

fluctuations in the partial pressure of oxygen on the feed and the permeate side. As the operating partial pressure of oxygen decreases and the temperature increases, the number of oxygen vacancies increases considerably, which may result in significant chemical expansion and cause stress across the membrane and, eventually, lead to membrane failure [43,44]. The thermal expansion coefficient of some perovskites and fluorite-type structures are presented in Table 2.2.

**Table 2.2.** Thermal expansion coefficient of some perovskites and fluorites for different temperature ranges and oxygen partial pressures, P(O<sub>2</sub>). RT = room temperature

Membrane	p(O <sub>2</sub> ) (atm)	Temperature Range (°C)	$\alpha \cdot 10^6$ (K <sup>-1</sup> )	Reference
SrCo <sub>0.8</sub> Fe <sub>0.2</sub> O <sub>3-δ</sub>	1.00	RT-430	18.5	[45]
	1.00	430-1000	31.1	
	1.00	600-900	31.1	[46]
	0.21	RT-500	17.8	[45]
	0.21	500-1000	30.3	
	0.21	27-427	18.8 ± 0.3	[47]
	0.21	427-827	29.4 ± 0.8	
	0.21	RT-1000	17.9	[48]
	10 <sup>-4</sup>	RT-540	12.3	[45]
			540-1000	19.7
Ba <sub>0.5</sub> Sr <sub>0.5</sub> Co <sub>0.8</sub> F <sub>e<sub>0.2</sub>O<sub>3-δ</sub></sub>		RT-440	12.2	
	1.00	440-1000	24.5	[45]

		RT-440	13.6	
	0.21	440-1000	24.1	[45]
		RT-500	13.6	
	0.21	700-1000	24.8	[49]
	0.21	RT-1000	11.5	[48]
	10 <sup>-4</sup>	RT-1000	18.2	[45]
La <sub>0.5</sub> Sr <sub>0.5</sub> FeO <sub>3-δ</sub>	0.21	RT-400	15.3	[50]
		700-800	16.1	
La <sub>0.5</sub> Sr <sub>0.5</sub> Co <sub>0.5</sub> F e <sub>0.5</sub> O <sub>3-δ</sub>	0.21	RT-400	16.9	[51]
		700-1000	28.6	
La <sub>0.5</sub> Sr <sub>0.5</sub> CoO <sub>3-δ</sub>	0.21	RT-400	17.9	[51]
		700-1000	30.6	
(ZrO <sub>2</sub> ) <sub>0.92</sub> - (Y <sub>2</sub> O <sub>3</sub> ) <sub>0.08</sub> (YSZ)	0.21	RT-1000	10.7	[45]
(ZrO <sub>2</sub> ) <sub>0.85</sub> - (Y <sub>2</sub> O <sub>3</sub> ) <sub>0.15</sub> (YSZ)	0.21	50-1000	10.8	[20]
CeO <sub>2</sub>	0.21	50-1000	12.3	[20]
Ce <sub>0.9</sub> Gd <sub>0.1</sub> O <sub>2-δ</sub>	0.21	Room-1000	12.4	[45]
Ce <sub>0.8</sub> Gd <sub>0.2</sub> O <sub>2-δ</sub>	0.21	50-1000	12.5	[20]
Ce <sub>0.6</sub> Gd <sub>0.4</sub> O <sub>2-δ</sub>	0.21	50-1000	12.1	[20]
Ce <sub>0.5</sub> Er <sub>0.5</sub> O <sub>2-δ</sub>	0.21	50-1000	11.4	[20]
Ce <sub>0.9</sub> Ca <sub>0.1</sub> O <sub>2-δ</sub>	0.21	50-1000	12.8	[20]

$\text{Ce}_{0.8}\text{Ca}_{0.2}\text{O}_{2-\delta}$	0.21	50-1000	13.6	[20]
---	------	---------	------	------

Choi and co-workers [49] reported on the thermochemical expansion of BSCF perovskites that are often employed as oxygen membrane. The thermal expansion was measured for  $\text{Ba}_{0.5}\text{Sr}_{0.5}\text{Co}_{0.8}\text{Fe}_{0.2}\text{O}_{3-\delta}$  at around  $13.6 \cdot 10^{-6} \text{ }^\circ\text{C}^{-1}$  up to  $500 \text{ }^\circ\text{C}$ , while, from  $700 \text{ }^\circ\text{C}$  to  $1000 \text{ }^\circ\text{C}$ , the total expansion measured was  $24.8 \cdot 10^{-6} \text{ }^\circ\text{C}^{-1}$ . This increase is related to the chemical expansion. On the other hand, fluorite type structures exhibit lower expansion than perovskites, which represents an advantage in avoiding (or decreasing) stress problems and membrane failure [23]. Bishop et al. studied the chemical expansion of gadolinium and un-doped cerium oxide [44]. The study reported a chemical expansion for very low oxygen partial pressures that are less than  $10^{-16} \text{ atm}$ . Omar et al. [43] studied the expansion effect of doping ceria with different cations. The experimental data were compared with results obtained employing a mathematical model proposed by Hong and Virkar. As the radius of the trivalent doping increases, the chemical expansion (or chemical elastic strain induced by the non-stoichiometry) of the material increases. The expansion coefficients of ceria and doped-ceria with Gd, Er, and Ca have been reported by Mogensen et al. [20]. Their constant expansion coefficient over a large temperature range ( $50\text{-}1000 \text{ }^\circ\text{C}$ ) indicates that their chemical expansion can be considered negligible. Besides, ceria stabilized with Gd and Sm are promising materials since their fluorite structure does not show high chemical expansion compared to most perovskites [23].

### **2.3.2. Phase transformation**

As previously explained, perovskite materials present a relatively high oxygen flux. Between all the possible phases that a perovskite can adopt, the cubic perovskite phase is the most favourable structure for oxygen permeation. The examples are the BSCF and SCF, which present high permeation rates at high

temperatures ( $>850$  °C) due to the relatively stable cubic phase. Below  $850$  °C, these cubic perovskite transforms into an orthorhombic brownmillerite phase [52,53], with a concomitant dramatic decrease in the oxygen permeation rate. The ordered arrangement of oxygen vacancies in the brownmillerite structure, in which one-sixth of the oxygen sites are vacant, reduces the oxygen flux. Nevertheless, the brownmillerite phase can change again into a perovskite phase when the temperature is increased [54,55]. The lattice expansion associated with the phase transition results in mechanical instability issues [56].

In order to improve the phase stability of the perovskite material, several strategies have been reported [18]. For instance, cations with higher valence (i.e., La) were introduced into the A site [57] or (i.e., Ti, Cr) [47,58] into the B site cation. Moderate amounts of Ti or Cr into the Co or Fe sub-lattice improves the structural stability, but might decrease the electron conductivity and oxygen permeability [59].

Partial substitution of the A site or the B site cation with ions of larger radius is another option. For instance, the Zr doping was found to reduce the lower temperature limit of the perovskite phase stability range to below  $800$  °C. Ravkina et al. [60] extended the research done with Zr-doped BSCF on long-term experiments at an intermediate temperature range and they could conclude that a BSCF membrane with up to 3 mol% Zr content at an intermediate temperature range (i.e.,  $773$ – $1123$  K) showed improved phase stability compared with pure BSCF. In case of introducing Ba into  $\text{SrCo}_{0.8}\text{Fe}_{0.2}\text{O}_{3-\delta}$  by partial substitution of Sr, improved phase stability is obtained while the conductivity remain unaffected [10,61]. Unger et al. [62] studied the effect of Y doped BSCF for different Y concentrations to analyze the partial transformation to an Fe-depleted hexagonal phase during long term annealing in ambient air for 240 h at intermediate temperatures, as well as cobalt precipitates and anomalies in the morphology.

They concluded that the partial B site doped with 10% of Y extended the stability range of the cubic BSCF perovskite phase at lower temperatures. In addition, no secondary phase formation was observed at 800 °C and, at lower temperatures, the degradation was significantly reduced.

The development of perovskite compounds without cobalt can help improving the phase stability of the membranes. Cobalt based perovskite type membranes present high oxygen permeability but the stability at intermediate temperatures or under reducing conditions is poor because the cobalt easily reduces, which results in large changes in the unit cell dimension. Development of cobalt-free MIEC membranes could also be a strategy to solve the long-term stability problems caused by the reaction with gas species like CO<sub>2</sub>, SO<sub>2</sub>, or water vapor [63]. One of the most studied cobalt-free membranes is the BaFeO<sub>3-δ</sub>, but it shows a low oxygen permeability because it crystalizes in the hexagonal structure, which permeates less than the cubic structure. Tan et al. [64] fabricated a cobalt-free La<sub>0.7</sub>Sr<sub>0.3</sub>FeO<sub>3-δ</sub> hollow fiber membrane and observed that the stability in a He and CO<sub>2</sub> atmosphere was higher than for the LSCF membrane. However, the LSF membrane still suffered from a reaction with H<sub>2</sub> and CH<sub>4</sub> and porous debris were formed, which resulted in membrane leaking or even in a mechanical stability decrease.

Many of the fluorite-type structures do not show phase changes, but ZrO<sub>2</sub> presents a mixed phase and/or phase transition, depending on the operating conditions. This phase transformation vanishes with Y<sub>2</sub>O<sub>3</sub> or Bi<sub>2</sub>O<sub>3</sub> addition, since they stabilize the cubic phase [65].

### ***2.3.3. Cationic diffusion and creep***

When MIEC membranes are employed for oxygen separation, the oxygen



chemical potential gradient across the membranes would result in an inverse cation chemical potential gradient. Cation diffusion is, therefore, expected through the membranes. Although, for most perovskite materials, the activation energy for cation diffusion is several times higher than the oxygen ionic diffusion, and its contribution to the electrical conductivity is also negligible, cation diffusion is still necessary to be studied with regards to the long-term stability of some materials. At an elevated temperature, cations tend to diffuse from the low oxygen chemical potential side to the high oxygen chemical potential side. Different diffusivities of the cations may result in de-mixing of the material or precipitation of certain elements on the surface of the membrane. For instance, Lein and co-workers [66] observed several secondary phases on the oxidizing side of LSCF membranes after 1 month of operation at 1150 °C, which was attributed to the higher mobility of Fe and Co than that of Sr and La.

Apart from cation diffusion, a high oxygen partial pressure also applies stress and sufficient activation energy to provoke creep deformation of some MIEC membranes. Creep refers to the non-elastic or plastic deformation of some solid materials, influenced by temperature, time, and the material properties. For MIEC oxides, the oxygen partial pressure is also one of the key factors that may cause creep [67]. For engineering ceramics, the acceptable strain is reported to be lower than 1% per year.

#### ***2.3.4. Gas poisoning***

Membrane surfaces exposed to atmospheres containing carbon dioxide (CO<sub>2</sub>), sulphur compounds (H<sub>2</sub>S and SO<sub>2</sub>), or steam (H<sub>2</sub>O) could be poisoned, which results in a decrease in the oxygen flux and, in the worst case, cause the membrane failure. The effects of the gases on the membranes depend on the membrane material. The surface morphology is modified as those materials react with the

gases to create new phases, which may result in permeation losses. Doping strategies can again improve the tolerance towards these gases. However, in many cases, the stability improvement comes at the expense of decreased permeability.

#### 2.3.4.1. CO<sub>2</sub> poisoning

When exposed to CO<sub>2</sub>, some MIEC perovskite membranes show a decrease in the O<sub>2</sub> permeation. This variation could be attributed to the absorption of CO<sub>2</sub> on the surface of the membrane or to a carbonation process. For instance, carbonation of some alkaline earth elements (e.g., Ba or/and Sr) can destroy the perovskite structure. On top of it, the formation of a new phase may produce a partial or complete loss of oxygen permeation [18].

Arnold et al. [68] reported an immediate decrease in the oxygen flux for a BSCF membrane when CO<sub>2</sub> was used as sweep gas. Tong's group [69] also found that exposure of BCFZ membranes to CO<sub>2</sub> could lead to a significant decrease in the oxygen permeability. This process is also associated with the formation of some metal oxides such as the CoO and/or Fe<sub>3</sub>O<sub>4</sub> [10,68,70]. Efimov et al. evaluated the stability of the carbonates for metals such as Ca, Sr, Ba, and La [71] using the Ellingham diagram, and found that the carbonate of Ba is more stable than SrCO<sub>3</sub> and CaCO<sub>3</sub>, which means the BaCO<sub>3</sub> is much easier to be formed. Although Ba<sup>2+</sup> (large alkaline earth cation) favours a high oxygen conductivity, this cation can also lead to inferior CO<sub>2</sub> tolerance. On the other hand, the smaller cation of Ca<sup>2+</sup> shows better stability but disfavours the oxygen permeability. Substitution of Fe with Ti also improves the CO<sub>2</sub> tolerance while the O<sub>2</sub> permeability decreases slightly [72]. Moreover, a high cobalt-containing perovskite also presents a low chemical stability in CO<sub>2</sub>-containing atmospheres [73]. According to the research of Waandich et al. [74], Ba<sub>0.3</sub>Sr<sub>0.7</sub>Fe<sub>0.8</sub>Co<sub>0.2</sub>O<sub>3-δ</sub> is more stable than Ba<sub>0.5</sub>Sr<sub>0.5</sub>Fe<sub>0.2</sub>Co<sub>0.8</sub>O<sub>3-δ</sub> in the presence of CO<sub>2</sub>.

Zeng et al. [75] improved the CO<sub>2</sub> tolerance of SCF perovskite oxides by introducing Ti into SCF oxides, and they found that the sample with a low Ti content showed a dramatic decrease in the oxygen flux after exposure to CO<sub>2</sub> for 70 h, while higher Ti-substituted samples remained almost stable after 90 h. The author attributed the improved CO<sub>2</sub> tolerance to the stronger chemical bond between Ti and O than the Fe-O and Co-O bonds.

Another possibility is doping with a highly charged metal B<sup>5+</sup> like Ta and Nb. Chen et al. [76] found that, when SCF is doped with Ta, the CO<sub>2</sub> erosion is almost negligible. Yi et al. [77] investigated the corrosion of BaCo<sub>1-x-y</sub>Fe<sub>x</sub>Nb<sub>y</sub>O<sub>3-δ</sub> (x=0.2-0.8, y=0.1-0.5) in the temperature range of 800 to 1000 °C. The chemical stability was found to be improved when increasing the Nb content, while no significant degradation was observed when Co was totally substituted by Fe and Nb. The Ba and/or Co substituted perovskite materials can provide increased chemical stability, but the oxygen permeability may also be decreased. The addition of metals B<sup>6+</sup> (Mo, W) can stabilize the membrane in a CO<sub>2</sub> environment as well as suppress the polymorphic transition. Popov et al. [78] reported that substitution of Co by W to a BSCF not only improves the CO<sub>2</sub> tolerance, but the O<sub>2</sub> permeability was also enhanced by one order of magnitude. The same effect has been reported by Shubnikoba et al. [79] when cobalt was substituted with molybdenum.

Another type of perovskite, La<sub>0.6</sub>Ca<sub>0.4</sub>Co<sub>0.8</sub>Fe<sub>0.2</sub>O<sub>3-δ</sub>, was studied under a continuous gas flow containing CO<sub>2</sub>, which revealed a higher resistance than the one considered from Ellingham diagrams [71]. Un-doped cobalt La<sub>0.6</sub>Ca<sub>0.4</sub>FeO<sub>3-δ</sub> can resist the presence of CO<sub>2</sub> in the stream.

Many fluorite type materials have good phase stability under CO<sub>2</sub> atmospheres. Due to this reason, a dual phase type membrane could help increase the tolerance

to CO<sub>2</sub> poisoning.

#### 2.3.4.2. Sulphur poisoning

The presence of CO<sub>2</sub>, which commonly comes from the combustion of light hydrocarbons, is, in many cases, accompanied with the presence of SO<sub>2</sub> coming from sulphur containing feedstocks (like coals, natural gas, or biomass). It has been proven that this SO<sub>2</sub> can lead to a degradation of the oxygen flux and decrease in the mechanical stability of oxygen membranes. Specifically, alkaline and alkaline earth metals compounds, commonly present in MIEC membranes, can form sulphur compounds.

BSCF-based membranes exhibit a low stability in the presence of sulphur compounds, since the heat formation of BaS and SrS are very high, which are -406 kJ/mol and -472 kJ/mol, respectively. YSZ is also a sensitive material under sulphur compound containing atmospheres since yttrium present a high tendency to form the corresponding sulphate with a heat formation of -1260 kJ/mol. In addition, lanthanum-based perovskites are strongly affected by sulphur and the corresponding heat formation for La<sub>2</sub>S<sub>3</sub> is -1205 kJ/mol [80]. The influence of SO<sub>2</sub> on the oxygen permeation of LSCF hollow fiber membranes was studied after the membrane was exposed to SO<sub>2</sub> [81]. Surface decomposition was observed, which resulted in a significant decrease in the oxygen permeation flux. The XRD analysis showed a peak related to the formation of SrSO<sub>4</sub>. In another study, an LSCF membrane was exposed to 200 ppm of H<sub>2</sub>S for 100 h at 900 °C [82]. Again, strontium sulphate was formed with the corresponding decay in the oxygen flux. The membrane performance was, however, completely recovered when air was switched back.

Alkaline earth elements should be avoided to obtain MIEC membranes, which

can offer a stable performance under CO<sub>2</sub> and SO<sub>2</sub> containing atmospheres. A CO<sub>2</sub> stable NFO-CTO dual-phase membrane also showed sulphur resistance after exposure to SO<sub>2</sub> for 170 h at 800 °C [83], which makes this membrane very interesting for applications where CO<sub>2</sub> and SO<sub>2</sub> are both present in the feed gas stream. However, there is a need to use a less expensive and toxic material for the development of CO<sub>2</sub> and SO<sub>2</sub> resistant oxygen membranes. Cheng et al. [84] reported ZnO-based dual phase membranes as an alternative. They fabricated an Al<sub>0.02</sub>Ga<sub>0.02</sub>Zn<sub>0.96</sub>O<sub>1.02</sub>-CGO membrane and the post XRD characterization indicated that the membrane showed sufficient stability when in contact with CO<sub>2</sub> for 120 h at 850 °C and in contact with SO<sub>2</sub> for 2 h at 850 °C.

Garcia et al. [85] prepared a LaCo<sub>0.2</sub>Ni<sub>0.4</sub>Fe<sub>0.4</sub>O<sub>3-δ</sub> (50 vol%)-Ce<sub>0.8</sub>Gd<sub>0.2</sub>O<sub>2-δ</sub> (50 vol%) membrane activated by the deposition of a 30 μm thick porous layer of Ce<sub>0.8</sub>Gd<sub>0.2</sub>O<sub>2-δ</sub> (50 vol %)-La<sub>0.8</sub>Sr<sub>0.2</sub>MnO<sub>3-δ</sub> (50 vol %) at both sides of the membrane. The oxygen flux permeation under a SO<sub>2</sub> atmosphere for the coated membrane was higher than the un-coated one, which shows that the coating composite works as a protective layer to preserve the performance of the membrane.

It is also worthy to underline that not only the SO<sub>2</sub> coming from the process can affect the membrane performance, but also sulphur coming from impurities of the raw materials used in the membrane preparation can result in a detrimental effect on the membrane performance. Wu et al. [86] showed that a dual phase membrane Ce<sub>0.9</sub>Gd<sub>0.1</sub>O<sub>2-δ</sub>-SrCo<sub>0.8</sub>Fe<sub>0.1</sub>Nb<sub>0.1</sub>O<sub>3-δ</sub> prepared with low sulphur content raw materials presented a constant permeation rate of 30 ml/min·cm<sup>2</sup> in which the permeation is higher than the same composite prepared with high sulphur content (because of the impurities in the raw material), which contributed to sulphate formation in the membrane.

## **2.4. Oxygen permeation improvement**

As has been illustrated, the oxygen permeation through the membranes mainly involves five steps, and membranes of different thickness and materials were found to have different controlling steps. When the permeation was controlled by the bulk diffusion, the oxygen permeability through the membranes can be described by the Wagner equation:

$$j_{O_2} = -\frac{RT}{4^2 F^2} \frac{1}{L} \int_{\ln P'_{O_2}}^{\ln P''_{O_2}} \frac{\sigma_{el} \sigma_{ion}}{\sigma_{el} + \sigma_{ion}} d \ln p_{O_2} \quad (2-3)$$

where  $j_{O_2}$  is the oxygen permeation flux,  $F$  is the Faraday constant,  $R$  is the gas constant,  $L$  is the membrane thickness,  $P''_{O_2}$  and  $P'_{O_2}$  are the low and high oxygen partial pressure and  $\sigma_{el}$  and  $\sigma_{ion}$  are partial electronic and ionic conductivity, respectively. Accordingly, the oxygen permeability could be improved by increasing the partial pressure difference across the membrane, improving the operating temperature, choosing material with high conductivity or reducing the membrane thickness.

When the bulk diffusion resistance gets very small, which may be attributed to the reduced thickness and/or improved mixed-conductivity of the membrane, the limiting step would become the surface-exchange reaction. The dissociation and association processes at both sides of the membrane need to be promoted, and this can be realized by depositing an activation layer on the membrane.

### **2.4.1. Thickness reduction of the membranes**

Thinner membranes usually provide an improved permeation flux, but may also show decreased mechanical strength. Accordingly, asymmetric membranes were

developed with thin membrane layers on a thicker porous layer. This structure allows not only a high permeation flux, but also good mechanical strength of the membrane. For successful fabrication of a supported thin-film membrane, certain criteria must be fulfilled [4]:

1. The thermal and chemical expansion of the selective layer and the support should be as close as possible.
2. No reactions should take place between the different materials at high temperatures.
3. The dense selective layer should be free of defects, such as cracks and pinholes.

For the selection of the support material, there are two options including using the same material as employed for the selective layer or using a different material, but with good chemical and thermal compatibility. Fluorite type oxides are good candidate materials for the support material due to their good chemical and mechanical stability. There would be cracks and/or pin holes on the membrane layer, or the membrane layer may peel off from the support during the sintering process due to the a mismatch in thermal expansion of the different materials. For example, porous substrates made of  $\text{Al}_2\text{O}_3$  are very common in the water purification industry and can be applied as a support for hydrogen separation technologies, which takes advantage of their low cost. However, the low thermal expansion coefficient of this material may frustrate its application as support material for asymmetric oxygen transport membranes. Perovskites which are usually applied as the membrane layer because of their good mixed-conductivity generally have a much larger chemical and thermal expansion coefficient in comparison with aluminum oxide, and some perovskites, such as BSCF, was found to react with the aluminum oxide. Another support candidate is MgO

thanks to its good chemical and mechanical stability at high temperatures and lower cost compared to perovskite and fluorite materials. Since the thermal expansion coefficient of MgO ( $13.9 \cdot 10^{-6} \text{ }^\circ\text{C}^{-1}$ ) is close to that of CGO ( $12.7 \cdot 10^{-6} \text{ }^\circ\text{C}^{-1}$ ) [87], this material is preferred as support. Ovtar et al. [88] prepared a thin dense layer (10  $\mu\text{m}$ ) of CGO-LSF onto MgO. The measured oxygen flux at 850  $^\circ\text{C}$  was  $1.56 \cdot 10^{-6} \text{ mol/cm}^2 \cdot \text{s}$ , using  $\text{N}_2$  as sweep gas, while this value increased to  $1.16 \cdot 10^{-5} \text{ mol/cm}^2 \cdot \text{s}$  when  $\text{H}_2$  was employed as sweep gas. A larger flux ( $2.97 \cdot 10^{-6} \text{ mol/cm}^2 \cdot \text{s}$ ) was reported under the same conditions by Ramachandran et al. [87] for a 30  $\mu\text{m}$ -thick CGO dense layer deposited onto MgO. Apart from MgO,  $\text{CeO}_2$  may also be a good support candidate for the fabrication of CGO-based membranes because their thermal expansion coefficients closely resemble those of CGO. Yin et al. [89] tested the performance of a  $\text{CeO}_2$  supported CGO membrane (10-20  $\mu\text{m}$ -thick), where an oxygen flux of  $3.35 \cdot 10^{-7} \text{ mol/cm}^2 \cdot \text{s}$  was measured at 900  $^\circ\text{C}$ .

Metal supports are attractive because of their high mechanical strength and easier integration in the reactor. However, it is usually very hard to find metals with similar thermal expansion coefficients as the ceramic membrane layer material, and there are not many papers on metal-supported oxygen transport membranes. A successful example was given by Sadykov's group [90], which reported on the deposition of a mixture of LSFN and CGO onto a Ni-Al alloy foam substrate. Stainless steel is a common low-cost metal, but, depending on the steel grade, their use at high temperatures ( $>500 \text{ }^\circ\text{C}$ ) is hampered by loss of their mechanical properties due to the precipitation of carbides and differences in thermal expansion coefficient with the membrane layer also restricts their application as support. However, in recent years, some researchers have tried to apply oxygen selective materials onto a stainless-steel support using a plasma spray deposition method, which could avoid the problems caused by high-temperature sintering. Fan and Kesler [91] deposited a 55  $\mu\text{m}$ -thick LSCF layer onto a stainless-steel



support using the plasma spray deposition method, which showed a very low gas leakage during testing at high temperatures. Niu's group [92] tried to fabricate an LSCF layer onto a stainless-steel support with two plasma spray-based methods, where the plasma spray deposition method performed better by avoiding vertical cracks on the membrane layer.

Large oxygen fluxes are required for industrial exploitation of the oxygen permselective membranes. One of the best results for supported membranes were reported by Baumann et al. [93], who coated a BSCF layer (70  $\mu\text{m}$ ) onto a BSCF substrate that showed an outstanding  $\text{O}_2$  flux of  $4.62 \cdot 10^{-5} \text{ mol/cm}^2 \cdot \text{s}$  at 1000  $^\circ\text{C}$  using pure oxygen as feed and argon as sweep gas, whereas, when air was used as feed, a flux of  $8.32 \cdot 10^{-6} \text{ mol/cm}^2 \cdot \text{s}$  was measured. Cao et al. [94] reported a dual-phase supported membrane with a large oxygen flux ( $2.90 \cdot 10^{-6} \text{ mol/cm}^2 \cdot \text{s}$ ), composed of a 40- $\mu\text{m}$  dense layer of SDC-SSAF on top of a porous substrate made of the same material. Meng et al. [95] fabricated asymmetric membranes using the  $\text{BaCo}_{0.7}\text{Fe}_{0.2}\text{Nb}_{0.1}\text{O}_{3-\delta}$  (BCFN) as material for both the dense layer (20  $\mu\text{m}$ -thick) and porous support. At 900  $^\circ\text{C}$ , the oxygen flux was  $3.35 \cdot 10^{-6} \text{ mol/cm}^2 \cdot \text{s}$ .

The porosity of the support also has influence on the permeation flux, which was observed by Schulze-Küppers et al. [25]. They reported that, when the porosity of the BSCF support was increased from 26% to 41%, the oxygen flux of the supported dense BSCF layer with a thickness of 20  $\mu\text{m}$  increased by 50% ( $2.01 \cdot 10^{-6} \text{ mol/cm}^2 \cdot \text{s}$  at 1000  $^\circ\text{C}$ ).

Some advanced membrane preparation methods result in large channels in the support layer, which facilitates lower resistance for the gas permeation. Zhang et al. [96] prepared an YSZ–LSCrF asymmetric composite membrane with a dense layer of thickness  $\sim 30 \mu\text{m}$  and a finger-like porous support with a thickness of  $\sim 1$

mm by using a phase-inversion tape-casting method. The YSZ-LSCrF composite was subsequently coated with  $\text{Sm}_{0.2}\text{Ce}_{0.8}\text{O}_2$  nano-particles on the inner surfaces of the support, and the oxygen permeation flux observed was  $1.64 \cdot 10^{-6} \text{ mol/cm}^2 \cdot \text{s}$  at  $900 \text{ }^\circ\text{C}$ . Another membrane consisted of a micro-channelled CGO-LSF layer with a dense  $100 \text{ }\mu\text{m}$ -thick layer was prepared by one-step phase inversion [97]. This membrane showed an oxygen flux of  $7.51 \cdot 10^{-6} \text{ mol/cm}^2 \cdot \text{s}$  at  $900 \text{ }^\circ\text{C}$  using CO as sweep gas with air as feed gas. The freeze cast is another promising method for preparing asymmetric membranes with oriented pores and low gas transfer resistance. This method starts with the preparation of a colloidal suspension and this suspension was then freed in a mould. During the sublimation of the solvent in the suspension, a network of oriented holes is formed inside the membrane, which provides a shorter gas transfer distance than the sponge-like microstructure formed by burning the sacrifice phase. Liu et al. [98] fabricated a  $\text{Zr}_{0.84}\text{Y}_{0.6}\text{O}_{1.92}\text{-La}_{0.8}\text{Sr}_{0.2}\text{Cr}_{0.5}\text{Fe}_{0.5}\text{O}_{3-\delta}$  dual-phase asymmetric membrane by the frozen cast process and the oxygen permeability is proven to be better when compared with the one fabricated phase-inversion tap-casting strategy.

#### ***2.4.2. Membrane surface modification***

Modifying surface of the membrane can lead to an enhancement on the oxygen permeation when the limiting step is the surface-exchange reaction. As the surface per volume ratio increases in a porous top layer, the adsorption and dissociation of oxygen molecules is promoted [99]. A very thin layer composed of nanoparticles is an interesting approach to obtain a meso-structured layer on top of the oxygen selective layer [100,101]. The layer can be obtained by using sacrificial agents, which are removed during a sintering step, such as carbon black or polymeric nanoparticles [102]. The material used for the porous coating can be the same as the selective layer [97,103] or a different material [104], which possess ionic and/or electronic conductivity.

The oxygen permeation of a 20  $\mu\text{m}$ -thick LSFT membrane was improved by 50%, when the surface at the permeate side was modified, as described in [103]. At 1000  $^{\circ}\text{C}$ , the membrane permeation increases from  $2.23 \cdot 10^{-6}$  to  $4.31 \cdot 10^{-6}$   $\text{mol}/\text{cm}^2 \cdot \text{s}$  by increasing the roughness of the membrane at the permeate side. On the other hand, the addition of a porous LSC layer (20  $\mu\text{m}$ -thick) on both sides of a SDF-SSF (75wt%  $\text{Ce}_{0.85}\text{Sm}_{0.15}\text{O}_{1.925}$ -25wt%  $\text{Sm}_{0.6}\text{Sr}_{0.4}\text{FeO}_3$ ) membrane not only increased the oxygen permeation, but also provided a faster steady state permeation rate obtained (0-8 h) than without the presence of the porous LSC layer (18-40 h) [105]. For the case of a LSTF-coated BSFC membrane, an increase of 20% in the oxygen flux was obtained relative to the flux through a bare BSFC at 950  $^{\circ}\text{C}$  [104], which resulted in an oxygen flux of  $2.23 \cdot 10^{-6}$   $\text{mol}/\text{cm}^2 \cdot \text{s}$  at atmospheric pressure. The authors reported a reduction in the performance of both membranes after 12 days of testing, but the reduction for the coated membrane was significantly smaller (7.6%) compared to the decrease in performance for the non-coated BSCF (31%). Hayamizu et al. [106] reported a decrease in the activation energy by addition of a thin porous layer. The activation energy in the temperature range of 725-775  $^{\circ}\text{C}$  decreased from 177.8 kJ/mol to 102.6 kJ/mol after a 6.5  $\mu\text{m}$  thick porous BSCF layer was deposited onto a 120  $\mu\text{m}$  thick dense BSCF membrane, while the oxygen permeation flux increased by a factor of 3.6 and 1.35 at 700  $^{\circ}\text{C}$  and 850  $^{\circ}\text{C}$ , respectively. The addition of a ceramic catalytic layer of SDC-LSCF onto an asymmetric dual-phase membrane composed of CGO-LSM (30  $\mu\text{m}$ -thick dense layer) resulted in an increase in the oxygen permeation flux from  $7.16 \cdot 10^{-8}$  to  $5.32 \cdot 10^{-7}$   $\text{mol}/\text{cm}^2 \cdot \text{s}$  at 950  $^{\circ}\text{C}$  [107].

## **2.5. Conclusions**

Oxygen is an essential gas for many industrial processes, which is industrially produced by the expensive and energy intensive techniques, such as cryogenic distillation. The development of membrane technology with dense mixed ionic and electronic conducting ceramic membranes (MIEC) could open up the possibility to supply pure oxygen at reduced production costs. In this context, in the last few decades, significant efforts have been made to develop new materials to improve the oxygen permeation and stability of MIEC membranes.

Some perovskites materials are very unique because of their favourable capacity to transport oxygen ions and electrons, but these perovskite materials usually show insufficient chemical stability under certain operating conditions (especially in the presence of CO<sub>2</sub> and sulphur compounds). On the other hand, most fluorites show a better performance under atmospheres containing CO<sub>2</sub> and sulphur compounds, but their permeation is lower because of the insufficient electronic-conductivity. Combination of two phases may lead to a better membrane performance, but good compatibility of the two materials during the sintering and operation process is crucial.

Asymmetric membranes allow us to increase the oxygen flux while maintaining sufficient mechanical strength due to the possibility to deposit a very thin dense layer on top of porous support. However, for the successful fabrication of asymmetric membranes, the layer(s) should attach well with to each other, which requires good chemical and thermal compatibility between the selected material of the support and the selective layer during the preparation, sintering, and operation at high temperatures. Papers have been published about asymmetric membranes by focusing on the same or similar materials for both the support and selective layers, and most papers have proven that asymmetric membranes allow

reduced bulk diffusion resistances compared with single layer membranes by reducing the selective layer thickness. Some advanced membrane fabrication techniques allow the fabrication of asymmetric membrane structure in a single step and the formation of less tortuous channels for gas transfer in the support layer. For some asymmetric membranes, there is a point at which a further decrease of the membrane thickness no longer results in a higher oxygen permeability because of the limitation by surface kinetics. Activation layers can be applied on top of these membranes to improve the surface exchange rate.

## References

- [1] C. Li, J. J. Chew, A. Mahmoud, S. Liu, J. Sunarso, Modelling of oxygen transport through mixed ionic-electronic conducting (MIEC) ceramic-based membranes: an overview, *J. Memb. Sci.* 567 (2018) 228–260.
- [2] Y. Liu, X. Tan, K. Li, Mixed conducting ceramics for catalytic membrane processing, *Catal. Rev. - Sci. Eng.* 48 (2006) 145–198.
- [3] K. Zhang, J. Sunarso, Z. Shao, W. Zhou, C. Sun, S. Wang, S. Liu, Research progress and materials selection guidelines on mixed conducting perovskite-type ceramic membranes for oxygen production, *RSC Adv.* 1 (2011) 1661–1676.
- [4] X. Zhu, W. Yang, Critical factors affecting oxygen permeation through dual-phase membranes, 1st ed., Elsevier BV., 2011.
- [5] M. A. Peña, J. L. G. Fierro, Chemical structures and performance of perovskite oxides, *Chem. Rev.* 101 (2001) 1981–2017.
- [6] R. L. Cook, A. F. Sammells, On the systematic selection of perovskite solid electrolytes for intermediate temperature fuel cells, *Solid State Ionics.* 45 (1991) 311–321.
- [7] Y. Teraoka, H. M. Zhang, S. Furukawa, N. Yamazoe, Oxygen permeation through perovskite-type oxides, *Chem. Lett.* 14 (1985) 1743–1746.
- [8] J. W. Stevenson, Electrochemical properties of mixed conducting perovskites  $\text{La}_{1-x}\text{M}_x\text{Co}_{1-y}\text{Fe}_y\text{O}_{3-\delta}$  (M = Sr, Ba, Ca), *J. Electrochem. Soc.* 143 (1996) 2722.
- [9] S. Li, W. Jin, P. Huang, N. Xu, J. Shi, Y. S. Lin, M. Z. C. Hu, E. A. Payzant, Comparison of oxygen permeability and stability of perovskite type  $\text{La}_{0.2}\text{A}_{0.8}\text{Co}_{0.2}\text{Fe}_{0.8}\text{O}_{3-\delta}$  (A = Sr, Ba, Ca) membranes, *Ind. Eng. Chem. Res.* 38 (1999) 2963–2972.
- [10] Z. Shao, G. Xiong, H. Dong, W. Yang, L. Lin, Synthesis, oxygen permeation study and membrane performance of a  $\text{Ba}_{0.5}\text{Sr}_{0.5}\text{Co}_{0.8}\text{Fe}_{0.2}\text{O}_{3-\delta}$  oxygen-permeable dense ceramic reactor for partial oxidation of methane to syngas, *Sep. Purif. Technol.* 25 (2001) 97–116.

- [11] E. G. Babakhani, J. Towfighi, L. Shirazi, A. N. Pour, Order-disorder transition and phase stability of  $\text{Ba}_x\text{Sr}_{1-x}\text{Co}_{0.8}\text{Fe}_{0.2}\text{O}_{3-\delta}$  oxides, *J. Memb. Sci.* 376 (2011) 78–82.
- [12] E. G. Babakhani, J. Towfighi, L. Shirazi, A. Nakhaeipour, A. Zamaniyan, Z. Shafiei, Structure stability and oxygen permeability of perovskite-type oxides of  $\text{Ba}_{0.5}\text{Sr}_{0.5}\text{Co}_{0.8}\text{Fe}_{0.1}\text{R}_{0.1}\text{O}_{3-\delta}$  (R=Al, Mn, Fe, Ce, Cr, Ni, Co), *J. Mater. Sci. Technol.* 28 (2012) 177–183.
- [13] X. Li, T. Kerstiens, T. Markus, Oxygen permeability and phase stability of  $\text{Ba}_{0.5}\text{Sr}_{0.5}\text{Co}_{0.8}\text{Fe}_{0.2}\text{O}_{3-\delta}$  perovskite at intermediate temperatures, *J. Memb. Sci.* 438 (2013) 83–89.
- [14] H. Cheng, W. Yao, X. Lu, Z. Zhou, C. Li, J. Liu, Structural stability and oxygen permeability of  $\text{BaCo}_{0.7}\text{Fe}_{0.2}\text{M}_{0.1}\text{O}_{3-\delta}$  (M = Ta, Nb, Zr) ceramic membranes for producing hydrogen from coke oven gas, *Fuel Process. Technol.* 131 (2015) 36–44.
- [15] J. Liu, H. Cheng, B. Jiang, X. Lu, W. Ding, Effects of tantalum content on the structure stability and oxygen permeability of  $\text{BaCo}_{0.7}\text{Fe}_{0.3-x}\text{Ta}_x\text{O}_{3-\delta}$  ceramic membrane, *Int. J. Hydrogen Energy.* 38 (2013) 11090–11096.
- [16] W. Yao, H. Cheng, H. Zhao, X. Lu, X. Zou, S. Li, C. Li, Synthesis, oxygen permeability, and structural stability of  $\text{BaCo}_{0.7}\text{Fe}_{0.3-x}\text{Zr}_x\text{O}_{3-\delta}$  ceramic membranes, *J. Memb. Sci.* 504 (2016) 251–262.
- [17] M. Mogensen, D. Lybye, N. Bonanos, P. V. Hendriksen, F. W. Poulsen, Factors controlling the oxide ion conductivity of fluorite and perovskite structured oxides, *Solid State Ionics.* 174 (2004) 279–286.
- [18] J. Sunarso, S. Baumann, J. M. Serra, W. A. Meulenber, S. Liu, Y. S. Lin, J. C. Diniz da Costa, Mixed ionic-electronic conducting (MIEC) ceramic-based membranes for oxygen separation, *J. Memb. Sci.* 320 (2008) 13–41.
- [19] V. V. Kharton, F. M. B. Marques, A. Atkinson, Transport properties of solid oxide electrolyte ceramics: a brief review, *Solid State Ionics.* 174 (2004) 135–149.

- [20] M. Mogensen, Physical properties of mixed conductor solid oxide fuel cell anodes of doped CeO<sub>2</sub>, *J. Electrochem. Soc.* 141 (1994) 2122.
- [21] D. P. Fagg, A. L. Shaula, V. V. Kharton, J. R. Frade, High oxygen permeability in fluorite-type Ce<sub>0.8</sub>Pr<sub>0.2</sub>O<sub>2-δ</sub> via the use of sintering aids, *J. Memb. Sci.* 299 (2007) 1–7.
- [22] R. Srinivasan, R. J. De Angelis, G. Ice, B. H. Davis, Identification of tetragonal and cubic structures of zirconia using synchrotron x-radiation source, *J. Mater. Res.* 6 (1991) 1287–1292.
- [23] J. H. Joo, G. S. Park, C. Y. Yoo, J. H. Yu, Contribution of the surface exchange kinetics to the oxygen transport properties in Gd<sub>0.1</sub>Ce<sub>0.9</sub>O<sub>2-δ</sub>-La<sub>0.6</sub>Sr<sub>0.4</sub>Co<sub>0.2</sub>Fe<sub>0.8</sub>O<sub>3-δ</sub> dual-phase membrane, *Solid State Ionics.* 253 (2013) 64–69.
- [24] C. S. Chen, B. A. Boukamp, H. J. M. Bouwmeester, G. Z. Cao, H. Kruidhof, A. J. A. Winnubst, A. J. Burggraaf, Microstructural development, electrical properties and oxygen permeation of zirconia-palladium composites, *Solid State Ionics.* 76 (1995) 23–28.
- [25] F. Schulze-Küppers, S. Baumann, W. A. Meulenber, D. Stöver, H.P. Buchkremer, Manufacturing and performance of advanced supported Ba<sub>0.5</sub>Sr<sub>0.5</sub>Co<sub>0.8</sub>Fe<sub>0.2</sub>O<sub>3-δ</sub> (BSCF) oxygen transport membranes, *J. Memb. Sci.* 433 (2013) 121–125.
- [26] T. J. Mazanec, T. L. Cable, J. G. Frye, Electrocatalytic cells for chemical reaction, *Solid State Ionics.* 53–56 (1992) 111–118.
- [27] A. L. Shaula, V. V. Kharton, F. M. B. Marques, A. V. Kovalevsky, A. P. Viskup, E. N. Naumovich, Oxygen permeability of mixed-conducting composite membranes: Effects of phase interaction, *J. Solid State Electrochem.* 10 (2006) 28–40.
- [28] J. Kim, Y. S. Lin, Synthesis and oxygen-permeation properties of thin YSZ/Pd composite membranes, *AIChE J.* 46 (2000) 1521–1529.
- [29] C. S. Chen, H. Kruidhof, H. J. M. Bouwmeester, H. Verweij, A.J. Burggraaf, Oxygen permeation through oxygen ion oxide-noble metal dual phase composites, *Solid State Ionics.* 86–88 (1996) 569–572.



- [30] C. S. Chen, H. Kruidhof, H. J. M. Bouwmeester, H. Verweij, A.J. Burggraaf, Thickness dependence of oxygen permeation through erbiastabilized bismuth oxide-silver composites, *Solid State Ionics*. 99 (1997) 215–219.
- [31] K. Wu, S. Xie, G. S. Jiang, W. Liu, C. S. Chen, Oxygen permeation through  $(\text{Bi}_2\text{O}_3)_{0.74}(\text{SrO})_{0.26}$ -Ag (40%) composite, *188* (2001) 189–193.
- [32] E. Capoen, M.C. Steil, G. Nowogrocki, M. Malys, C. Pirovano, A. Löfberg, E. Bordes-Richard, J.C. Boivin, G. Mairesse, R.N. Vannier, Oxygen permeation in bismuth-based materials. Part I: Sintering and oxygen permeation fluxes, *Solid State Ionics*. 177 (2006) 483–488.
- [33] J. Kim, Y.S. Lin, Synthesis and oxygen permeation properties of ceramic-metal dual-phase membranes, *J. Memb. Sci.* 167 (2000) 123–133.
- [34] D. R. Lide, *CRC handbook of chemistry and physics*, CRC press, Boca Raton, FL, USA, 2004.
- [35] H. Luo, H. Jiang, T. Klande, Z. Cao, F. Liang, H. Wang, J. Caro, Novel cobalt-free, noble metal-free oxygen-permeable  $40\text{Pr}_{0.6}\text{Sr}_{0.4}\text{FeO}_{3-\delta}$ - $60\text{Ce}_{0.9}\text{Pr}_{0.1}\text{O}_{2-\delta}$  dual-phase membrane, *Chem. Mater.* 24 (2012) 2148–2154.
- [36] Z. Wang, W. Sun, Z. Zhu, T. Liu, W. Liu, A novel cobalt-free,  $\text{CO}_2$ -stable, and reduction-tolerant dual-phase oxygen-permeable membrane, *ACS Appl. Mater. Interfaces*. 5 (2013) 11038–11043.
- [37] X. Shao, D. Dong, G. Parkinson, C. Z. Li, Improvement of oxygen permeation through microchanneled ceramic membranes, *J. Memb. Sci.* 454 (2014) 444–450.
- [38] T. Chen, H. Zhao, N. Xu, Y. Li, X. Lu, W. Ding, F. Li, Synthesis and oxygen permeation properties of a  $\text{Ce}_{0.8}\text{Sm}_{0.2}\text{O}_{2-\delta}$ - $\text{LaBaCo}_2\text{O}_{5+\delta}$  dual-phase composite membrane, *J. Memb. Sci.* 370 (2011) 158–165.
- [39] K. J. Yoon, O. A. Marina, Highly stable dual-phase  $\text{Y}_{0.8}\text{Ca}_{0.2}\text{Cr}_{0.8}\text{Co}_{0.2}\text{O}_3$ - $\text{Sm}_{0.2}\text{Ce}_{0.8}\text{O}_{1.9}$  ceramic composite membrane for oxygen separation, *J. Memb. Sci.* 499 (2016) 301–306.

- [40] V. V. Kharton, A. V. Kovalevsky, A. P. Viskup, F. M. Figueiredo, A. A. Yaremchenko, E. N. Naumovich, F. M. B. Marques, Oxygen permeability and faradaic efficiency of, *J. Eur. Ceram. Soc.* 21 (2001) 1763–1767.
- [41] J. Xue, Q. Liao, Y. Wei, Z. Li, H. Wang, A CO<sub>2</sub>-tolerance oxygen permeable 60Ce<sub>0.9</sub>Gd<sub>0.1</sub>O<sub>2-δ</sub>-40Ba<sub>0.5</sub>Sr<sub>0.5</sub>Co<sub>0.8</sub>Fe<sub>0.2</sub>O<sub>3-δ</sub> dual phase membrane, *J. Memb. Sci.* 443 (2013) 124–130.
- [42] W. He, H. Huang, J. fen Gao, L. Winnubst, C. sheng Chen, Phase-inversion tape casting and oxygen permeation properties of supported ceramic membranes, *J. Memb. Sci.* 452 (2014) 294–299.
- [43] S. Omar, J. C. Nino, Consistency in the chemical expansion of fluorites: a thermal revision of the doped ceria, *Acta Mater.* 61 (2013) 5406–5413.
- [44] S. R. Bishop, K. L. Duncan, E. D. Wachsman, Surface and bulk oxygen non-stoichiometry and bulk chemical expansion in gadolinium-doped cerium oxide, *Acta Mater.* 57 (2009) 3596–3605.
- [45] A. A. Yaremchenko, S. M. Mikhalev, E. S. Kravchenko, J. R. Frade, Thermochemical expansion of mixed-conducting (Ba,Sr)Co<sub>0.8</sub>Fe<sub>0.2</sub>O<sub>3-δ</sub> ceramics, *J. Eur. Ceram. Soc.* 34 (2014) 703–715.
- [46] S. McIntosh, J. F. Vente, W. G. Haije, D. H. A. Blank, H. J. M. Bouwmeester, Phase stability and oxygen non-stoichiometry of SrCo<sub>0.8</sub>Fe<sub>0.2</sub>O<sub>3-δ</sub> measured by in situ neutron diffraction, *Solid State Ionics.* 177 (2006) 833–842.
- [47] V. V. Kharton, A. P. Viskup, A. V. Kovalevsky, J. R. Jurado, E. N. Naumovich, A. A. Vecher, J. R. Frade, Oxygen ionic conductivity of Ti-containing strontium ferrite, *Solid State Ionics.* 133 (2000) 57–65.
- [48] H. Wang, C. Tablet, A. Feldhoff, J. Caro, Investigation of phase structure, sintering, and permeability of perovskite-type Ba<sub>0.5</sub>Sr<sub>0.5</sub>Co<sub>0.8</sub>Fe<sub>0.2</sub>O<sub>3-δ</sub> membranes, *J. Memb. Sci.* 262 (2005) 20–26.

- [49] M. B. Choi, S. Y. Jeon, H. N. Im, E. D. Wachsman, S. J. Song, Oxygen exchange kinetics and ionic conductivity from chemical expansion relaxation of mixed conducting  $\text{Ba}_{0.5}\text{Sr}_{0.5}\text{Co}_{0.8}\text{Fe}_{0.2}\text{O}_{3-\delta}$ , *J. Electrochem. Soc.* 159 (2011) P23–P28.
- [50] A. Fossdal, M. Menon, K. Wiik, M. Einarsrud, T. Grande, Crystal structure and thermal expansion of  $\text{La}_{1-x}\text{Sr}_x\text{FeO}_{3-\delta}$  *Materials*, 1958 (2004) 1952–1958.
- [51] H. L. Lein, K. Wiik, T. Grande, Thermal and chemical expansion of mixed conducting  $\text{La}_{0.5}\text{Sr}_{0.5}\text{Fe}_{1-x}\text{Co}_x\text{O}_{3-\delta}$  materials, *Solid State Ionics*. 177 (2006) 1795–1798.
- [52] H. J. M. Bouwmeester, Dense ceramic membranes for methane conversion, *Catal. Today*. 82 (2003) 141–150.
- [53] H. J. M. Bouwmeester, A. J. Burggraaf, Chapter 10 Dense ceramic membranes for oxygen separation, *Membr. Sci. Technol.* 4 (1996) 435–528.
- [54] U. Balachandran, J. T. Dusek, P. S. Maiya, B. Ma, R. L. Mieville, M. S. Kleefisch, C. A. Udovich, Ceramic membrane reactor for converting methane to syngas, *Catal. Today*. 36 (1997) 265–272.
- [55] B. C. H. Steele, Oxygen ion conductors and their technological applications, *Mater. Sci. Eng. B*. 13 (1992) 79–87.
- [56] S. Švarcová, K. Wiik, J. Tolchard, H. J. M. Bouwmeester, T. Grande, Structural instability of cubic perovskite  $\text{Ba}_x\text{Sr}_{1-x}\text{Co}_{1-y}\text{Fe}_y\text{O}_{3-\delta}$ , *Solid State Ionics*. 178 (2008) 1787–1791.
- [57] F. Prado, N. Grunbaum, A. Caneiro, A. Manthiram, Effect of  $\text{La}^{3+}$  doping on the perovskite-to-brownmillerite transformation in  $\text{Sr}_{1-x}\text{La}_x\text{Co}_{0.8}\text{Fe}_{0.2}\text{O}_{3-\delta}$  ( $0 \leq x \leq 0.4$ ), *Solid State Ionics*. 167 (2004) 147–154.
- [58] W. Yang, H. Wang, X. Zhu, L. Lin, Development and application of oxygen permeable membrane in selective oxidation of light alkanes, *Top. Catal.* 35 (2005) 155–167.
- [59] V. V. Kharton, A. P. Viskup, A. A. Yaremchenko, P. F. Kerko, E. N. Naumovich, A. V. Kovalevsky, Ionic transport in  $\text{SrCo}_{0.85}\text{Ti}_{0.15}\text{O}_{3-\delta}$  ceramics at high oxygen pressures, *Mater. Res. Bull.* 34 (1999) 1921–1928.

- [60] O. Ravkina, T. Klande, A. Feldhoff, G. Wilhelm, L. Universit, Investigation of Zr-doped BSCF perovskite membrane for oxygen separation in the intermediate temperature range, *J. Solid State Chem.* 201 (2013) 101–106.
- [61] Z. Shao, W. Yang, Y. Cong, H. Dong, J. Tong, G. Xiong, Investigation of the permeation behavior and stability of a  $\text{Ba}_{0.5}\text{Sr}_{0.5}\text{Co}_{0.8}\text{Fe}_{0.2}\text{O}_{(3-\delta)}$  oxygen membrane, *J. Memb. Sci.* 172 (2000) 177–188.
- [62] L. S. Unger, R. Ruhl, M. Meffert, C. Niedrig, W. Menesklou, S. F. Wagner, D. Gerthsen, H. J. M. Bouwmeester, E. Ivers-Tiffée, Yttrium doping of  $\text{Ba}_{0.5}\text{Sr}_{0.5}\text{Co}_{0.8}\text{Fe}_{0.2}\text{O}_{3-\delta}$  part II: Influence on oxygen transport and phase stability, *J. Eur. Ceram. Soc.* 38 (2018) 2388–2395.
- [63] F. Liang, K. Partovi, H. Jiang, H. Luo, J. Caro, B-site La-doped  $\text{BaFe}_{0.95-x}\text{La}_x\text{Zr}_{0.05}\text{O}_{3-\delta}$  perovskite-type membranes for oxygen separation, *J. Mater. Chem. A.* 1 (2013) 746–751.
- [64] X. Tan, L. Shi, G. Hao, B. Meng, S. Liu,  $\text{La}_{0.7}\text{Sr}_{0.3}\text{FeO}_{3-\alpha}$  perovskite hollow fiber membranes for oxygen permeation and methane conversion, *Sep. Purif. Technol.* 96 (2012) 89–97.
- [65] M. N. Tahir, L. Gorgishvili, J. Li, T. Gorelik, U. Kolb, L. Nasdala, W. Tremel, Facile synthesis and characterization of monocrystalline cubic  $\text{ZrO}_2$  nanoparticles, *Solid State Sci.* 9 (2007) 1105–1109.
- [66] H. L. Lein, K. Wiik, T. Grande, Kinetic demixing and decomposition of oxygen permeable membranes, *Solid State Ionics.* 177 (2006) 1587–1590.
- [67] X. Zhu, W. Yang, *Mixed conducting ceramic membranes, Green Chemistry and Sustainable Technology*, 2017.
- [68] M. Arnold, H. Wang, A. Feldhoff, Influence of  $\text{CO}_2$  on the oxygen permeation performance and the microstructure of perovskite-type  $(\text{Ba}_{0.5}\text{Sr}_{0.5})(\text{Co}_{0.8}\text{Fe}_{0.2})\text{O}_{3-\delta}$  membranes, *J. Memb. Sci.* 293 (2007) 44–52.
- [69] J. Tong, W. Yang, B. Zhu, R. Cai, Investigation of ideal zirconium-doped perovskite-type

- ceramic membrane materials for oxygen separation, *J. Memb. Sci.* 203 (2002) 175–189.
- [70] H. Cheng, L. Luo, W. Yao, X. Lu, X. Zou, Z. Zhou, Novel cobalt-free CO<sub>2</sub>-tolerant dual-phase membranes of Ce<sub>0.8</sub>Sm<sub>0.2</sub>O<sub>2-δ</sub>-Ba<sub>0.95</sub>La<sub>0.05</sub>Fe<sub>1-x</sub>Zr<sub>x</sub>O<sub>3-δ</sub> for oxygen separation, *J. Memb. Sci.* 492 (2015) 220–229.
- [71] K. Efimov, T. Klande, N. Juditzki, A. Feldhoff, Ca-containing CO<sub>2</sub>-tolerant perovskite materials for oxygen separation, *J. Memb. Sci.* 389 (2012) 205–215.
- [72] K. Li, H. Zhao, Y. Lu, Y. Ma, Z. Du, Z. Zhang, High CO<sub>2</sub> tolerance oxygen permeation membranes BaFe<sub>0.95-x</sub>Ca<sub>0.05</sub>Ti<sub>x</sub>O<sub>3-δ</sub>, *J. Memb. Sci.* 550 (2018) 302–312.
- [73] Y. Kathiraser, Z. Wang, N.T. Yang, S. Zahid, S. Kawi, Oxygen permeation and stability study of La<sub>0.6</sub>Sr<sub>0.4</sub>Co<sub>0.8</sub>Ga<sub>0.2</sub>O<sub>3-δ</sub> (LSCG) hollow fiber membrane with exposure to CO<sub>2</sub>, CH<sub>4</sub> and He, *J. Memb. Sci.* 427 (2013) 240–249.
- [74] A. Waindich, A. Möbius, M. Müller, Corrosion of Ba<sub>1-x</sub>Sr<sub>x</sub>Co<sub>1-y</sub>Fe<sub>y</sub>O<sub>3-δ</sub> and La<sub>0.3</sub>Ba<sub>0.7</sub>Co<sub>0.2</sub>Fe<sub>0.8</sub>O<sub>3-δ</sub> materials for oxygen separating membranes under oxycoal conditions, *J. Memb. Sci.* 337 (2009) 182–187.
- [75] Q. Zeng, Y. bo Zuo, C. gang Fan, C. sheng Chen, CO<sub>2</sub>-tolerant oxygen separation membranes targeting CO<sub>2</sub> capture application, *J. Memb. Sci.* 335 (2009) 140–144.
- [76] W. Chen, C. S. Chen, L. Winnubst, Ta-doped SrCo<sub>0.8</sub>Fe<sub>0.2</sub>O<sub>3-δ</sub> membranes: Phase stability and oxygen permeation in CO<sub>2</sub> atmosphere, *Solid State Ionics.* 196 (2011) 30–33.
- [77] J. Yi, T. E. Weirich, M. Schroeder, CO<sub>2</sub> corrosion and recovery of perovskite-type BaCo<sub>1-x-y</sub>Fe<sub>x</sub>Nb<sub>y</sub>O<sub>3-δ</sub> membranes, *J. Memb. Sci.* 437 (2013) 49–56.
- [78] M. P. Popov, S. F. Bychkov, A. P. Nemudry, Modification of mixed conducting Ba<sub>0.5</sub>Sr<sub>0.5</sub>Co<sub>0.8</sub>Fe<sub>0.2</sub>O<sub>3-δ</sub> by partial substitution of cobalt with tungsten, *Russ. J. Electrochem.* 52 (2016) 648–654.
- [79] E. V. Shubnikova, O. A. Bragina, A. P. Nemudry, Mixed conducting molybdenum doped BSCF materials, *J. Ind. Eng. Chem.* 59 (2018) 242–250.
- [80] S. J. Khatib, S. Yun, S. T. Oyama, Sulfur resistant Pd and Pd alloy membranes by

- phosphidation, *J. Memb. Sci.* 455 (2014) 283–293.
- [81] J. Gao, L. Li, Z. Yin, J. Zhang, S. Lu, X. Tan, Poisoning effect of SO<sub>2</sub> on the oxygen permeation behavior of La<sub>0.6</sub>Sr<sub>0.4</sub>Co<sub>0.2</sub>Fe<sub>0.8</sub>O<sub>3-δ</sub> perovskite hollow fiber membranes, *J. Memb. Sci.* 455 (2014) 341–348.
- [82] Y. Alqaheem, A. Thursfield, G. Zhang, I. S. Metcalfe, The impact of sulfur contamination on the performance of La<sub>0.6</sub>Sr<sub>0.4</sub>Co<sub>0.2</sub>Fe<sub>0.8</sub>O<sub>3-δ</sub> oxygen transport membranes, *Solid State Ionics*. 262 (2014) 262–265.
- [83] M. Balaguer, J. García-Fayos, C. Solís, J.M. Serra, Fast oxygen separation through SO<sub>2</sub>- and CO<sub>2</sub>-stable dual-phase membrane based on NiFe<sub>2</sub>O<sub>4</sub>-Ce<sub>0.8</sub>Tb<sub>0.2</sub>O<sub>2-δ</sub>, *Chem. Mater.* 25 (2013) 4986–4993.
- [84] S. Cheng, M. Sjøgaard, L. Han, W. Zhang, M. Chen, A. Kaiser, P. V. Hendriksen, A novel CO<sub>2</sub>- and SO<sub>2</sub>-tolerant dual phase composite membrane for oxygen separation, *Chem. Commun.* 51 (2015) 7140–7143.
- [85] J. Garcia-Fayos, M. Balaguer, S. Baumann, J. M. Serra, Dual-phase membrane based on LaCo<sub>0.2</sub>Ni<sub>0.4</sub>Fe<sub>0.4</sub>O<sub>3-x</sub>-Ce<sub>0.8</sub>Gd<sub>0.2</sub>O<sub>2-x</sub> composition for oxygen permeation under CO<sub>2</sub>/SO<sub>2</sub>-rich gas environments, *J. Memb. Sci.* 548 (2018) 117–124.
- [86] C. Wu, J. Zhou, X. Tang, W. Luo, Y. Zhang, W. Ding, C. Sun, The migration behavior of sulfur impurity contained in the dual-phase membrane of Ce<sub>0.9</sub>Gd<sub>0.1</sub>O<sub>2-δ</sub>-SrCo<sub>0.8</sub>Fe<sub>0.1</sub>Nb<sub>0.1</sub>O<sub>3-δ</sub> under CO<sub>2</sub> atmosphere, *J. Memb. Sci.* 511 (2016) 162–169.
- [87] D. K. Ramachandran, M. Sjøgaard, F. Clemens, J. Gurauskis, A. Kaiser, Fabrication and performance of a tubular ceria based oxygen transport membrane on a low cost MgO support, *Sep. Purif. Technol.* 147 (2015) 422–430.
- [88] S. Ovtar, J. Gurauskis, A. Bjørnetun Haugen, C. Chatzichristodoulou, A. Kaiser, P. V. Hendriksen, Oxygen transport properties of tubular Ce<sub>0.9</sub>Gd<sub>0.1</sub>O<sub>1.95</sub>-La<sub>0.6</sub>Sr<sub>0.4</sub>FeO<sub>3-δ</sub> composite asymmetric oxygen permeation membranes supported on magnesium oxide, *J. Memb. Sci.* 523 (2017) 576–587.

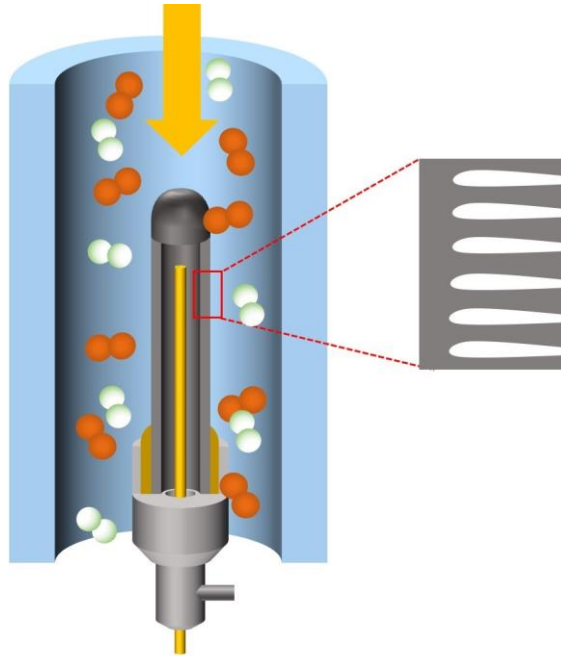
- [89] X. Yin, L. Hong, Z. L. Liu, Development of oxygen transport membrane  $\text{La}_{0.2}\text{Sr}_{0.8}\text{CoO}_{3-\delta}/\text{Ce}_{0.8}\text{Gd}_{0.2}\text{O}_{2-\delta}$  on the tubular  $\text{CeO}_2$  support, *Appl. Catal. A Gen.* 300 (2006) 75–84.
- [90] V. Sadykov, V. Zarubina, S. Pavlova, T. Krieger, G. Alikina, A. Lukashevich, V. Muzykantov, E. Sadovskaya, N. Mezentseva, E. Zevak, V. Belyaev, O. Smorygo, Design of asymmetric multilayer membranes based on mixed ionic-electronic conducting composites supported on Ni-Al foam substrate, *Catal. Today.* 156 (2010) 173–180.
- [91] E. S. C. Fan, O. Kesler, Deposition of lanthanum strontium cobalt ferrite (LSCF) using suspension plasma spraying for oxygen transport membrane applications, *J. Therm. Spray Technol.* 24 (2015) 1081–1092.
- [92] S. Niu, K. Zhou, L. Xu, C. Deng, M. Liu, J. Mao, A comparative study of  $\text{La}_{0.6}\text{Sr}_{0.4}\text{Co}_{0.2}\text{Fe}_{0.8}\text{O}_{3-\delta}$  oxygen transport membranes deposited on porous metal supports prepared by supersonic air-gas plasma spraying (SAPS) and low pressure plasma spraying-physical vapor deposition (PS-PVD), *Surf. Coatings Technol.* 307 (2016) 963–970.
- [93] S. Baumann, J. M. Serra, M. P. Lobera, S. Escolástico, F. Schulze-Küppers, W. A. Meulenber, Ultrahigh oxygen permeation flux through supported  $\text{Ba}_{0.5}\text{Sr}_{0.5}\text{Co}_{0.8}\text{Fe}_{0.2}\text{O}_{3-\delta}$  membranes, *J. Memb. Sci.* 377 (2011) 198–205.
- [94] Z. Cao, X. Zhu, W. Li, B. Xu, L. Yang, W. Yang, Asymmetric dual-phase membranes prepared via tape-casting and co-lamination for oxygen permeation, *Mater. Lett.* 147 (2015) 88–91.
- [95] X. Meng, W. Ding, R. Jin, H. Wang, Y. Gai, F. Ji, Y. Ge, D. Xie, Two-step fabrication of  $\text{BaCo}_{0.7}\text{Fe}_{0.2}\text{Nb}_{0.1}\text{O}_{3-\delta}$  asymmetric oxygen permeable membrane by dip coating, *J. Memb. Sci.* 450 (2014) 291–298.
- [96] Y. Zhang, R.H. Yuan, Z.Y. He, J.F. Gao, C.S. Chen, Phase inversion tape casting and oxygen permeation properties of supported planar  $\text{Zr}_{0.84}\text{Y}_{0.16}\text{O}_{1.92}\text{-La}_{0.8}\text{Sr}_{0.2}\text{Cr}_{0.5}\text{Fe}_{0.5}\text{O}_{3-\delta}$  composite membrane, *Solid State Ionics.* 288 (2016) 342–346.
- [97] S. Cheng, H. Huang, S. Ovtar, S. B. Simonsen, M. Chen, W. Zhang, M. Søggaard, A. Kaiser,

- P. V. Hendriksen, C. Chen, High-performance microchanneled asymmetric  $\text{Gd}_{0.1}\text{Ce}_{0.9}\text{O}_{1.95-\delta}\text{-La}_{0.6}\text{Sr}_{0.4}\text{FeO}_{3-\delta}$ -based membranes for oxygen separation, *ACS Appl. Mater. Interfaces*. 8 (2016) 4548–4560.
- [98] T. Liu, W. Zhao, Y. Wang, Robust freeze-cast bilayer dual-phase oxygen transport membrane targeting chemical reactor application, *ACS Appl. Nano Mater.* 1 (2018) 3774–3778.
- [99] Q. Jiang, S. Faraji, D. A. Slade, S. M. Stagg-Williams, A review of mixed ionic and electronic conducting ceramic membranes as oxygen sources for high-temperature reactors, 1st ed., Elsevier BV., 2011.
- [100] E. Crepaldi, J. Soler-Illia, A. Bouchara, D. Grosso, D. Durand, C. Sanchez, Controlled formation of highly ordered cubic and hexagonal mesoporous nanocrystalline yttria–zirconia and ceria–zirconia thin films exhibiting high thermal stability, *Angew. Chemie*. 0 (2003) 361–365.
- [101] A. Corma, P. Atienzar, H. García, J. Y. Chane-Ching, Hierarchically mesostructured doped  $\text{CeO}_2$  with potential for solar-cell use, *Nat. Mater.* 3 (2004) 394–397.
- [102] J. M. Serra, S. Uhlenbruck, W. A. Meulenber, H. P. Buchkremer, D. Stöver, Nanostructuring of solid oxide fuel cells cathodes, *Top. Catal.* 40 (2006) 123–131.
- [103] J. Gorauskis, F. Lohne, K. Wiik,  $\text{La}_{0.2}\text{Sr}_{0.8}\text{Fe}_{0.8}\text{Ta}_{0.2}\text{O}_{3-\delta}$  based thin film membranes with surface modification for oxygen production, *Solid State Ionics*. 225 (2012) 703–706.
- [104] J. P. Kim, J. H. Park, E. Magnone, Y. Lee, Significant improvement of the oxygen permeation flux of tubular  $\text{Ba}_{0.5}\text{Sr}_{0.5}\text{Co}_{0.8}\text{Fe}_{0.2}\text{O}_{3-\delta}$  membranes covered by a thin  $\text{La}_{0.6}\text{Sr}_{0.4}\text{Ti}_{0.3}\text{Fe}_{0.7}\text{O}_{3-\delta}$  layer, *Mater. Lett.* 65 (2011) 2168–2170.
- [105] X. Zhu, H. Liu, Q. Li, Y. Cong, W. Yang, Unsteady-state permeation and surface exchange of dual-phase membranes, *Solid State Ionics*. 185 (2011) 27–31.
- [106] Y. Hayamizu, M. Kato, H. Takamura, Effects of surface modification on the oxygen permeation of  $\text{Ba}_{0.5}\text{Sr}_{0.5}\text{Co}_{0.8}\text{Fe}_{0.2}\text{O}_{3-\delta}$  membrane, *J. Memb. Sci.* 462 (2014) 147–152.



- [107] T. Liu, Y. Chen, S. Fang, L. Lei, Y. Wang, C. Ren, F. Chen, A dual-phase bilayer oxygen permeable membrane with hierarchically porous structure fabricated by freeze-drying tape-casting method, *J. Memb. Sci.* 520 (2016) 354–363.

# Chapter 3 Dead-end CGO-BSCF membranes fabricated with modified phase-inversion casting method



*A modified phase inversion casting method was employed for the fabrication of dead-end tubular membranes, applying dual-phase composites of CGO-BSCF as the membrane material. Performances of the membranes were optimised by adjusting the processing conditions and the CGO:BSCF ratio.*

*This chapter is based on the paper: Performance control of dead-end tubular membranes fabricated with a modified phase inversion casting method. *Ceramics International*, 2020, 46(14): 22429-22437.*

### 3.1. Introduction

Compared with planar discs and hollow fibres, tubular membranes are preferred for industrial processes especially when integrated in membrane reactors. For lab tests or practical applications, it is necessary to seal the tubular membrane with a gas-tight connection to the permeation cell/reactor. A smaller sealing area can reduce the probability of leakage from the joining parts. To simplify the sealing process and to reduce the stress caused by the thermal expansion difference between the connection part and the membrane, it is preferred to produce dead-end membranes so that only one side of the membrane tubes needs to be sealed.

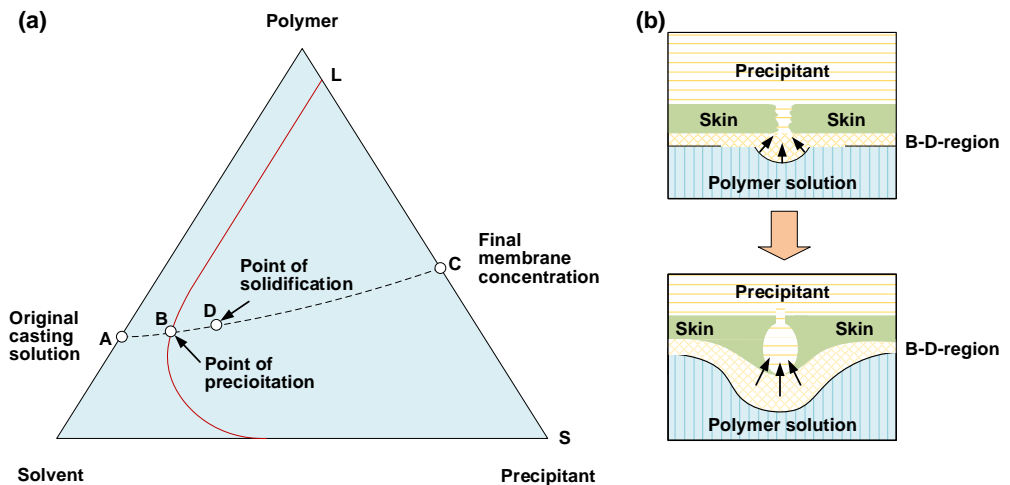


**Figure 3.1.** (a) Phase diagram for the precipitation process and (b) schematic presentation for the formation process of finger-like channels during phase inversion [1].

In this chapter, dead-end tubular membranes were fabricated with a novel phase-inversion casting method. With this method the dead-end membrane shape is formed in a single step. The phase inversion process was initially developed for the polymer membrane fabrication. This process starts with adding certain

polymers into a solvent forming a polymer solution. The solution is then cast into a desired shape and introduced into a precipitant (e.g. water) bath for phase inversion. In the precipitant-bath, the solvent in the polymer solution exchanges with the precipitant, and since the dissolved polymer exhibits low solubility in the precipitant, the system solidifies due to polymer precipitation. Phenomenon for the solidification process of the membrane in the precipitant-bath can be explained by the phase diagram (Figure 3.1a). The three corners of the diagram represent the precipitant, solvent and polymer respectively, and the triangle can be divided into two regions, namely a single-phase region and a dual-phase region. In the single-phase region everything is miscible, while the system separates to a polymer-lean phase and a polymer-rich phase in the dual-phase region [1]. The phase is a liquid with low viscosity when the polymer concentration is low. However, the viscosity increases rapidly with the polymer concentration improved, and the system is regarded as a solid when the polymer reaches a certain concentration. In the phase diagram, point A is the initial solution, C represents the membrane system obtained finally, and the path from A to C is the membrane formation process. At point C, two phases are considered to be equilibrium, which are a polymer-rich phase (point S) forming the membrane structure and a polymer-lean phase (point L) filling the pores of the membrane. Point B on the path is the start point for the polymer precipitation. As the polymer-rich phase lose more solvent, the viscosity of which increased and then at point D the phase is considered as solid.

Finger-like channels can be formed inside the membrane due to the fast phase inversion process. The formation of the channels can be divided into two stages [1], including the initiation of the channels and the channel growth (Figure 3.1b). At the moment when the solution brought into contact with the precipitant, a thin skin layer of precipitated polymer was formed. The skin layer protects the solution underneath from the direct exposure to the precipitant. As a result,

sponge structure is formed due to the slowed-down precipitation. However, the syneresis cause a shrinkage stress on the skin layer. When the polymer creep relaxation cannot relieve the stress, the skin would fracture, which means the channels are initiated. Afterwards, the channels grow with draining the mixture at the precipitation front.

In recent years the phase inversion technique has found its application in the formation of asymmetric ceramic membranes. Ceramic-based slurries are prepared by adding ceramic powders into the polymer solution. The green membranes, which are formed by the ceramic powders together with the polymer precipitated during the phase inversion, are densified after sintering process. Although many researchers reported the fabrication of ceramic oxygen transport membranes with phase inversion technique, most works were focused on flat membranes [2–5] or hollow fibres [6–10]. Application of this technique to the fabrication of tubular membranes and especially dead-end tubes is rather limited. The processing parameters of the phase-inversion-based membrane fabrication process has great impact on the microstructure and performance of the dead-end tubes. For instance, the micro-channelled structure favours slurries with low viscosity, while high fluidity of the slurries would bring difficulties in the formation of a dead-end membrane shape. Thus, selection of optimised processing parameters to obtain highly performing dead-end membrane tubes is an area of great interest.

Some of the perovskite materials, typically BSCF, shows a very high oxygen permeability, but low stability in a CO<sub>2</sub>-containing atmosphere, so the perovskites were mixed with some CO<sub>2</sub>-stable material to form the dual-phase membranes [11–14]. In this chapter, the CGO-BSCF composites are applied for the preparation of the dead-end membrane tubes. The effect of the ceramic loading in the casting slurry on the micro-channel length in the dead-end tubular

membrane was investigated to obtain reduced resistance for oxygen permeation. Dual-phase membranes with different CGO:BSCF ratios were prepared, and the performance of these membranes were compared in detail based on their oxygen permeation flux, CO<sub>2</sub> resistance and mechanical strength.

## 3.2. Experimental procedure

### 3.2.1. Manufacturing of the dead-end membranes by phase-inversion casting method

The dual-phase membranes of CGO/BSCF composites were fabricated using commercially available powders. The CGO powder provided by Ningbo Sofcman Energy was applied as the oxygen-ionic conductor after milling with a planetary ball mill (Pulverisette 6, Fritsch) for 3 h, while the BSCF powder (Cerpotech) was used as received for the formation of the electronic conductive phase.

**Table 3.1.** Ceramic loadings in the slurries, BSCF concentrations and sintering temperatures of the dead-end membranes under study.

Membrane	Ceramic loading, (CGO+BSCF)/ (CGO+BSCF+NMP), wt%	BSCF concentration, BSCF/ (CGO+BSCF), wt%	Sintering T, °C
CGO/BSCF40-I	73	40	1170
CGO/BSCF40-II	71	40	1170
CGO/BSCF40-III	69	40	1170
CGO/BSCF40-III	67	40	1170
CGO/BSCF50	69	50	1160
CGO/BSCF60	69	60	1150
CGO	69	0	1350
BSCF	69	100	1130

For preparation of the green dead-end tubes (i.e. before calcination), a starting polymer solution was prepared by adding 5 g of polyethersulfone (PES, Veradel

3000P, Solvay Advanced Polymers) and 1 g of polyvinylpyrrolidone (PVP, Sigma-Aldrich) into 20 g of 1-methyl-2-pyrrolidone (NMP, 99.5%, Sigma-Aldrich), which were mixed in a centrifugal mixer (ARE-250, Thinky) for 20 min to ensure that the polymers were fully dissolved in the solvent. Then the ceramic powder for each phase was added to the polymer solution in a predetermined ratio and mixed for 90 min, followed by a defoaming procedure of 30 min in the same mixer to remove the bubbles that may influence gas tightness and mechanical strength of the formed membranes. A mixer rotational speed of 1900 rpm (after optimization) was used for both the mixing and defoaming procedures. The slurry compositions and relative abbreviations of the membranes are listed in Table 3.1.

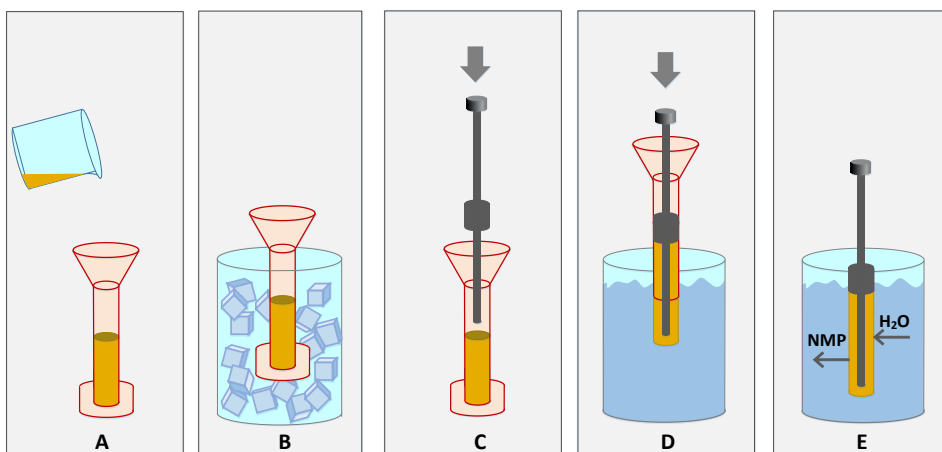


**Figure 3.2.** Schematic representation of the dead-end membrane manufacturing process.

The defoamed slurries were poured into a simple cylindrical casting device to perform the phase-inversion casting process (Figure 3.2). A screw cap is connected to the cylindrical mould to prevent outflow of the casting pastes. Good slurry fluidity and a slow pouring speed are required to avoid air trapped in the mould (A). The casting device which was filled with the ceramic slurry was kept in ice for 30 min to reduce the slurry fluidity, because insufficient viscosity of the



slurry would give difficulties to the formation of dead-end membrane shape (B). Subsequently, the cap of the casting mould was taken off and a piston was used to push the slurries out into water for the phase inversion process (C-D). After 12 h in the water bath (E), the solidified green bodies of the membranes were removed from the piston and dried for 48 h at room temperature. The green dead-end membrane tubes were sintered at high temperature for 4 h to obtain gas-tight membranes with sufficient mechanical strength. The sintering temperature was varied for membranes with different components (Table 3.1); these temperatures have been optimized in a separate study (data not reported here). The samples were heated to the sintering temperature with a slow rate of 30 °C/h to void nonuniform heating and breakage of the membranes inside the oven. Finally, a cooling rate of 60 °C/h was used to cool the membranes back to room temperature.

### ***3.2.2. Characterisation of the dead-end membranes***

The morphology of the membrane tubes was studied by scanning electron microscopy (SEM) using a Quanta 3D FEG, which operated at a voltage of 5 kV with the secondary-electron mode. The element distribution on the cross section of the membranes was obtained at an excitation voltage of 15 kV with the EDS mapping coupled to another SEM (Phenom ProX). A rheometer (Physica MCR 301) was used to study the rheological behavior of the casting slurries. A three-point bending test was performed to measure the mechanical strength of the dense membranes with the assistance of the Zwick Zmart Pro universal testing machine equipped with a 10 kN load cell. The span length was fixed at 30 mm while a crosshead speed of 1 mm/min was used during the testing process. The specific surface area of the membranes with different channel lengths was obtained from the BET nitrogen adsorption isotherm using TriStar II, Micromeritics. The adsorption of CO<sub>2</sub> by the CGO/BSCF40-III membrane samples was studied by TGA experiments at three operation temperatures (850 °C, 900 °C and 950 °C).

The in-house developed TGA setup is described by Coenen et al. [15]. The TGA test can be divided into three sections, with pure helium fed into the quartz reactor in the first and last stages for 12 h and CO<sub>2</sub> as the fed gas in the middle stage for 24 h. Flow rate of the feed gas was fixed at 500 mL/min. Phase structure of the membrane samples was determined by XRD (Rigaku MiniFlex 600).

### 3.2.3. Oxygen permeation measurement

A helium setup was used to examine the gas tightness of the sintered membranes and only gas-tight membranes were used in the permeation test. The oxygen permeation fluxes through the membranes were tested with a high-temperature experimental setup (Figure 3.3).

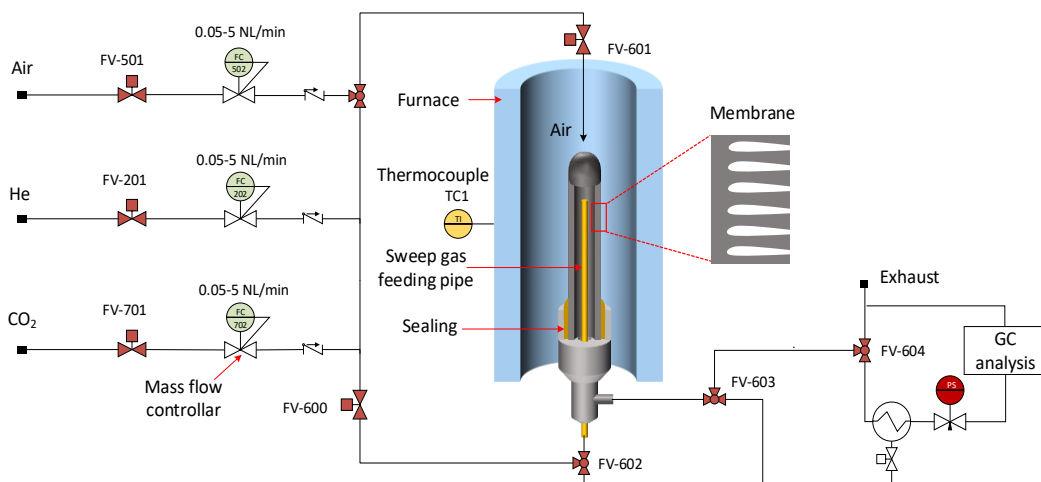


**Figure 3.3.** Simplified scheme of the experimental system used for oxygen permeation.

An Ag-CuO braze paste was used to seal the open-end side of the membrane to a vertically positioned tube of Fe-Cr alloy at 1020 °C for 30 min (via reactive air brazing). A rate of 60 °C/h was used to heat the permeation cell to 1020 °C, which

was then cooled down to 825 °C with the same speed for the permeation test. The oxygen permeation flux was measured in the temperature range of 825-950 °C. Several digital mass flow controllers were used for delivering the gas mixtures to the permeation cell after calibration with a film flow meter (STEC SF, Horiba). Helium/CO<sub>2</sub> mixtures were fed as the sweep gas inside the membrane tube while air was used as feed gas. The concentration of the permeate side was detected with a micro-GC (Varian, CP-4900), while the flowrate was measured by the film flow meter. The leakage resulted from the imperfect sealing, which was always less than 2% of the flux of oxygen for each membrane, was subtracted during the calculation of the permeation flux:

$$J_{\text{O}_2} (\text{mL}/\text{min} \cdot \text{cm}^2) = (C_{\text{O}_2} - C_{\text{N}_2} \times 0.21 / 0.79 \times \sqrt{28 / 32}) \times f / S \quad (1)$$

where  $C_{\text{O}_2}$  and  $C_{\text{N}_2}$  are the calculated concentrations of oxygen and nitrogen from the GC,  $f$  (mL/min) is the outlet flowrate measured from the sweep side, and  $S$  (cm<sup>2</sup>) is the area of the dead-end membrane.

### 3.3. Results and discussion

#### 3.3.1. Oxygen permeation and chemical stability of the CGO-BSCF membrane

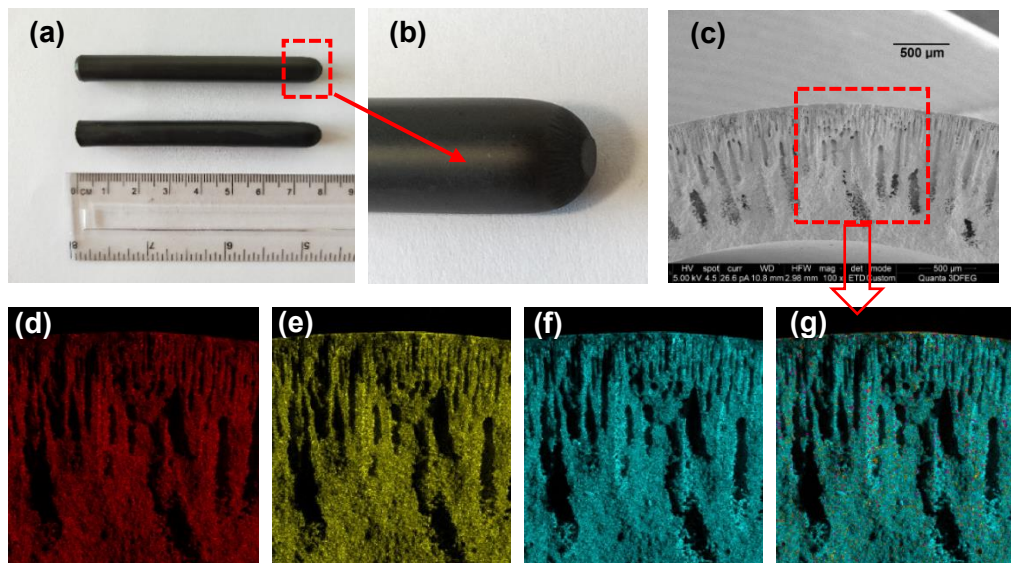


**Figure 3.4.** (a, b) Photographs; (c) SEM image of the cross section; Element distribution: (d) Iron mapping; (e) Barium mapping; (f) Cerium mapping; (g) Combined mapping of the CGO/BSCF40-III membrane.

The dead-end CGO-BSCF dual-phase membrane tubes of ~8 mm outer diameter and ~1.2 mm thickness were successfully prepared with the phase inversion casting method (Figure 3.4a, b). The length of the membranes can be tailored by adjusting size of the casting mould. A SEM micrograph of the overall cross section of membrane CGO/BSCF40-III is given in Figure 3.4c. The membrane tube showed a clear asymmetric microstructure consisting of a membrane layer and a support layer with large finger-like micro-channels. The channels initiate from the outer surface and extended into the bulk of the membrane. The diameters of the channels near the membrane surface were less than 10 μm, which merged

into larger ones in the bulk. The internal membrane layer was found to be free of defects and connected holes which might influence the selectivity of the membranes. Figure 3.4d-g present the element distributions over the cross section of the CGO/BSCF40-III membrane. A homogeneous distribution was observed for each element, suggesting a good mixing of the two phases, and it can be seen from Figure 3.4g that the distribution of Ce in the dual-phase membrane was much higher than the other elements, owing to the lower concentration of BSCF compared with CGO.

The oxygen permeation flux through the CGO/BSCF40-III membrane was measured as a function of the sweep gas (helium) flowrate and temperature. Each data set was collected when a steady state was reached for the oxygen permeation and the results are summarized in Figure 3.5. It has been generally accepted that higher surface exchange and bulk diffusion rate, which means higher permeability of oxygen, can be obtained by increasing the operating temperature; besides, an increase in the sweep gas flow rate reduces the oxygen partial pressure on sweep side of the membrane, which results in a higher oxygen permeation flux because of the increased driving force. Similar trends can be observed for the CGO-BSCF dual phase membrane in Figure 3.5a. It is noteworthy that the Arrhenius plots in Figure 3.5b exhibit constant slopes, which indicates constant activation energies of the oxygen permeation throughout the investigated temperature range, and a close correspondence was observed for the activation energies at different helium flow rates. Constant activation energy is one of the key factors that suggests good phase stability of the membranes during the test period [16,17].

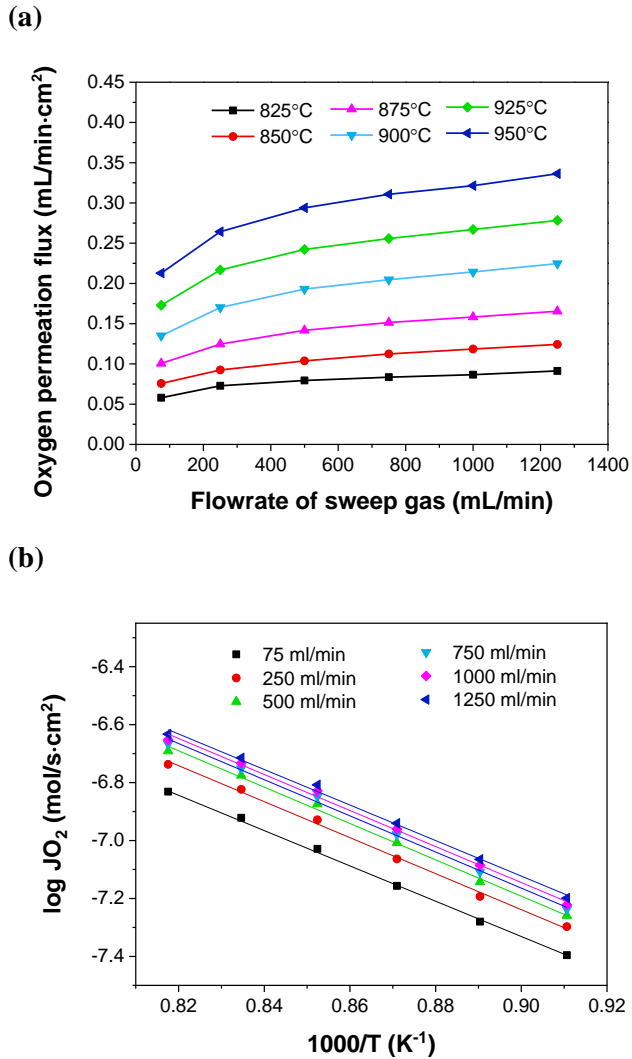


**Figure 3.5.** (a) Helium flowrate dependence of oxygen permeation fluxes through the CGO/BSCF40-III membrane at different temperatures; (b) Arrhenius plots of oxygen fluxes through the CGO/BSCF40-III dual-phase membrane.

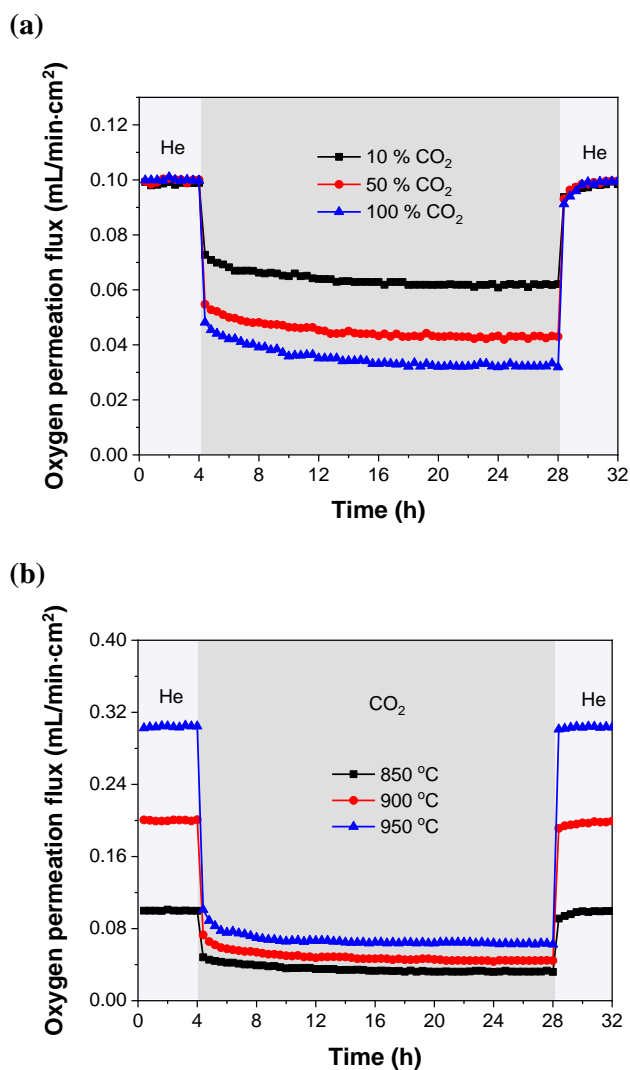


**Figure 3.6.** Stability test of the CGO/BSCF40-III membrane with (a) sweep gases of different CO<sub>2</sub> concentrations and (b) pure CO<sub>2</sub> as sweep gas at different operation temperatures.

The chemical stability of the CGO/BSCF40-III membrane was investigated under an oxygen partial pressure gradient with pure helium, CO<sub>2</sub> or a mixture of the two gases on the permeate side and air on the feed side. Figure 3.6a reports the effect

of CO<sub>2</sub> presence in the sweep gas in different concentrations on the oxygen permeation flux. The operating temperature was fixed at 850 °C and the total flowrate of the sweep gas was 500 mL/min. When the membrane was swept with pure helium during the first 4 h of the test, the oxygen permeation flux was found to be stable at ~0.1 mL/min·cm<sup>2</sup>, which instantaneously reduced when CO<sub>2</sub> was introduced to permeate side of the membrane. Additionally, from Figure 3.6a a gradual drop of oxygen flux was observed with increased CO<sub>2</sub> concentration in the sweep gas, and the maximum cutting down of the flux was 67% with 100% CO<sub>2</sub>. However, the oxygen permeability can reach a stable value in the CO<sub>2</sub> containing atmosphere even when pure CO<sub>2</sub> was fed inside the membrane tube, and almost a full recovery (and almost immediately) of the permeation flux was obtained with the sweep gas switched back to helium, which proved good CO<sub>2</sub> resistance of the CGO/BSCF40-III dual-phase membrane.

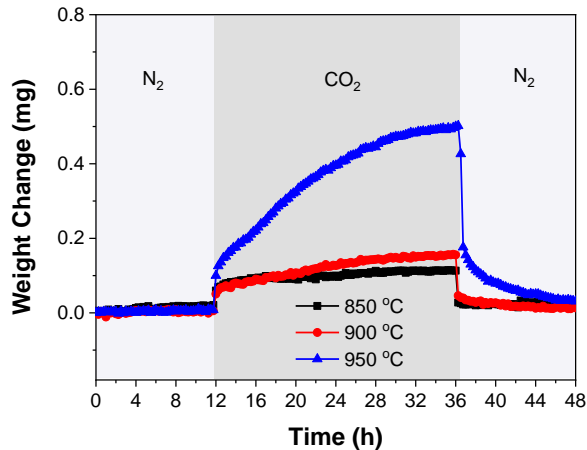
Figure 3.6b presents the temperature influence on the oxygen permeation flux through the CGO/BSCF40-III membrane with pure CO<sub>2</sub> fed to the permeate side. As swept with helium, the membrane exhibited an improved permeation flux at higher temperatures when pure CO<sub>2</sub> was used as sweep gas, and the highest oxygen flux is 0.063 mL/min·cm<sup>2</sup> at 950 °C. However, a maximum cutting down of 79% in the oxygen flux was also observed at 950 °C when 100% CO<sub>2</sub> was used. It should be noted that, at all the operation temperatures the oxygen permeation rates could be recovered when switching back to helium as sweep gas. The oxygen permeability reduction in CO<sub>2</sub> atmosphere can be attributed to mainly two reasons [18]. Firstly, alkaline earth metals, which occupy A-site of many perovskite phases, can be eroded by forming carbonates in the presence of CO<sub>2</sub>. Besides, adsorption of CO<sub>2</sub> on the membrane surface lowers the exchange rate of oxygen on the interface between the membrane and the sweep gas, but due to the weak adsorption at high temperature, the oxygen permeation flux can be recovered when the sweep gas is switched back to helium. Permeability



degradation of the CGO/BSCF40-III membrane under a  $\text{CO}_2$  atmosphere can result from both factors because of the alkaline earth metals of Ba and Sr contained in the BSCF phase. However, less alkaline earth metal is exposed to the  $\text{CO}_2$  atmosphere on the membrane surface due to the presence of CGO in the dual-phase membrane, which is assumed to be the cause of the higher  $\text{CO}_2$  resistance of the CGO-BSCF membranes compared with the BSCF membranes.

To further examine the stability of CGO/BSCF40-III membrane in  $\text{CO}_2$ , a weight recovery test under  $\text{N}_2\text{-CO}_2\text{-N}_2$  at different temperatures was carried out with the assistance of TGA. At each temperature the starting weight was collected when the desorption of the lattice oxygen reached a steady state in  $\text{N}_2$ . The membrane sample was found to lose weight after being heated up in  $\text{N}_2$ , but in order to compare the weight gains when the sample was exposed to a  $\text{CO}_2$  atmosphere, the starting weight at each temperature was set at 0 mg. A piece of 78.7 mg was cut off from a fresh CGO/BSCF40-III membrane and was used for the TGA test.

(a)



(b)

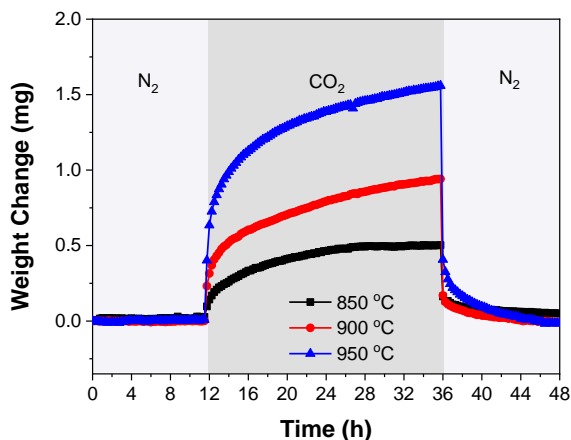


**Figure 3.7.** TGA test results for the (a) piece-formed and (b) powder-formed CGO/BSCF40-III samples with feed gas periodically changed at 850 °C, 900 °C and 950 °C.

The test results are given in Figure 3.7a. The results show that the sample weight increased immediately when pure CO<sub>2</sub> was fed into the reactor instead of N<sub>2</sub>, and higher operation temperatures were found to result in larger weight gains. Moreover, when it was shifted back to N<sub>2</sub> as the feed gas, the weight of the sample almost fully returned to the initial value because of desorption of CO<sub>2</sub>. Due to the small surface area of a single membrane piece, the amount of CO<sub>2</sub> adsorbed on the membrane surface is relatively small, with the maximum weight gain of 0.49 mg at 950 °C, which is only 0.6% of the fresh sample weight. To make a comparison, a piece (73.9 mg) of the CGO/BSCF40-III membrane was crushed into powder and tested at the same conditions, and the result is shown in Figure 3.7b. Similar to the results obtained using the single membrane piece, a higher temperature caused a larger weight increase of the powders when CO<sub>2</sub> was fed into the reactor. However, compared with the single membrane piece, the powder showed a much higher weight increase in CO<sub>2</sub> because of the much larger surface

area.

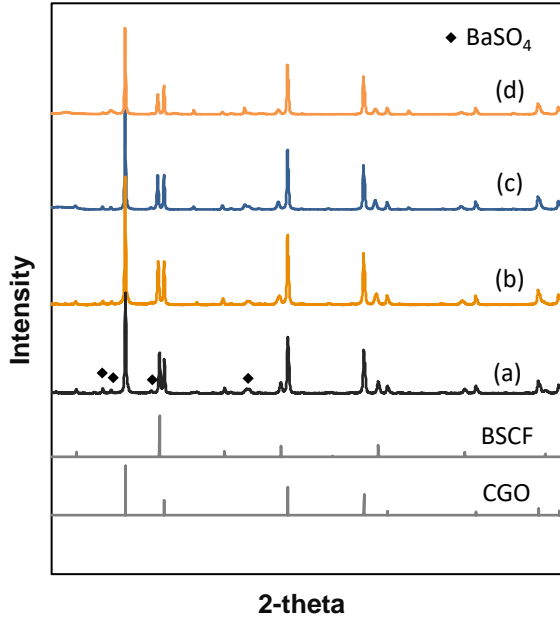


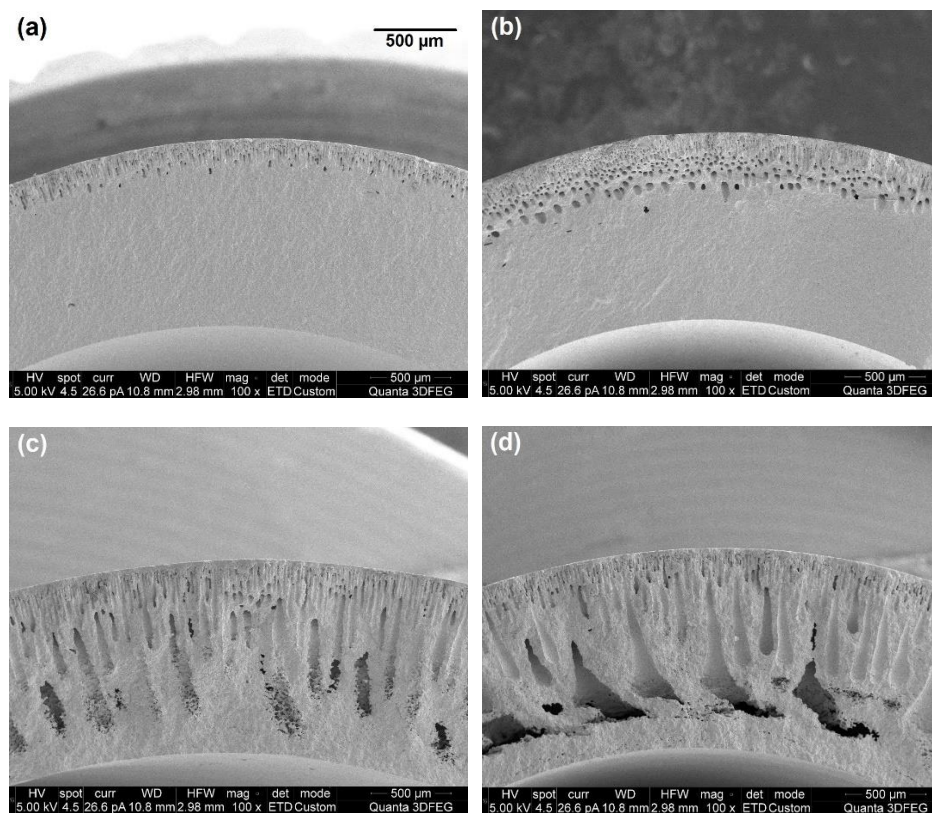
**Figure 3.8.** XRD patterns of the CGO/BSCF40-III membrane: (a) Fresh membrane; (b) Membrane after oxygen permeation test with CO<sub>2</sub> as sweep gas; (c) Piece-formed sample after TGA test; (d) Powder-formed sample after TGA test.

The XRD patterns of the CGO/BSCF40-III membrane before and after the oxygen permeation test in CO<sub>2</sub>, together with the membrane piece and powder after the TGA test are presented in Figure 3.8. It can be observed that BSCF and CGO retained their major phases after sintering at high temperature, with only a very small amount of impurity phase of BaSO<sub>4</sub> found in the fresh CGO/BSCF40-III sample. The formation of BaSO<sub>4</sub> phase is assumed to result from the generation of SO<sub>2</sub> during the burning of PES in the ceramic slurry. Figure 3.8 also shows that although the peaks of BSCF were weakened after the permeation and TGA test in CO<sub>2</sub>, no new phases were observed from the XRD patterns, or

only a very small amount of impurities was formed on the membrane surface, which are very hard to be detected by the XRD and this small amount of impurities did not have a significant effect on the oxygen permeability of the membrane.

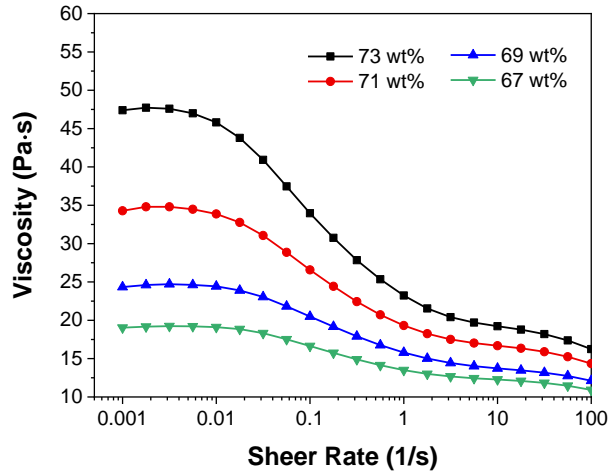
### ***3.3.2. Influence of ceramic loading in the casting slurry***

The asymmetric structure with finger-like channels is a unique microstructure formed with the phase inversion technique. The channels facilitate the oxygen permeation through the membranes. Concentration of the ceramic slurry is a key parameter that affects the channel growth during the phase inversion process. In this work the channel length and the oxygen permeability are compared for the membranes fabricated with different ceramic loadings in the slurries. If the ceramic loading was below 67 wt%, it would be difficult for the membrane to be fully densified during the sintering process because of the high ratio between the polymer and ceramic powder in the green tube, and the slurry would be difficult to be shaped into dead-end tubular shape due to its high fluidity (several concentrations below 67% were tested and the results are not reported here). Accordingly, ceramic loadings from 67 wt% to 73 wt% were applied during the membrane fabrication. For each 20 g of solvent, 40 g, 45 g, 50 g and 55 g ceramic powders with a fixed weight ratio of CGO to BSCF (60:40) was added to the polymer solution, which resulted in ceramic loadings of 67 wt%, 69 wt%, 71 wt% and 73 wt%.



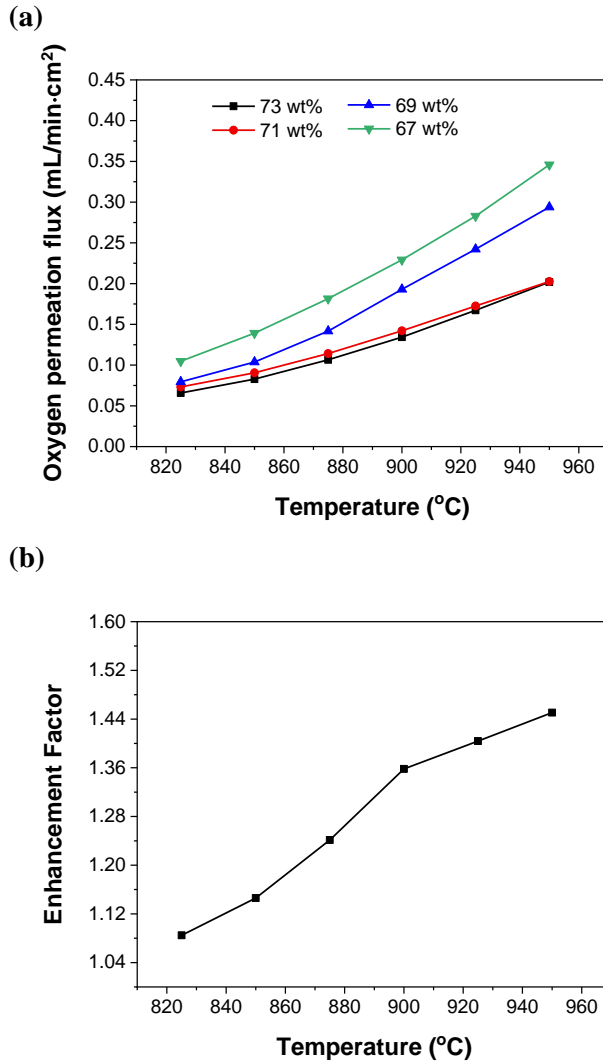
**Figure 3.9.** Cross section of CGO-BSCF dual-phase membranes fabricated from the slurries with (a) 73 wt%, (b) 71 wt%, (c) 69 wt% and (d) 67 wt% ceramic loadings.

Figure 3.9 gives the SEM images of the CGO-BSCF dual phase membranes prepared at varied ceramic loadings. From the cross sections of the membrane tubes it is clear that all membranes had two layers: one fully densified layer and the other one with finger-like channels. It can also be observed that the loading of ceramic powder in the recipe had a great influence on thickness of the micro-channelled layer. The largest volume of channels was obtained in the membrane prepared using a casting slurry with 67 wt% ceramic loading, while the finger-like pores tended to be smaller with ceramic powders added into the slurries.



**Figure 3.10.** Rheological behaviours of casting slurries with varied ceramic loadings.

The rheological behaviour of the casting slurries with different ceramic loadings is compared in Figure 3.10. A shear thinning behaviour was observed for all the ceramic pastes, and the slurry viscosity was found to increase with improved ceramic loading, which provided a higher resistance for the growth of the micro-channels.



**Figure 3.11.** Temperature dependence of (a) oxygen fluxes through membranes with different ceramic loadings and (b) permeation enhancement factor of CGO/BSCF40-III membrane compared with the CGO/BSCF40-II membrane.

Figure 3.11a shows the oxygen permeation flux as a function of temperature for the dual phase membranes prepared with different ceramic loadings. For each

membrane the effect of increasing the operating temperature was an increase of the oxygen permeability. Figure 3.11a also reveals that membranes fabricated with lower ceramic loading provided a higher oxygen permeation flux, which can be attributed to the longer channels formed during the phase inversion process. Especially when the loading of ceramic powder was reduced from 71 wt% to 69 wt%, a significant improvement in the oxygen flux from 0.20 ml/min to 0.29 ml/min was obtained at 950 °C. The enhancement factor (ratio of the permeation flux) of the CGO/BSCF40-III relative to CGO/BSCF40-II membrane is plotted as a function of temperature in Figure 3.11b. It can be seen that the oxygen permeation enhancement factor increased with temperature. The explanation of the observed phenomena is assumed to be as follows. The permeation rate-determining step is the surface exchange reaction at lower operation temperatures, which shifts to bulk diffusion at higher temperatures [19]. Compared with the CGO/BSCF40-II membrane, the thickness of the selective layer in the CGO/BSCF40-III membrane is reduced because of the improved channel length. However, the increase in the surface area is not obvious, as given in Table 3.2. This is because although the length and diameter of the channels are improved in the CGO/BSCF40-III membrane, the number of channels was not significantly increased owing to the combination of the small channels in the bulk of the membrane.

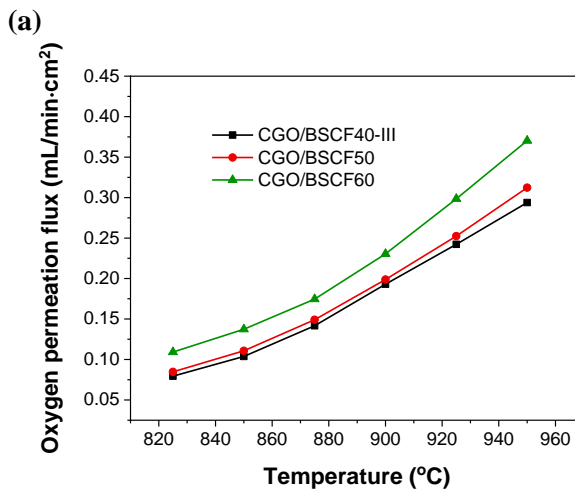


**Table 3.2.** Measured specific surface areas and mechanical strengths of membranes fabricated with slurries of varied ceramic loadings.

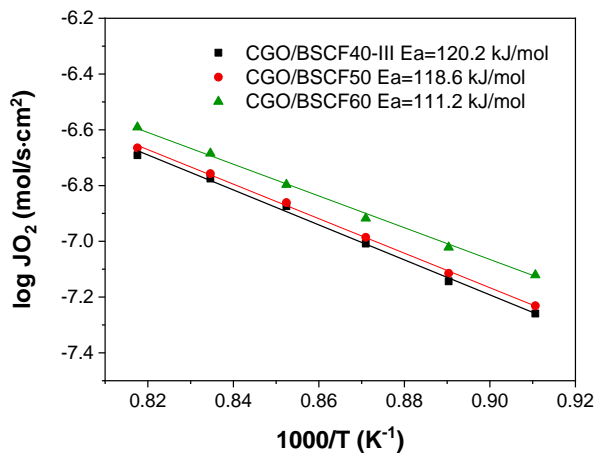
Membrane	Specific surface areas ( $\text{m}^2/\text{g}$ )	Mechanical strength (N)
CGO/BSCF40-I	0.011	208.2
CGO/BSCF40-II	0.019	208.0
CGO/BSCF40-III	0.022	205.9
CGO/BSCF40-III	0.056	203.2

Table 3.2 provides the effect of ceramic loadings on the mechanical strengths of the membranes. A rather small decrease in the mechanical strength was observed with improved channel length resulting from a lower ceramic loading in the casting slurry. The test results proved that the micro-channels formed with the phase inversion casting process provided low resistance for the oxygen permeation without obvious sacrifice of the membrane mechanical strength.

### 3.3.3. Influence of the weight ratio between CGO and BSCF



(b)



**Figure 3.12.** (a) Temperature dependence of oxygen permeation fluxes; (b) Arrhenius plots of oxygen fluxes through the membranes with different CGO:BSCF ratios.

The oxygen permeation fluxes, chemical stabilities in CO<sub>2</sub> and the mechanical strengths were compared for the CGO-BSCF membranes with different CGO:BSCF ratios, while the ceramic loading in the casting slurries was fixed at 69 wt%. The CGO:BSCF ratio is one of the factors that controls the oxygen permeation flux through the dual-phase membranes as shown in Figure 3.12a. At fixed operating temperature the oxygen flux with helium as sweep gas increased with improved BSCF percentage in the preparation recipe, while the permeation activation energies (E<sub>a</sub>) were observed to drop gradually in the order of CGO/BSCF40-III (E<sub>a</sub> =120.2 kJ/mol) > CGO/BSCF50 (E<sub>a</sub> =118.6 kJ/mol) > CGO/BSCF60 (E<sub>a</sub> =111.2 kJ/mol), which is given in Figure 3.12b. The membrane that provided higher oxygen flux showed a lower permeation activation energy. Additionally, each membrane showed a constant activation energy in the operation temperature range, which proves the phase stability of the tested CGO-BSCF membranes.

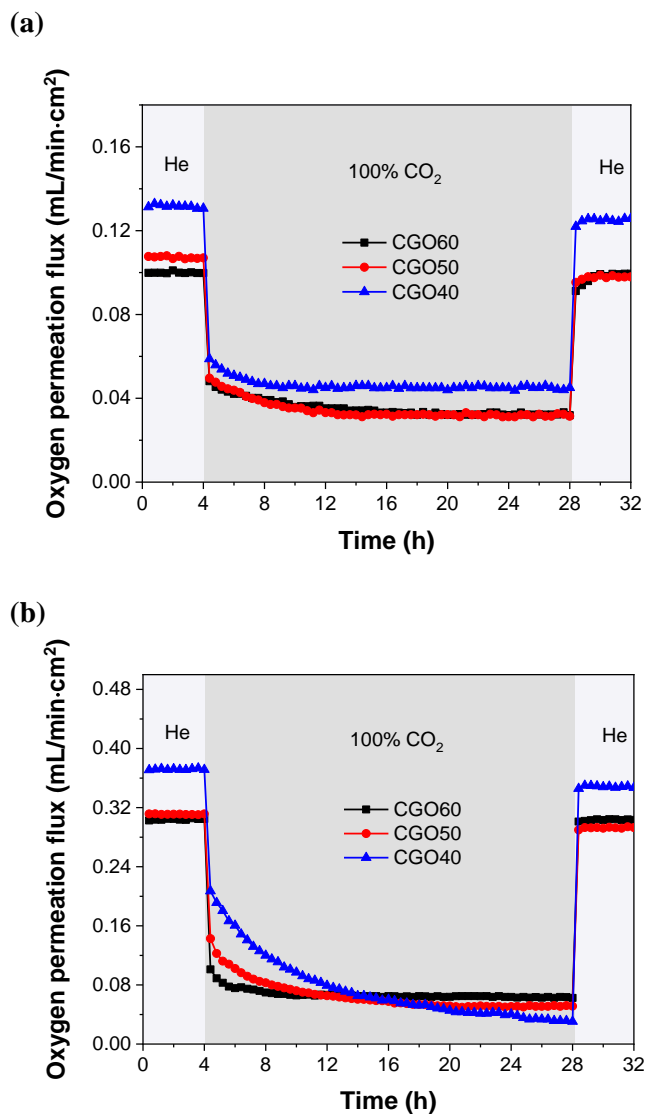


**Figure 3.13.** (a) Oxygen fluxes through the membranes with different CGO:BSCF ratios while alternating sweep gas between pure helium and CO<sub>2</sub> at (a) 850 °C and (b) 950 °C.

Since a favoured CGO:BSCF ratio in terms of the oxygen permeation flux is selected, further tests were focused on the CO<sub>2</sub> resistance of the membranes with

different BSCF concentrations. Permeation recovery tests with pure helium or CO<sub>2</sub> as sweep gas were conducted at two different temperatures. Figure 3.13a exhibits that at 850 °C the permeation flux through all the three membranes could reach a stable value while pure CO<sub>2</sub> was fed to the permeate side. The membranes with more BSCF showed larger degradation of the permeation fluxes when the sweep gas was shifted from helium to CO<sub>2</sub>, but the CGO/BSCF60 membrane still provided the highest permeability with CO<sub>2</sub> as sweep gas. Compared with their performance at 850 °C, it can be observed from Figure 3.13b that when the membranes were swept with pure CO<sub>2</sub> at 950 °C, the CGO/BSCF60 membrane provided the lowest oxygen flux among the three dual-phase membranes, which is totally different from the result obtained with helium as sweep gas. Moreover, from the plots in Figure 3.13, it is clear that at both temperatures the permeability of the CGO/BSCF60 and CGO/BSCF50 membranes could not be fully recovered after helium was switched back, suggesting lower stability of CGO/BSCF60 and CGO/BSCF50 membranes in CO<sub>2</sub> atmosphere compared with the CGO/BSCF40-III membrane.

**Table 3.3.** Measured mechanical strengths of membranes with different CGO: BSCF ratios.

<b>Membrane</b>	<b>Mechanical strength (N)</b>
CGO/BSCF40-III	205.9
CGO/BSCF50	181.6
CGO/BSCF60	81.0
CGO	251.3
BSCF	69.4

Table 3.3 gives the results of the mechanical strength measurements conducted for the three dual-phase membranes with different CGO:BSCF ratios, as well as

the single-phase CGO and BSCF membranes. The three-point bending strength of the CGO membrane is 251.3 N, which is more than three times the strength of BSCF membrane (69.4 N), and the forces needed to break the membranes were observed to reduce in the order of CGO/BSCF40-III > CGO/BSCF50 > CGO/BSCF60, proving the enhancing role of the CGO content on the mechanical strength of the membrane.

### **3.4. Conclusions**

Dead-end CGO-BSCF membrane tubes with a finger-like-channelled microstructure were successfully manufactured with a low-cost phase inversion casting technique. The dead-end tubular membrane geometry assures simple sealing process and ease of handling in membrane reactors. Although a drop of oxygen permeation rate through the CGO/BSCF40-III membrane was observed when CO<sub>2</sub>-containing sweep gas was fed to the permeate side instead of helium, the oxygen flux was found to be recovered with helium switched back. Higher CO<sub>2</sub> concentration in the sweep gas caused lower oxygen flowrate through the membranes. Increased operation temperature caused more CO<sub>2</sub> adsorbed onto the membrane and bigger drop of the permeation flux, but the oxygen flux still increased with temperature when pure was CO<sub>2</sub> fed as sweep gas. Ceramic loading in the casting slurry was a key factor that affected channel length in the CGO-BSCF membranes. Reduced ceramic loadings facilitated channel growth and resulted in higher oxygen permeability of the membranes. With fixed CGO:BSCF ratio, no obvious sacrifice of the mechanical strength was observed with longer channels inside the membranes. Oxygen permeability of the membranes with different CGO:BSCF ratio was observed to reduce in the order of CGO/BSCF60 > CGO/BSCF50 > CGO/BSCF40-III, while CGO/BSCF60 and CGO/BSCF50 membranes exhibited a lower CO<sub>2</sub> resistance than the CGO/BSCF40-III membrane. Moreover, higher CGO concentration caused improvement of the mechanical strength of the CGO-BSCF membranes.

## References

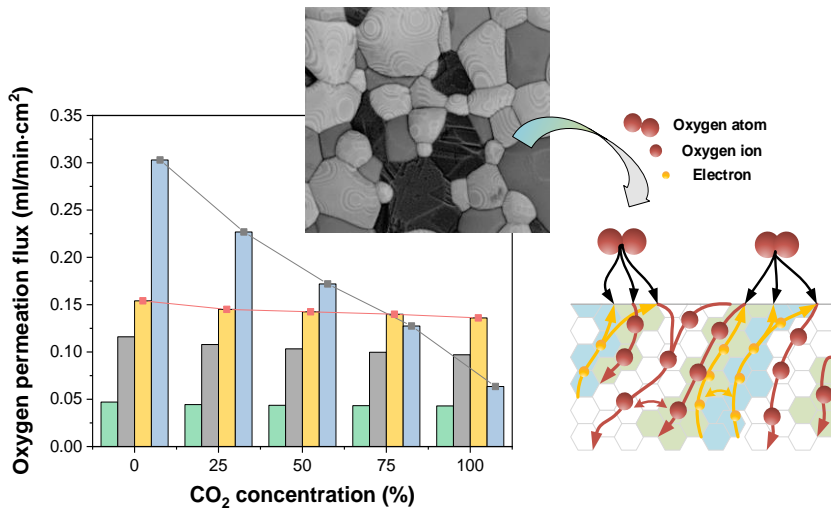
- [1] H. Strathmann, K. Kock, The formation mechanism of phase inversion membranes, *Desalination*. 21 (1977) 241–255.
- [2] W. He, H. Huang, J. Gao, L. Winnubst, C. Chen, Phase-inversion tape casting and oxygen permeation properties of supported ceramic membranes, *J. Memb. Sci.* 452 (2014) 294–299.
- [3] Y. Meng, W. He, X. Li, J. Gao, Z. Zhan, J. Yi, C. Chen, H. J. M. Bouwmeester, Asymmetric  $\text{La}_{0.6}\text{Sr}_{0.4}\text{Co}_{0.2}\text{Fe}_{0.8}\text{O}_{3-\delta}$  membrane with reduced concentration polarization prepared by phase-inversion tape casting and warm pressing, *J. Memb. Sci.* 533 (2017) 11–18.
- [4] X. Shao, D. Dong, G. Parkinson, C.Z. Li, Thin ceramic membrane with dendritic microchanneled sub structure and high oxygen permeation rate, *J. Memb. Sci.* 541 (2017) 653–660.
- [5] S. D. Nurherdiana, Effect of the sintering process on the morphology and mechanical properties of  $\text{La}_{0.6}\text{Sr}_{0.4}\text{Co}_{0.2}\text{Fe}_{0.8}\text{O}_{3-\delta}$  asymmetric flat membranes prepared by the phase inversion method, *Ceram. - Silikaty*. 63 (2019) 1–9.
- [6] Z. Wu, N. Hidayati Othman, G. Zhang, Z. Liu, W. Jin, K. Li, Effects of fabrication processes on oxygen permeation of  $\text{Nb}_2\text{O}_5$ -doped  $\text{SrCo}_{0.8}\text{Fe}_{0.2}\text{O}_{3-\delta}$  micro-tubular membranes, *J. Memb. Sci.* 442 (2013) 1–7.
- [7] D. Yang, N. Han, D. Han, B. Meng, G. Wang, S. Liu, Novel  $\text{SrCo}_{0.9}\text{W}_{0.1}\text{O}_{3-\delta}$  hollow fiber ceramic membrane with enhanced oxygen delivery performance and  $\text{CO}_2$  resistance ability, *ChemistrySelect*. 3 (2018) 13700–13704.
- [8] J. Song, B. Feng, X. Tan, N. Han, J. Sunarso, S. Liu, Oxygen selective perovskite hollow fiber membrane bundles, *J. Memb. Sci.* 581 (2019) 393–400.

- [9] N. Han, Q. Wei, H. Tian, S. Zhang, Z. Zhu, J. Liu, S. Liu, Highly stable dual-phase membrane based on  $\text{Ce}_{0.9}\text{Gd}_{0.1}\text{O}_{2-\delta}$ - $\text{La}_2\text{NiO}_{4+\delta}$  for oxygen permeation under pure  $\text{CO}_2$  atmosphere, *Energy Technol.* 7 (2019) 1–10.
- [10] C. Ren, Y. Gan, C. Yang, M. Lee, X. Xue, A rational asymmetric hollow fiber membrane for oxygen permeation, *Int. J. Appl. Ceram. Technol.* 16 (2019) 791–801.
- [11] X. Zhu, M. Li, H. Liu, T. Zhang, Y. Cong, W. Yang, Design and experimental investigation of oxide ceramic dual-phase membranes, *J. Memb. Sci.* 394–395 (2012) 120–130.
- [12] J. Xue, Q. Liao, Y. Wei, Z. Li, H. Wang, A  $\text{CO}_2$ -tolerance oxygen permeable  $60\text{Ce}_{0.9}\text{Gd}_{0.1}\text{O}_{2-\delta}$ - $40\text{Ba}_{0.5}\text{Sr}_{0.5}\text{Co}_{0.8}\text{Fe}_{0.2}\text{O}_{3-\delta}$  dual phase membrane, *J. Memb. Sci.* 443 (2013) 124–130.
- [13] J. Yi, Y. Zuo, W. Liu, L. Winnubst, C. Chen, Oxygen permeation through a  $\text{Ce}_{0.8}\text{Sm}_{0.2}\text{O}_{2-\delta}$ - $\text{La}_{0.8}\text{Sr}_{0.2}\text{CrO}_{3-\delta}$  dual-phase composite membrane, *J. Memb. Sci.* 280 (2006) 849–855.
- [14] V. V. Kharton, A. V. Kovalevsky, A. P. Viskup, A. L. Shaula, F. M. Figueiredo, E. N. Naumovich, F. M. B. Marques, Oxygen transport in  $\text{Ce}_{0.8}\text{Gd}_{0.2}\text{O}_{2-\delta}$ -based composite membranes, *Solid State Ionics.* 160 (2003) 247–258.
- [15] K. Coenen, F. Gallucci, P. Cobden, E. van Dijk, E. Hensen, M. van Sint Annaland, Chemisorption working capacity and kinetics of  $\text{CO}_2$  and  $\text{H}_2\text{O}$  of hydrotalcite-based adsorbents for sorption-enhanced water-gas-shift applications, *Chem. Eng. J.* 293 (2016) 9–23.
- [16] H. Luo, H. Jiang, K. Efimov, F. Liang, H. Wang, J. Caro,  $\text{CO}_2$ -tolerant oxygen-permeable  $\text{Fe}_2\text{O}_3$ - $\text{Ce}_{0.9}\text{Gd}_{0.1}\text{O}_{2-\delta}$  dual phase membranes, *Ind. Eng. Chem. Res.* 50 (2011) 13508–13517.
- [17] J. Tong, W. Yang, B. Zhu, R. Cai, Investigation of ideal zirconium-doped perovskite-type ceramic membrane materials for oxygen separation, *J. Memb. Sci.* 203 (2002) 175–189.



- [18] H. Cheng, L. Luo, W. Yao, X. Lu, X. Zou, Z. Zhou, Novel cobalt-free CO<sub>2</sub>-tolerant dual-phase membranes of Ce<sub>0.8</sub>Sm<sub>0.2</sub>O<sub>2-δ</sub>-Ba<sub>0.95</sub>La<sub>0.05</sub>Fe<sub>1-x</sub>Zr<sub>x</sub>O<sub>3-δ</sub> for oxygen separation, *J. Memb. Sci.* 492 (2015) 220–229.
- [19] Z. Wang, H. Liu, X. Tan, Y. Jin, S. Liu, Improvement of the oxygen permeation through perovskite hollow fibre membranes by surface acid-modification, *J. Memb. Sci.* 345 (2009) 65–73.

# Chapter 4 Dual-phase and triple-phase membranes with high CO<sub>2</sub>-tolerance



*In this chapter, the oxygen ionic conductor CGO was paired with NFO, LNO and BSCF, forming three kinds of dual-phase membranes. Performance of the membranes was compared. Based on the results for the dual-phase membranes, some CGO/BSCF/NFO triple-phase membranes were developed. The application of the two triple-phase composites promoted the oxygen permeation fluxes when the membranes were swept with pure CO<sub>2</sub>. This chapter provides valuable information for the material selection and performance optimization of the CGO-based multi-phase membranes.*

***This chapter is based on paper: Ce<sub>0.9</sub>Gd<sub>0.1</sub>O<sub>2-δ</sub>-based multi-phase membranes with high CO<sub>2</sub>-tolerance. Under review.***

## 4.1. Introduction

For a dual-phase membrane, compatible materials need to be selected to avoid the reactions between the two phases and to minimize the chemical-thermal expansion mismatch between both ceramics. Several combinations of crystalline materials, including fluorite, perovskite, spinel and Ruddlesden–Popper-type oxides, have been reported in the literatures [1-11]. The material with fluorite crystalline structure is generally applied as the oxygen-ionic phase in the composites since the ionic conductivity is dominant, while the Ruddlesden–Popper-type oxides and the perovskites can serve as electronic phase. Because of the much higher mobility of electrons than the oxygen ions, an increase in the oxygen-ionic conductivity of the membrane may allow the improvement of the total oxygen permeation flux. Following this strategy, the mixed conducting perovskites instead of the pure electronic conductors were combined with the fluorites by some researchers for the fabrication of dual-phase membranes [7]. Such composites ensure that both phases can provide the paths for the oxygen-ionic percolation. However, the presence of alkaline-earth-metal-containing perovskites would cause the formation of carbonate and immediate reduction of the oxygen permeation when the dual-phase membrane was exposed to CO<sub>2</sub>, although this reduction was found to be reversible. Therefore, CO<sub>2</sub>-stable electronic conductors are preferred by some researchers. For example, several fluorite-spinel composites, such as CGO-NiFe<sub>2</sub>O<sub>4</sub> (NFO) and Ce<sub>0.8</sub>Tb<sub>0.2</sub>O<sub>2-δ</sub> (CTO)-NFO membranes were tested in CO<sub>2</sub>-containing atmospheres and excellent results were obtained in terms of the membrane stability [6,8]. However, the studies of different dual-phase composites were mostly based on varied membrane thicknesses, geometries (tubular, hollow fibre and planar) and surface modifications, and were tested under varied test conditions, which bring difficulties to the comparison between the performance of the fluorite-perovskites and other the dual-phase composites with the pure electronic and

ionic conductors.

The CGO-BSCF membranes have been investigated in Chapter 3. In this chapter, the strategy to composite the dual-phase membranes with CGO as the oxygen-ionic conductor is further investigated. The modified phase-inversion casting method, which has been reported in Chapter 3, was applied to the production of the dead-end tubular membrane geometry. The permeability of the formed CGO-BSCF, CGO-NFO and CGO-  $\text{La}_2\text{NiO}_{4+\delta}$  (LNO) membranes is compared in detail together with an investigation in their permeation behaviour in CO<sub>2</sub> atmosphere. Based on the test results of the dual-phase membranes, some CGO/BSCF/NFO triple-phase membranes are developed, with the purpose of optimizing the membrane performance in CO<sub>2</sub>-containing atmosphere. Large amount of each phase is required for the formation of continuous ionic/electronic paths in the dual-phase membranes. However, in the triple-phase membranes, concentration of BSCF can be reduced with maintaining the continuous electronic network by adding the electronic conductor NFO. The oxygen permeability and CO<sub>2</sub>-tolerance of the triple-phase membranes are compared with that of the CGO-BSCF and CGO-NFO membranes.

## 4.2. Experimental methods

CGO powders purchased from Ningbo Sofcman Energy were milled for 3 h in a ball mill (Pulverisette 6, Fritsch) before being used for the formation of the oxygen-ionic conductive phase. The NFO powders for the electronic conductive phase was supplied by Alfa Aesar, while the BSCF and LNO powders was ordered from Cerpotech.

The fabrication of the dead-end tubular membranes has been reported in Chapter 3, which stated with the preparation of a solution by adding 5 g PES and 1 g PVP in to 20 g NMP. Subsequently, ceramic powders were then mixed with the solution. The total amount of the ceramic powders was set at 45 g for each 20 g of the NMP, while the components were varied for different multi-phase membranes, as listed in Table 4.1. The defoamed ceramic slurries were transferred into the home-made casting device, cooled with ice and pushed into water for phase inversion. Those solidified tubes formed after phase-inversion process were dried and sintered at ultra-high temperature. The green membranes with varied components required different sintering temperatures (Table 4.1) to achieve gas-tight membranes showing good mechanical stability, and the optimized sintering temperature for each kind of membrane has been determined in a separate study. A slow heating ramp of 30 °C/h was used to heat the membranes up to the sintering temperatures which was cooled down with a higher ramp of 60 °C/h.

**Table 4.1.** Weight percentage of each phase and sintering temperatures for the multi-phase membranes under study.

<b>Membrane</b>	<b>CGO content, wt%</b>	<b>BSCF content, wt%</b>	<b>NFO content, wt%</b>	<b>LNO content, wt%</b>	<b>Sintering temperature, °C</b>
C6L4	60	0	0	40	1400
C6N4	60	0	40	0	1450
C6B4	60	40	0	0	1170
C4B4N2	40	40	20	0	1235
C6B2N2	60	20	20	0	1245

The multi-phase membranes before or after oxygen permeation were observed by SEM and the element analysis was performed with EDX, and XRD was used to determine phase structure of the membranes. Gas-tightness of the multi-phase membranes after sintering process was tested with a helium setup, and only leakage-free membranes were selected for the permeation tests. A high-temperature experimental system, which was described in Chapter 3, was employed for the study of the oxygen permeation fluxes through the different multi-phase membranes. The open side of the dead-end membrane was sealed to the Fe-Cr tube. The permeation cell was heated to 1020 °C with a rate of 60 °C/h, kept for 30 min, and directly cooled down to 825 °C for the permeation test after the sealing procedure. Helium and/or CO<sub>2</sub> were used as the sweep gas for the permeation test with air applied as feed gas.

### 4.3. Results and discussion

#### 4.3.1 Oxygen permeation and CO<sub>2</sub>-tolerance of the dual-phase membranes

Measurements for the oxygen permeation as a function of operation temperature were performed on the dual-phase membranes with fixed sweep gas flowrate of 500 ml/min. The performance of three type of membranes, including C6L4, C6N4 and C6B4, were compared.

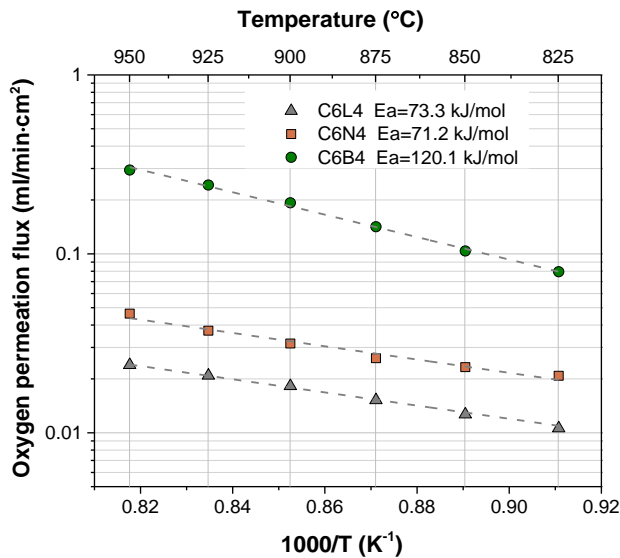


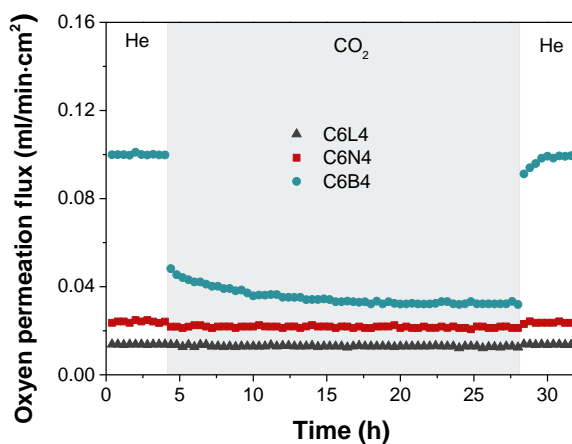
**Figure 4.1.** Temperature dependence of the permeation fluxes through the C6L4, C6N4 and C6B4 dual-phase membranes, together with the corresponding activation energies.

For the ceramic oxygen transport membranes, it was generally found that increased operation temperatures led to a rise in the permeation fluxes, which is because of the enhanced surface-exchange and bulk-diffusion rate of oxygen. This trend also applies to these three dual-phase composites, as shown in Figure 4.1. Of the three membranes, it can be observed that the C6B4 provided much

higher permeation value than the other two composites. Taking the data at 950 °C as a reference, the permeation flux through the C6B4 was 0.29 ml/min·cm<sup>2</sup>, which is more than 6 times the value obtained for the C6N4 and 12 times the value achieved for the C6L4 at the same conditions. These results prove the promoting effect of using mixed-conductive material instead of the pure electronic conductor in the dual-phase membranes on the oxygen permeation flux, which results from the increased paths for oxygen ion percolation. The activation energies ( $E_a$ ) for oxygen permeation through the three membrane samples are also included in Figure 4.1. Constant activation energies were observed for all of the three dual-phase membranes, and it is one of the factors that proves the good phase stability of the membranes under the test conditions [12,13]. The highest activation energy is obtained for the C6B4 membrane which is 120.1 kJ/mol. This could be attributed to two factors: Since both CGO and BSCF provide paths for the oxygen ion conduction, travel of the oxygen ions through the borders of the two phases may contribute to the high activation energy; The sintering temperature of 1170 °C for the composite is lower than the desired sintering temperature of the CGO phase (although a gas-tight membrane was obtained because of the presence of BSCF), and the increased grain boundary area of CGO due to the lower sintering temperature may lead to higher activation energy for the oxygen permeation [10].



(a)



(b)

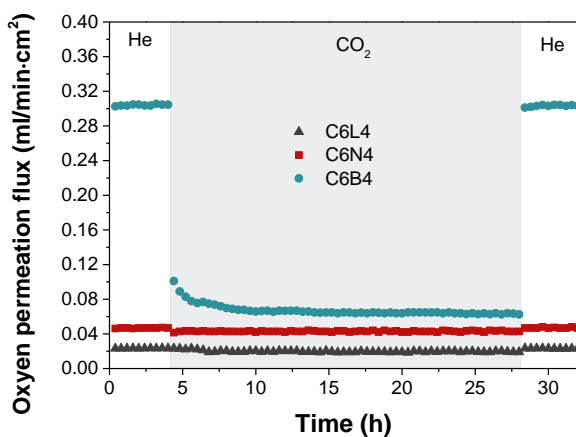


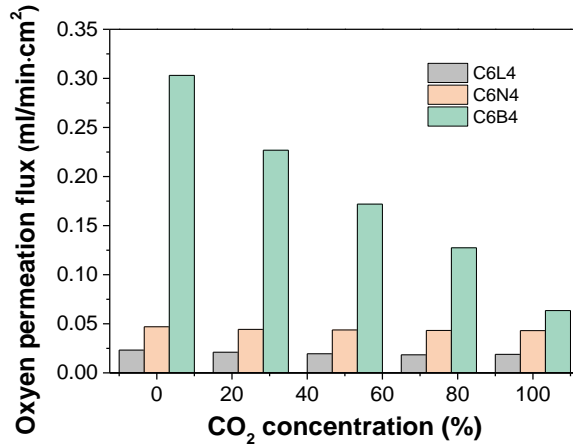
**Figure 4.2.** Permeation fluxes through the C6L4, C6N4 and C6B4 membranes with the sweep gas alternated between He and CO<sub>2</sub> at (a) 850 °C and (b) 950 °C.

The chemical stability of the three dual-phase membranes was studied by feeding CO<sub>2</sub>-containing sweep gas to the permeate side of the membranes at varied temperatures. Flowrate of the sweep gas was fixed at 500 ml/min. Figure 4.2a

reports the permeation evolution for the three composite membranes as a function of time with the sweep gas switched between 100% CO<sub>2</sub> and He at 850 °C. The experiment started with pure helium fed to the permeate side, and after the permeation had become stable for 4 h in helium, CO<sub>2</sub> was feed instead of helium as sweep gas. It can be observed that the permeation flux through the C6B4 membrane dropped instantly to 0.048 ml/min·cm<sup>2</sup> when the sweep gas was switched to pure CO<sub>2</sub>. Afterwards, a gradual decline was observed and then the flux tended to be stable at ~0.032 ml/min·cm<sup>2</sup>. The O<sub>2</sub>-CO<sub>2</sub> competitive adsorption on the membranes and the carbon formation due to the reactions was found to be the two factors that may cause the permeation loss of the membranes in CO<sub>2</sub> [14]. The sharp decline of the oxygen permeation may be mainly attributed to the competitive adsorption of the two gasses, while the gradual drop afterwards may be due to the reaction forming the carbonate, since the carbonate-formation process would take longer time. The carbonates such as SrCO<sub>3</sub> were reported to be decomposed to oxides with exposed to CO<sub>2</sub>-rare atmosphere at temperatures above 800 °C followed by the possible recovery of the perovskite structure due to the reactions of the solid-state oxides [15,16]. This explains the recovery of the permeation flux through the C6B4 when He was switched back as sweep gas. The performance loss with the exposure to CO<sub>2</sub>-containing atmosphere was also observed for some other membranes (not reported here) e.g. the permeation value dropped to zero when the BSCF membrane was swept with CO<sub>2</sub>. The comparatively high oxygen flux through the C6B4 membrane when exposed to CO<sub>2</sub> proves the enhancing role of CGO on the CO<sub>2</sub>-resistance of the membrane. Figure 4.2a also shows that the CO<sub>2</sub> atmosphere brought little poisoning effect on the C6N4 and C6L4 membranes. However, it is noticeable that although a large drop of the oxygen flux was observed for the C6B4 membrane, the stable permeation value was still higher than that of the other two composites. Similar results were obtained at 950 °C (Figure 4.2b). The

permeation performance of the three dual-phase membranes all can reach to a steady state in CO<sub>2</sub> atmosphere and the C6B4 composite provided the highest oxygen flux when swept with either He or pure CO<sub>2</sub>.

(a)



(b)

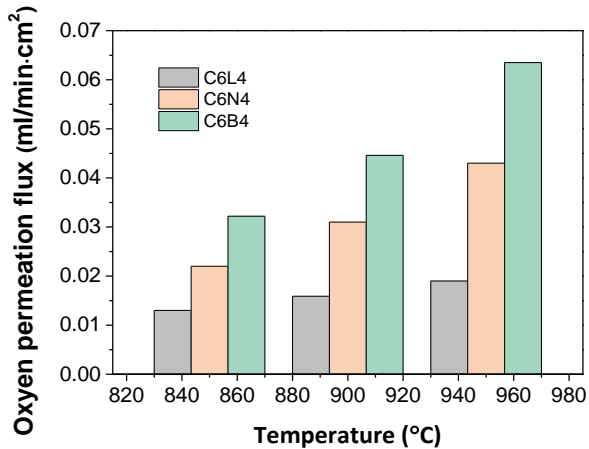


**Figure 4.3.** Permeation fluxes through C6L4, C6N4 and C6B4 membranes (a) with sweep gas of different CO<sub>2</sub> concentrations at 950 °C and (b) with CO<sub>2</sub> as the sweep gas at varied temperatures.

The effect of CO<sub>2</sub> concentration in the sweep gas on the oxygen permeation flux through the three dual-phase membranes with the operation temperature fixed at 950 °C is presented in Figure 4.3a. The permeation value was observed to decline with the rise of CO<sub>2</sub> content in the sweep gas for the C6B4 membrane, while the CO<sub>2</sub> produced little poisoning effect on the C6N4 and C6L4 membranes. This result can be explained by the higher concentration of oxygen vacancies on surface of the C6B4 membrane compared to the other two membranes, which means more CO<sub>2</sub> could be adsorbed on the C6B4 composite. However, it should be noticed that, at each CO<sub>2</sub> concentration, C6B4 provided the highest oxygen permeation value among the three composites.

Figure 4.3b shows the temperature effect on the permeability of the three composites when 100 % CO<sub>2</sub> was fed as the sweep gas. It can be observed that, as swept by He, rise of the operating temperature caused a permeation flux increase for all the three dual-phase membranes, because of the improved surface exchange and bulk diffusion speed at higher temperature. It can also be seen from Figure 4.3b that at each temperature C6B4 provided the highest permeation flux of the three investigated membranes.

#### ***4.3.2 Phase and morphology of the triple-phase membranes***

The C6B4 exhibited superior permeability but also a larger reduction of oxygen permeation than the C6N4 and C6L4 compounds when swept by CO<sub>2</sub>. Accordingly, some triple-phase membranes were prepared using the CGO, NFO and the mixed conductive BSCF oxides. Several types of triple-phase membranes can be obtained by adjusting the ratio between the different phases, and two of these composites were investigated and compared with C6B4 and C6N4 dual-phase membranes in this work.

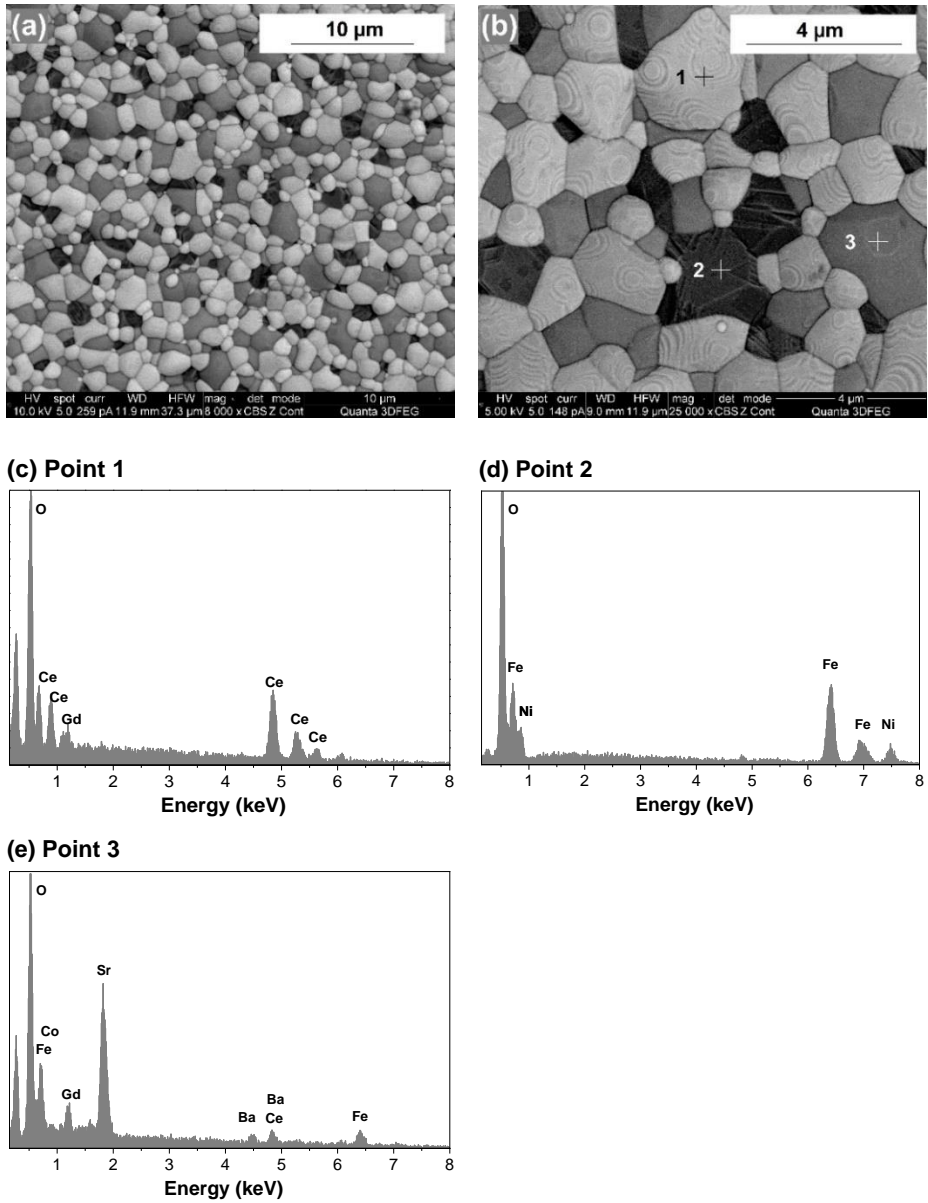


**Figure 4.4.** (a,b) Back-scattered electron microscopy and (c-e) EDS analysis of three points on surface of the C6BN membrane.

Figure 4.4a/b are the SEM images of the C6BN triple-phase membrane. With the

BSD mode of SEM, three kinds of grains can be clearly observed on the membrane surface. These uniformly distributed grains are sized between 1-4  $\mu\text{m}$ . According to the EDS analysis, the light grey blocks (point 1) are the CGO phase, the ones in darker grey (point 3) are supposed to be BSCF phase, and the black grains (point 2) can be assigned to the NFO phase (Figure 4.4c-e). The SEM images show well-connected network of the CGO phase, while the other two phases appear less continuous. However, connected electronic pathways can be obtained due to the collective effect of BSCF and NFO. No new phases were observed on the C6BN membrane after sintered at ultra-high temperature, and this can be confirmed by the XRD test result (Figure 4.5). A weak signal of Gd was detected on the BSCF grains, which was repeatable in the EDX tests. This result can be explained by the trace Gd diffusion from CGO to the BSCF phase at high sintering temperature. Gd of the CGO was also found to diffuse into  $\text{La}_{0.6}\text{Sr}_{0.4}\text{Co}_{0.2}\text{Fe}_{0.8}\text{O}_{3-\delta}$  during sintering of the dual-phase membrane by Han et al. [10] From the XRD patterns of the fresh C6BN membranes (Figure 4.5), it is obvious that the characteristic peaks of the BSCF phase all have shifted to the left, and this can be explained by the large amount of lattice oxygen release during sintering process.

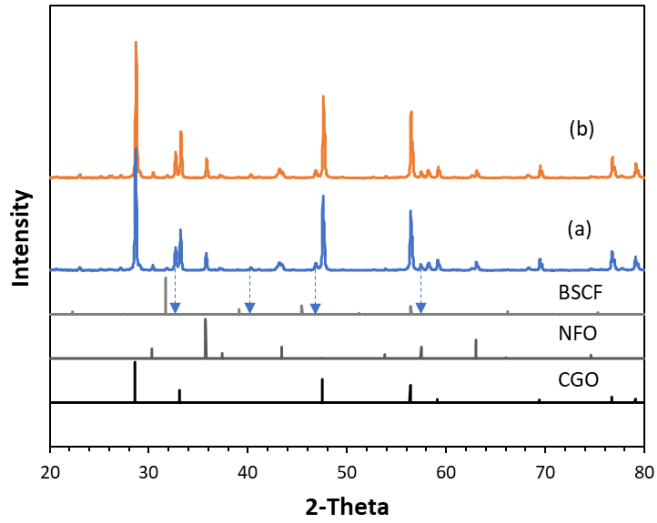
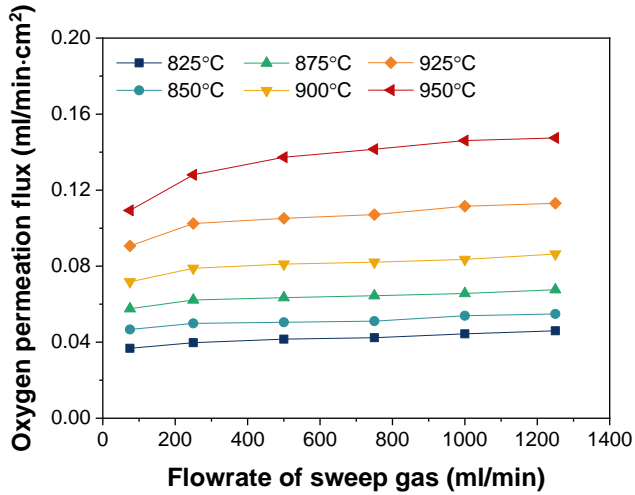


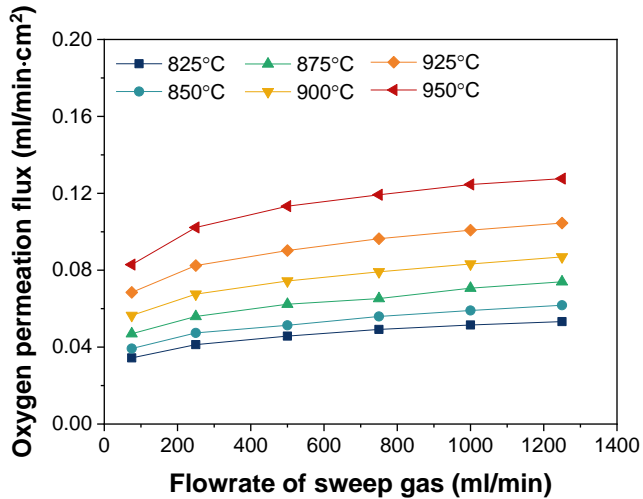
**Figure 4.5.** XRD pattern of the C6BN membrane (a) before and (b) after the permeation test with CO<sub>2</sub> as sweep gas.

### 4.3.3 Performance comparison between the triple-phase and dual-phase membranes

(a)



(b)





(c)

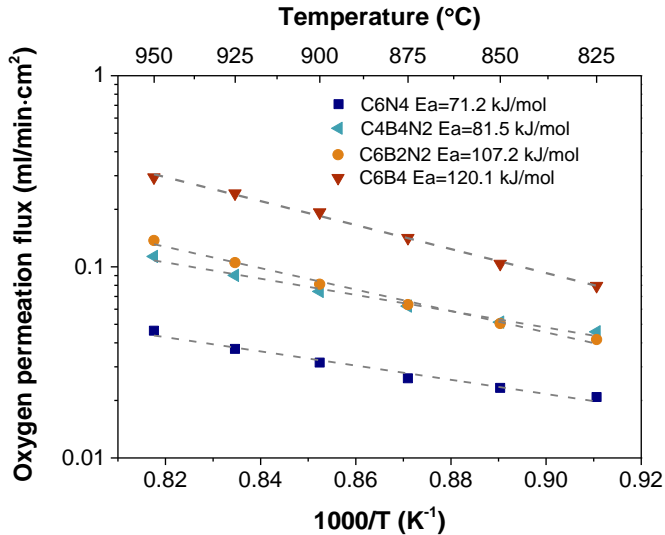


**Figure 4.6.** Helium flowrate dependence of the permeation value for the (a) C6B2N2 and (b) C4B2N2 membranes; (c) Temperature dependence of the permeation fluxes through the C6N4, C4B4N2, C6B2N2 and C6B4 membranes.

Figure 4.6a/b give the permeation fluxes through the C6B2N2 and C4B4N2 membranes when swept by helium with different flow rates at the temperatures ranging from 825 to 950 °C. A positive correlation was observed between the permeation value and the flowrate of helium for both of the membranes e.g. at 950 °C the oxygen flux through the C6B2N2 and C4B4N2 rose from 0.13 to 0.15 and from 0.10 to 0.12 ml/min·cm<sup>2</sup>, respectively, when flowrate of the sweep gas increased from 250 to 750 ml/min. The rise in the oxygen permeation flux can be attributed to the reduced oxygen partial pressure on permeate side of the membranes. Besides, the permeation was found to be less sensitive to the helium flowrate increase at higher feeding rate of the sweep gas.

The temperature dependence of the permeation values for the two triple-phase

membranes together with the C6B4 and C6N4 dual-phase membranes are presented in Figure 4.6c. Apparently, the permeation fluxes of both triple-phase membranes are higher than that of the C6N4 but lower compared with that of the C6B4 membrane at the same temperature. The activation energies of the four composites are also given in Figure 4.6c. Constant activation energies for the oxygen permeation through the two triple-phase membranes were observed over the test temperature range, and similar as their permeation fluxes, activation energies of the C6B2N2 and C4B4N2 are between those of the two dual-phase composites. The C6B2N2 membrane was observed to show a higher activation energy than the C4B4N2, which can be due to the low activation energy of the oxygen-ion percolation in BSCF compared to that of the ionic conduction in CGO [17].

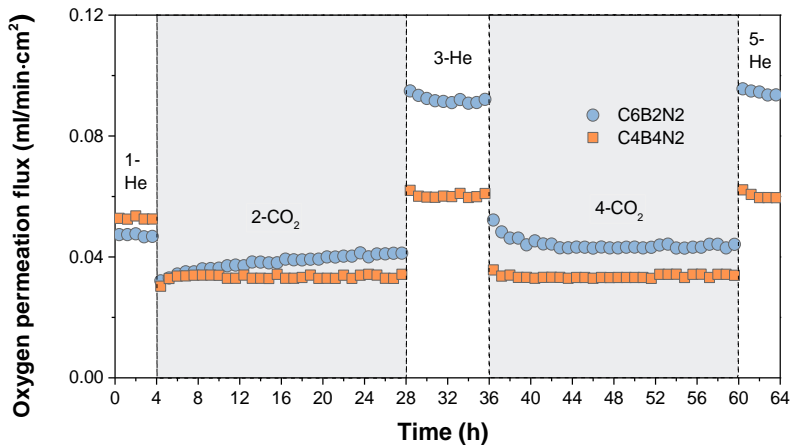


**Figure 4.7.** Oxygen fluxes through the C6B2N2 and C4B4N2 membranes with the sweep gas alternated between helium and 100 % CO<sub>2</sub> at 850 °C.

Figure 4.7 exhibits the permeation evolution trend for the C6B2N2 and C4B4N2 membranes versus experiment time with the sweep gas switched between pure

CO<sub>2</sub> and He at 850 °C. Similar as the C6B4 membrane, an instant breakdown of the permeability was observed for both triple-phase membranes when CO<sub>2</sub> was fed as sweep gas instead of helium. However, in the following 24 h, the permeation fluxes through C6B2N2 and C4B4N2 were found to rise gradually to 0.041 ml/min·cm<sup>2</sup> and 0.034 ml/min·cm<sup>2</sup>, respectively, as illustrated by curve-2. When helium was switched back as the sweep gas, the oxygen permeation through the C6B2N2 membrane restored to 0.092 ml/min·cm<sup>2</sup> immediately. It is worth noting that the restored permeation value is much higher than the original level of curve-1, which is 0.047 ml/min·cm<sup>2</sup>. This upgrade of the oxygen permeation flux can be explained by the postulation that the formation and decomposition process of the carbonates on the membrane could increase roughness of the membrane surface, and the resulted larger surface area would facilitate the surface-exchange reactions of oxygen. The postulation is supported by the SEM images of the C6B2N2 before and after the permeation test in CO<sub>2</sub> atmosphere (Figure 4.8). It is obvious that the surface of the membrane tube, which was exposed to the sweep gas, became rough and porous after the exposure to CO<sub>2</sub>, while a smooth surface was observed for the fresh C6B2N2 membrane. However, the XRD pattern of the membrane after exposure to CO<sub>2</sub> shows no new phases (Figure 4.5), which can be explained by the decomposition of the carbonate and recovery of the perovskite structure in the CO<sub>2</sub>-rare atmosphere or that the trace amount of the carbonate is hard to be detected by XRD.

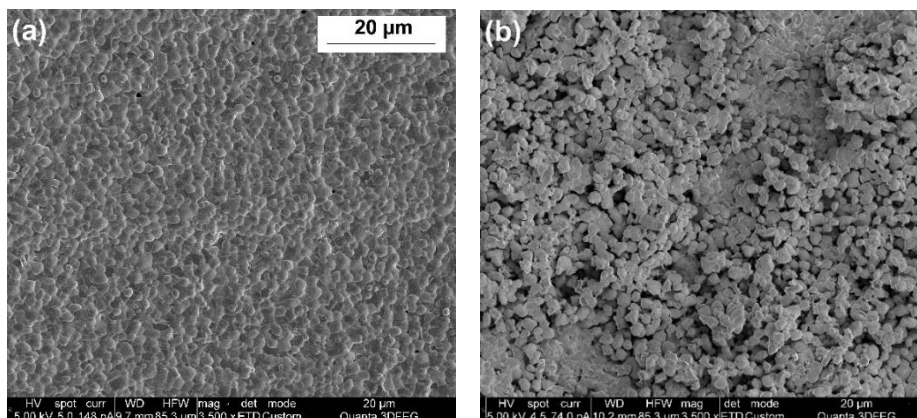


**Figure 4.8.** SEM images of the C6B2N2 membrane tube: (a) fresh inner surface and (b) inner surface after the permeation test with pure CO<sub>2</sub> as sweep gas at 850 °C.

When CO<sub>2</sub> was fed again to the permeate side of the C6B2N2 membrane, the permeation flux instantly dropped to 0.052 ml/min·cm<sup>2</sup> and then gradually reduced 0.043 ml/min·cm<sup>2</sup> (stage-4 in Figure 4.7). Then, as helium was switch back, the permeation value restored to 0.093 ml/min·cm<sup>2</sup>, which is at the similar level of curve-3, and this is because of the already-formed surface microstructure of the membrane. Similar trend was observed for the oxygen permeation of C4B4N2 when CO<sub>2</sub> and helium was fed alternatively to the permeate side, but permeability of the C4B4N2 seems to be less sensitive to the microstructure changes, that resulted from the CO<sub>2</sub> corrosion, compared to the C6B2N2 membrane.

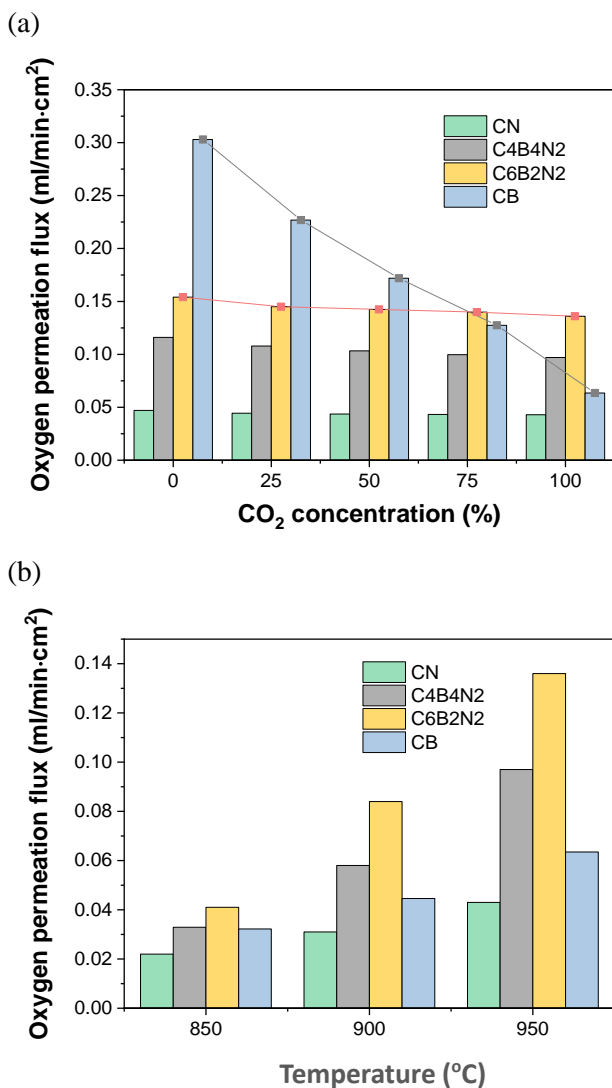


**Figure 4.9.** Permeation fluxes through the C6N4, C4B4N2, C6B2N2 and C6B4 membranes (a) with sweep gas of different CO<sub>2</sub> concentrations at 950 °C and (b) with pure CO<sub>2</sub> feed as the sweep gas at different temperatures.

Permeation of the two triple-phase membranes were compared with that of the C6B4 and C6N4 at 950 °C by feeding the sweep gas with varied CO<sub>2</sub>

concentrations. As can be seen in Figure 4.9a, although the oxygen fluxes through the C6B2N2 and C4B4N2 also declined with increased CO<sub>2</sub> concentration in the permeate side, the slopes of the permeation rates were much smaller than that of the C6B4 membrane. For instance, with 25 % CO<sub>2</sub> in the sweep gas, permeation flux through the C6B4 membrane reached 0.23 ml/min·cm<sup>2</sup>, but reduced by 74 % to 0.06 ml/min·cm<sup>2</sup> when feeding pure CO<sub>2</sub> to the permeate side, whereas the permeation rate of the C6B2N2 decreased from 0.15 ml/min·cm<sup>2</sup> to 0.14 ml/min·cm<sup>2</sup> with the CO<sub>2</sub> concentration in the sweep gas rising from 25 % to 100 %. The application of the triple-phase composites instead of the C6B4 and C6N4 promoted the oxygen permeation when the high CO<sub>2</sub>-containing sweep gas was fed to permeation side of the membranes.

Figure 4.9b gives the oxygen permeation flux through the C6N4, C6B2N2, C4B4N2 and C6B4 membranes with pure CO<sub>2</sub> fed as the sweep gas at varied temperatures. Permeation value of the four membranes all exhibited positive correlation with the temperature, and the triple-phase membranes showed higher permeability than both the C6N4 and C6B4 membranes at each temperature.

#### 4.4. Conclusions

Several CGO-based dual-phase and triple-phase membranes with a dead-end tubular geometry were fabricated. Performance of the membranes were compared at varied conditions. Three dual-phase membranes were obtained by paring BSCF, NFO and LNO oxides with CGO. Results of the oxygen permeation tests exhibited that the C6B4 membrane provided the highest permeation flux, and the constant activation energies reflected good phase stabilities of the three composites over the operation temperature range. CO<sub>2</sub>-tolerance of the membranes was investigated by feeding CO<sub>2</sub> and helium alternatively as the sweep gas. Large drop of the oxygen flux was observed for the C6B4 composites when CO<sub>2</sub> was fed instead of helium to the permeate side, but eventually a stable permeation was obtained which was still higher than that of the other two membranes. Two triple-phase membranes, C6B2N2 and C4B4N2, were fabricated with CGO, BSCF and NFO powders. The permeation values and corresponding activation energies obtained for the triple-phase composites were higher than that of the C6N4 but lower compared with that of the C6B4. When CO<sub>2</sub> was fed instead of helium as the sweep gas, the permeation fluxes through C6B2N2 and C4B4N2 exhibited only a small reduction compared to the C6B4 membrane, and the C6B2N2 was found to provide the highest oxygen permeability among all the dual-phase and triple-phase membranes investigated in this work, when 100 % CO<sub>2</sub> was fed as the sweep gas.

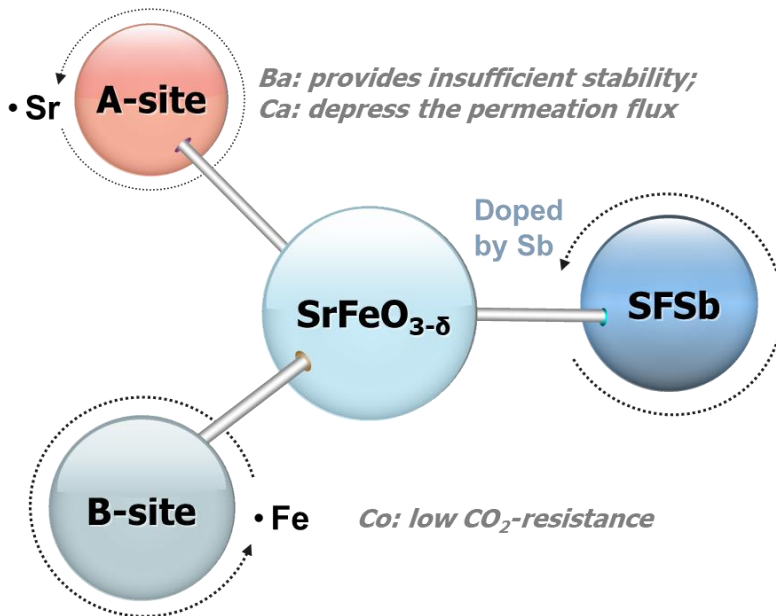
## References

- [1] B. Wang, J. Yi, L. Winnubst, C. Chen, Stability and oxygen permeation behavior of Ce<sub>0.8</sub>Sm<sub>0.2</sub>O<sub>2-δ</sub>-La<sub>0.8</sub>Sr<sub>0.2</sub>CrO<sub>3-δ</sub> composite membrane under large oxygen partial pressure gradients, *J. Memb. Sci.* 286 (2006) 22–25.
- [2] X. Zhu, M. Li, H. Liu, T. Zhang, Y. Cong, W. Yang, Design and experimental investigation of oxide ceramic dual-phase membranes, *J. Memb. Sci.* 394–395 (2012) 120–130.
- [3] J. García-Fayos, R. Ruhl, L. Navarrete, H. J. M. Bouwmeester, J. M. Serra, Enhancing oxygen permeation through Fe<sub>2</sub>NiO<sub>4</sub>-Ce<sub>0.8</sub>Tb<sub>0.2</sub>O<sub>2-δ</sub> composite membranes using porous layers activated with Pr<sub>6</sub>O<sub>11</sub> nanoparticles, *J. Mater. Chem. A.* 6 (2018) 1201–1209.
- [4] V. V. Kharton, A. V. Kovalevsky, A. P. Viskup, A. L. Shaula, F. M. Figueiredo, E. N. Naumovich, F. M. B. Marques, Oxygen transport in Ce<sub>0.8</sub>Gd<sub>0.2</sub>O<sub>2-δ</sub>-based composite membranes, *Solid State Ionics.* 160 (2003) 247–258.
- [5] J. Xue, Q. Zheng, Y. Wei, K. Yuan, Z. Li, H. Wang, Dual phase composite oxide of Ce<sub>0.9</sub>Gd<sub>0.1</sub>O<sub>2-δ</sub>-Ba<sub>0.5</sub>Sr<sub>0.5</sub>Co<sub>0.8</sub>Fe<sub>0.2</sub>O<sub>3-δ</sub> with excellent oxygen permeation, *Ind. Eng. Chem. Res.* 51 (2012) 4703–4709.
- [6] H. Luo, H. Jiang, K. Efimov, Influence of the preparation methods on the microstructure and oxygen permeability of a CO<sub>2</sub>-stable dual phase membrane, *AIChE J.* 57 (2011) 2738–2745.
- [7] S. K. Kim, M. J. Shin, J. Rufner, K. van Benthem, J. H. Yu, S. Kim, Sr<sub>0.95</sub>Fe<sub>0.5</sub>Co<sub>0.5</sub>O<sub>3-δ</sub>-Ce<sub>0.9</sub>Gd<sub>0.1</sub>O<sub>2-δ</sub> dual-phase membrane: Oxygen permeability, phase stability, and chemical compatibility, *J. Memb. Sci.* 462 (2014) 153–159.
- [8] M. Balaguer, J. García-Fayos, C. Solís, J.M. Serra, Fast oxygen separation through SO<sub>2</sub>- and CO<sub>2</sub>-stable dual-phase membrane based on NiFe<sub>2</sub>O<sub>4</sub>-Ce<sub>0.8</sub>Tb<sub>0.2</sub>O<sub>2-δ</sub>, *Chem. Mater.* 25 (2013) 4986–4993.
- [9] J. Xue, L. Chen, Y. Wei, H. Wang, CO<sub>2</sub>-stable Ce<sub>0.9</sub>Gd<sub>0.1</sub>O<sub>2-δ</sub>-perovskite dual phase oxygen separation membranes and the application in partial oxidation of methane to syngas, *Chem. Eng. J.* 327 (2017) 202–209.
- [10] N. Han, Q. Wei, H. Tian, S. Zhang, Z. Zhu, J. Liu, S. Liu, Highly Stable Dual-Phase Membrane Based on Ce<sub>0.9</sub>Gd<sub>0.1</sub>O<sub>2-δ</sub>-La<sub>2</sub>NiO<sub>4+δ</sub> for Oxygen Permeation under Pure CO<sub>2</sub>



- Atmosphere, Energy Technol. 7 (2019) 1–10.
- [11] H. Huang, S. Cheng, J. Gao, C. Chen, J. Yi, Phase-inversion tape-casting preparation and significant performance enhancement of  $\text{Ce}_{0.9}\text{Gd}_{0.1}\text{O}_{1.95}\text{-La}_{0.6}\text{Sr}_{0.4}\text{Co}_{0.2}\text{Fe}_{0.8}\text{O}_{3-\delta}$  dual-phase asymmetric membrane for oxygen separation, *Mater. Lett.* 137 (2014) 245–248.
- [12] J. Tong, W. Yang, B. Zhu, R. Cai, Investigation of ideal zirconium-doped perovskite-type ceramic membrane materials for oxygen separation, *J. Memb. Sci.* 203 (2002) 175–189.
- [13] H. Luo, H. Jiang, K. Efimov, F. Liang, H. Wang, J. Caro,  $\text{CO}_2$ -tolerant oxygen-permeable  $\text{Fe}_2\text{O}_3\text{-Ce}_{0.9}\text{Gd}_{0.1}\text{O}_{2-\delta}$  dual phase membranes, *Ind. Eng. Chem. Res.* 50 (2011) 13508–13517.
- [14] H. Cheng, L. Luo, W. Yao, X. Lu, X. Zou, Z. Zhou, Novel cobalt-free  $\text{CO}_2$ -tolerant dual-phase membranes of  $\text{Ce}_{0.8}\text{Sm}_{0.2}\text{O}_{2-\delta}\text{-Ba}_{0.95}\text{La}_{0.05}\text{Fe}_{1-x}\text{Zr}_x\text{O}_{3-\delta}$  for oxygen separation, *J. Memb. Sci.* 492 (2015) 220–229.
- [15] S. Liu, X. Tan, K. Li, R. Hughes, Synthesis of strontium cerates-based perovskite ceramics via water-soluble complex precursor routes, *Ceram. Int.* 28 (2002) 327–335.
- [16] O. Czuprat, M. Arnold, S. Schirmeister, T. Schiestel, J. Caro, Influence of  $\text{CO}_2$  on the oxygen permeation performance of perovskite-type  $\text{BaCo}_x\text{Fe}_y\text{Zr}_z\text{O}_{3-\delta}$  hollow fiber membranes, *J. Memb. Sci.* 364 (2010) 132–137.
- [17] W. K. Hong, G. M. Choi, Oxygen permeation of BSCF membrane with varying thickness and surface coating, *J. Memb. Sci.* 346 (2010) 353–360.

# Chapter 5 Co-free $\text{SrFe}_{0.8}\text{Sb}_{0.2}\text{O}_{3-\delta}$ -based membranes



*In this chapter, B-site doped  $\text{SrFeO}_{3-\delta}$  material was used for the preparation of oxygen transport membranes. New phases were observed on the surface of the SFSb membrane after the permeation test. Adding CGO into the membrane preparation recipe resulted in a better thermal stability of the membrane.*

## 5.1 Introduction

As elaborated in previous chapters, the operation condition for the oxygen transport membranes include the exposure to CO<sub>2</sub>-containing gases, which generates the demand for membranes with good chemical stability when operated in presence of CO<sub>2</sub>. Several dual-phase and triple-phase membranes have been fabricated and compared in Chapter 3 and Chapter 4, and some of these membranes provided good CO<sub>2</sub>-resistance. However, the fabrication cost of multi-phase composites can be relatively high compared with that of the single-phase membranes, and the high cost may limit the industrial application of those membranes. As a result, some doped single-phase oxides were adopted for the membrane fabrication by researchers with the purpose of developing low-cost CO<sub>2</sub>-tolerant membranes [1–7].

Perovskite material is an attractive candidate for the membrane assisted oxygen separation process under the premise of the good CO<sub>2</sub>-tolerance. ABO<sub>3-δ</sub> is the structural formula for ideal perovskite-type oxides. The A-site of the perovskite crystals can be occupied by alkaline earth metals, e.g. Sr, Ba or Ca, and/or lanthanides, e.g. Pr or La. The B-site cations are normally chosen from transition metals. The electronic conductivity of the membranes with a ABO<sub>3-δ</sub> crystal structure originates from the valence changes of the transition metals, while the oxygen ionic conductivity is mainly influenced by the oxygen non-stoichiometry [8]. Permeability as well as the chemical stability of the perovskites are strongly affected by the selection of the A-site and B-site metals. Using a rare earth metal instead of an alkaline earth element as the A-site cation would reduce the oxygen permeability. Ba-based perovskites usually show high oxygen permeability but rather low CO<sub>2</sub> stability [9]. Ca<sup>2+</sup> favour good chemical stability but disfavours the permeation flux [10]. Accordingly, Sr is a better choice as the A-site element among the alkaline earth metals. Co and Fe are the popular transition metals for

the B-site of the perovskite-type oxides because of the variable valence state [11]. Considering the relatively low CO<sub>2</sub>-resistance of the Co-containing perovskites, Fe is preferred for the B-site. Nevertheless, the SrFeO<sub>3-δ</sub> did not show sufficient CO<sub>2</sub> tolerance, so some other transition metals are applied to substitute the B-site elements with the purpose to improve the chemical stability of the material. A good dopant on the B-site provides high valence and high metal bond energy after doping. Ta, Ti, Nb, Sb, Mo and Zr are all the candidates that meet the requirements and may be suitable dopants for the perovskite oxides [12–14].

In this work, SrFe<sub>0.8</sub>Sb<sub>0.2</sub>O<sub>3-δ</sub> (SFSb), SrFe<sub>0.8</sub>Nb<sub>0.2</sub>O<sub>3-δ</sub> (SFN) and SrFe<sub>0.8</sub>Ta<sub>0.2</sub>O<sub>3-δ</sub> (SFT) green tubes are fabricated with the a phase-inversion casting method. However, SFN and SFT were found to react with the Al<sub>2</sub>O<sub>3</sub> holding plate at ultra-high sintering temperatures (1350 °C and 1400 °C), which restrained the shrinkage of the membrane during the sintering process and caused failure of the membrane. As a result, only the permeability and stability of SFSb were tested. According to the performance of the SFSb membrane, some CGO-SFSb membranes are prepared, the performance of which are compared with that of the single-phase membranes.

## 5.2 Experimental methods

### 5.2.1. Manufacturing of the membranes

SFSb powders used for the preparation of the single-phase and dual-phase membranes were supplied by Marion Technologies, while the CGO powders used for the fabrication of CGO-BSCF membranes were also applied as the ionic-conductive phase in the CGO-SFSb membranes. 5 g PES and 1 g PVP were added into 20 g NMP to obtain a polymer solution after mixing for 30 min. 45 g ceramic powders were mixed with the polymer solution for preparation of the casting slurries. For the CGO- SFSb dual-phase membrane, the weight ratio between CGO and SFSb is 60 : 40.

Dead-end green membrane tubes were prepared with the phase-inversion casting method reported in Chapter 3. Both of the green SFSb and CGO-SFSb dual-phase membranes were sintered at 1310 °C for 4 hr. It is noticeable that, although the reaction between SFSb and the alumina plate is not as obvious as that of the SFN and SFT membranes due to the lower sintering temperature, the reaction can also cause the SFSb membrane stick to the holding plate. To solve this problem, a thick layer of MgO powders was spread between the SFSb membrane and the plate during the sintering process. Contrary, the CGO-SFSb dual-phase membrane was placed directly on the alumina plate, since the presence of CGO depressed the reaction.

### 5.2.2. Characterisation and permeation test

Microstructure of the membranes were observed with the secondary electron detector (SED) of SEM (Phenom ProX), while the backscattered electron detector (BSD) was used to detect the phase composition. EDX-point and mapping were applied to investigate the element distribution on the membrane surface and phase

structure of the membranes after sintering and permeation test were determined with the assistance of XRD.

Permeability and CO<sub>2</sub>-stability of the membranes were tested in the high-temperature experimental setup with air as the feed gas and He/CO<sub>2</sub> as sweep gas. The dead-end membranes were sealed with the gas-tight Fe-Cr tube with an Ag-Cu paste, which was densified at 1020 °C.

## 5.3 Results and discussion

### 5.3.1 Performance of the SFSb membrane

Figure 5.1(a, b) give the XRD patterns of the SFSb powders and the fresh SFSb membrane after sintering process, respectively. It shows that SFSb retained the major phase after sintering at ultra-high temperature, but very small peaks of  $\text{SrSO}_4$  can be observed in the plot of the fresh membrane.

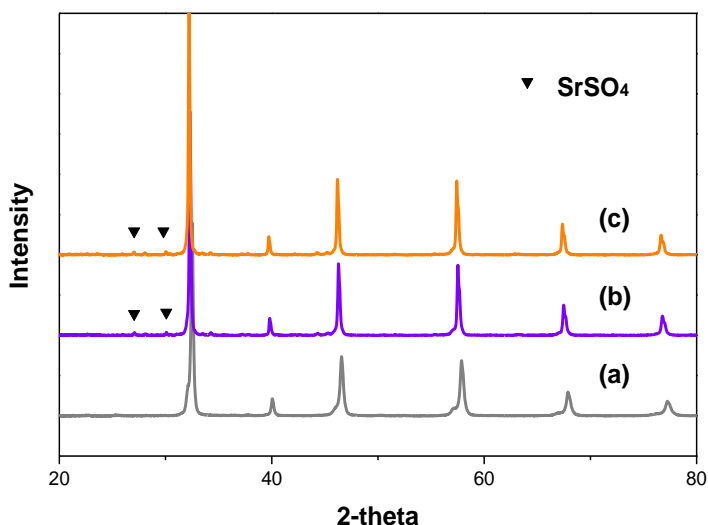


**Figure 5.1.** XRD patterns of (a) SFSb powders, (b) fresh SFSb membrane and (c) SFSb membrane after permeation test with  $\text{CO}_2$  as sweep gas.

The reason for the formation of the trace amount of  $\text{SrSO}_4$  is assumed to be the reaction between the Sr in SFSb with the  $\text{SO}_2$  released during the polymer (PES) burning. The amount of  $\text{SrSO}_4$  formed on the SFSb membrane is relatively small compared to that of the  $\text{BaSO}_4$  formed on the CGO-BSCF membranes (Figure 3.7), because Ba-containing perovskites exhibit a lower chemical stability in  $\text{SO}_2$

atmosphere.

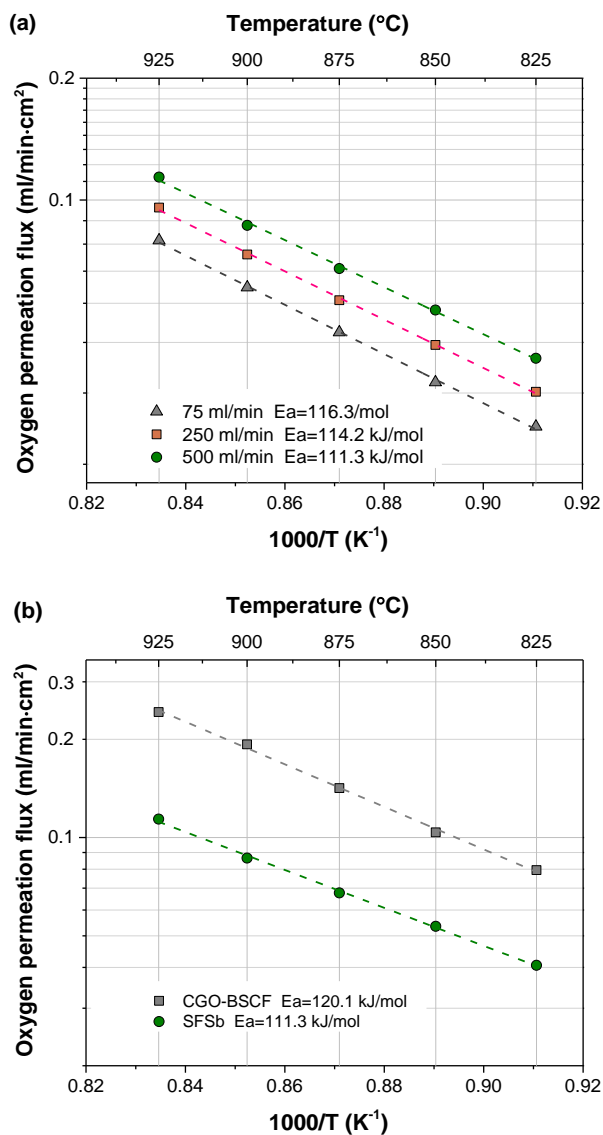
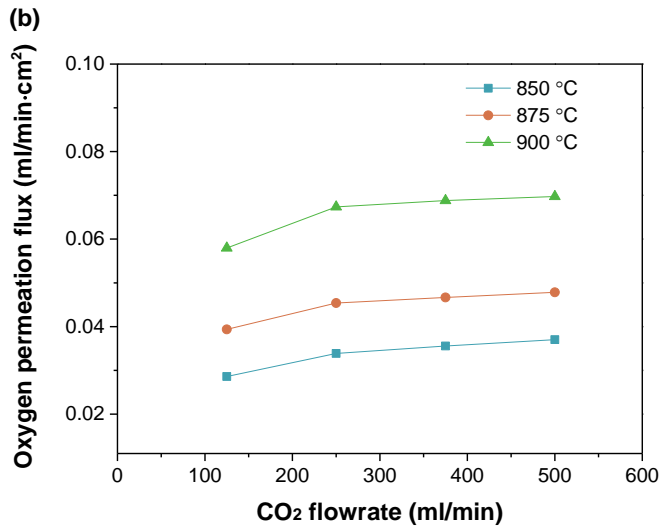
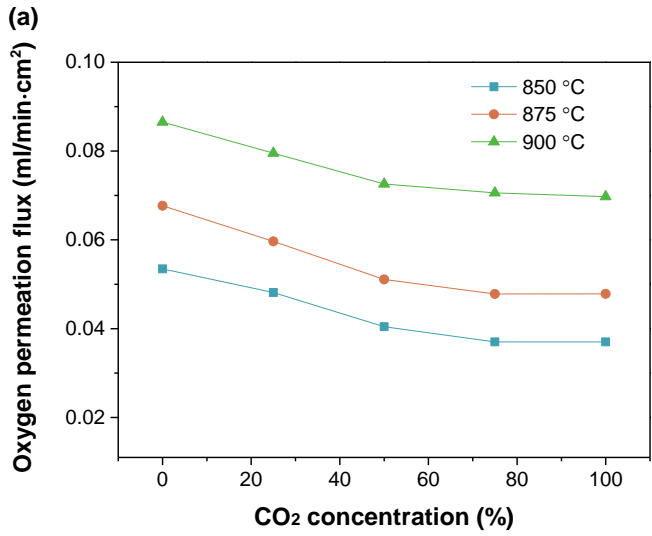


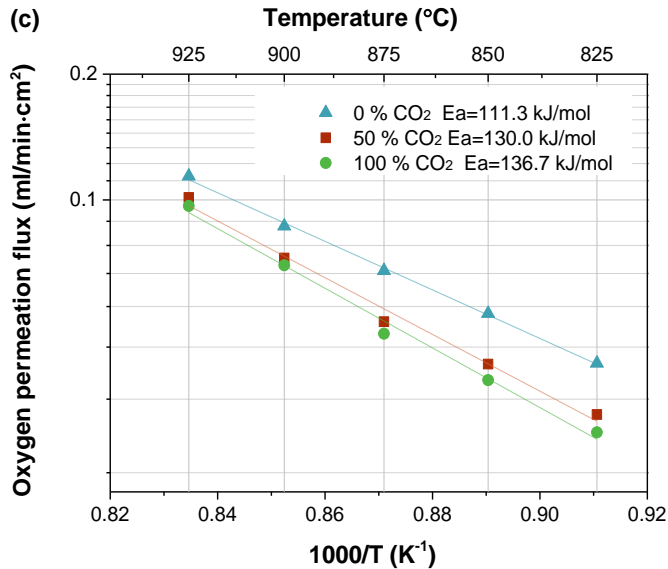
**Figure 5.2.** (a) Temperature dependence of the permeation fluxes through the SFSb membrane with varied flowrates of the sweep gas; (b) comparison of the permeation fluxes through CGO-BSCF and SFSb membranes.



The oxygen fluxes through the SFSb single-phase membrane as a function of temperature were measured at different He flowrates. As shown in Figure 5.2, the increases in the sweep gas flow rate and the operation temperature both resulted in higher permeation fluxes. For example, when the flowrate of He was 250 ml/min, the oxygen permeation flux through the membrane was 0.034 ml/min·cm<sup>2</sup> at 825 °C, which increased to 0.096 ml/min·cm<sup>2</sup> at 925 °C, while the permeation flux increased from 0.041 ml/min·cm<sup>2</sup> to 0.114 ml/min·cm<sup>2</sup> with the temperature raised from 825 °C to 925 °C at the He flowrate of 500 ml/min. The activation energies for oxygen permeation through SFSb appeared to be constant over the test temperature range with different flowrates of sweep gas, and only a slight rise of the activation energy was observed for a lower He sweep flow rate.

The permeation fluxes through the SFSb and CGO-BSCF membranes are compared in Figure 5.2b. The CGO-BSCF dual-phase composite provided higher permeation fluxes than the SFSb membrane, e. g. at the 925 °C the oxygen fluxes through the CGO-BSCF and SFSb membranes are 0.114 ml/min·cm<sup>2</sup> and 0.242 ml/min·cm<sup>2</sup>, respectively. However, the dual-phase membrane also exhibited higher activation energy than the SFSb membrane which can be attributed to the travel of oxygen ions through the borders between the two phases of the CGO-BSCF membrane.

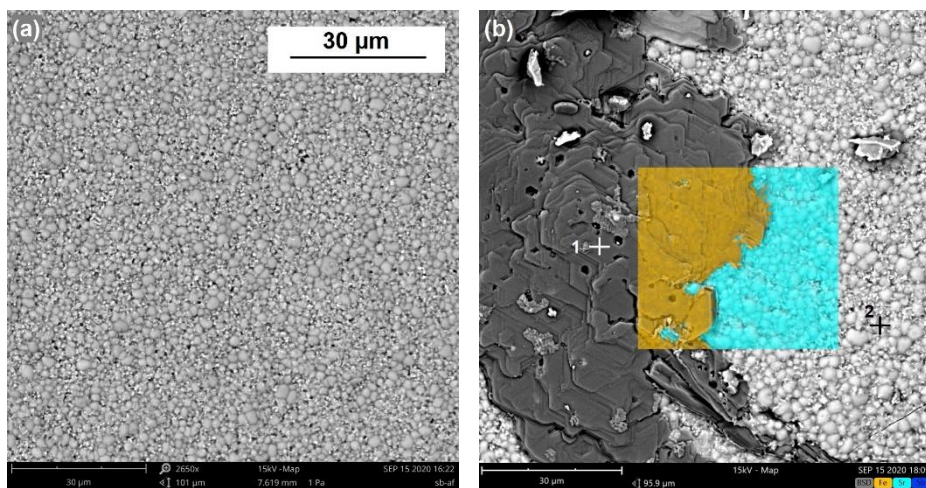




**Figure 5.3.** Permeation fluxes through the SFSb membrane as functions of (a) CO<sub>2</sub> concentration and (b) flowrate of CO<sub>2</sub> at different temperatures; (c) Arrhenius plots of the permeation through the SFSb membrane with pure CO<sub>2</sub> as sweep gas.

Subsequently, CO<sub>2</sub> was introduced into the sweep gas to test chemical stability of the SFSb membrane. Figure 5.3a gives the effect of CO<sub>2</sub> concentration in the sweep gas on permeability of the SFSb membrane with a fixed sweep gas flowrate of 500 ml/min. It is clear that adding more CO<sub>2</sub> in the sweep gas depressed the permeability of the membrane. The permeation flux was 0.080 ml/min·cm<sup>2</sup> when 25 % CO<sub>2</sub>-containing sweep gas was applied to the permeate side and the flux dropped to 0.070 ml/min·cm<sup>2</sup> when the CO<sub>2</sub> concentration was increased to 100 % at 900 °C. Permeation of oxygen was blocked by the adsorption of CO<sub>2</sub> on the membrane. Then, pure CO<sub>2</sub> with varied flowrates was used to sweep the membrane for the permeation test. It can be seen in Figure 5.3b that similar to the case using He as sweep gas the permeability of the membrane rose with increased flowrate of CO<sub>2</sub> due to the increased oxygen partial pressure difference across the

membrane. Similarly, a rise of the operation temperature brought an increase of the membrane permeability even with pure CO<sub>2</sub> fed as sweep gas (Figure 5.3c), which is due to the enhanced surface-exchange and bulk-diffusion rate. The activation energies of the oxygen permeation with different CO<sub>2</sub> concentration in the sweep gas are also given in Figure 5.3c. The activation energy was 111.3 kJ/mol when the membrane was swept with pure He but increased to 126.7 kJ/mol when the sweep gas was switched to pure CO<sub>2</sub>. This can be explained by the lower oxygen vacancies on the membrane surface due to the adsorption of CO<sub>2</sub>. It should be noted that, when swept with pure CO<sub>2</sub>, performance of the SFSb membrane is better than that of the CGO-BSCF dual-phase membrane, for instance, a permeation flux of 0.070 ml/min·cm<sup>2</sup> was measured for the SFSb membrane at 900 °C, which was only 0.044 ml/min·cm<sup>2</sup> for the CGO-BSCF membrane at the same condition (Figure 4.3b).



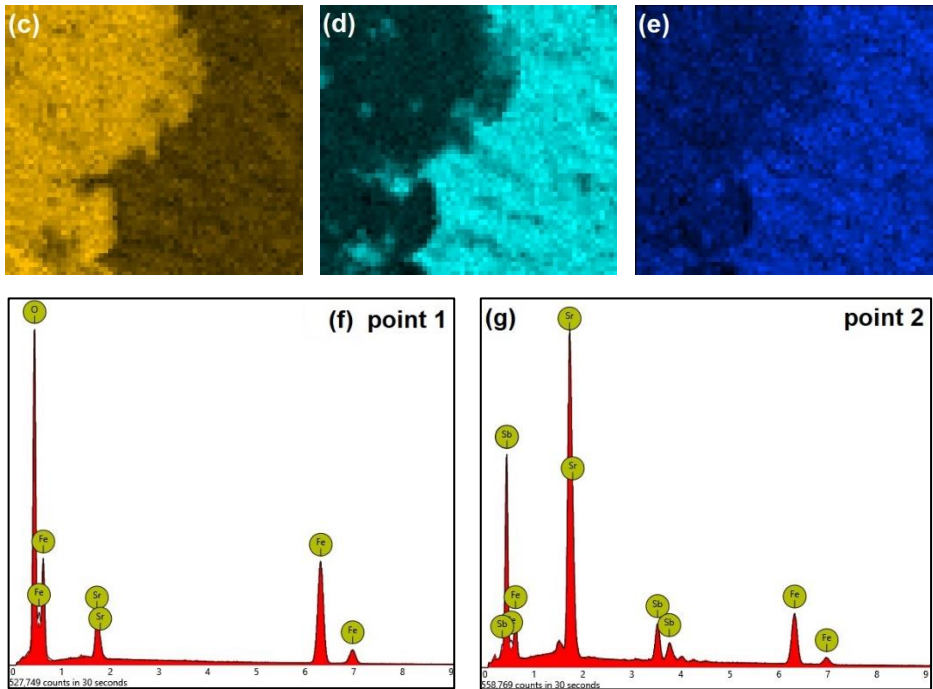
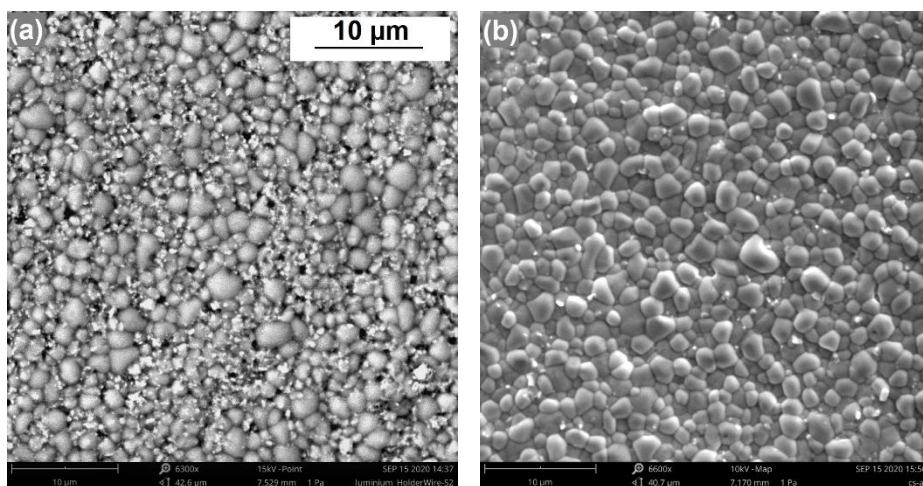


**Figure 5.4.** BSD microscopy of the SFSb membrane (a) before and (b) after the permeation test; (c) EDS-mapping of Fe; (d) EDS-mapping of Sr; (e) EDS-mapping of Sb (f, g) EDS analysis of two points on the membrane surface.

The SEM images of the SFSb membrane before and after the permeation test is given in Figure 5.4(a, b). A large amount of new phase was found on the membrane surface after the permeation test. EDS mapping and point analysis embedded in the SEM were used to identify the element composition of the new phase. The Figure 5.4(c-g) exhibit that this new phase is enriched with Fe and O, so it can be inferred from the EDS results that some iron oxides precipitated during the high-temperature operation of the SFSb membrane. To further investigate the reason for the formation of the new phase, a piece of fresh SFSb membrane was heated up to 950 °C and kept for 3 days in air. It was found that even without the oxygen partial pressure difference or CO<sub>2</sub> contact, there was still some new phase precipitated from the SFSb oxide at high temperature, which

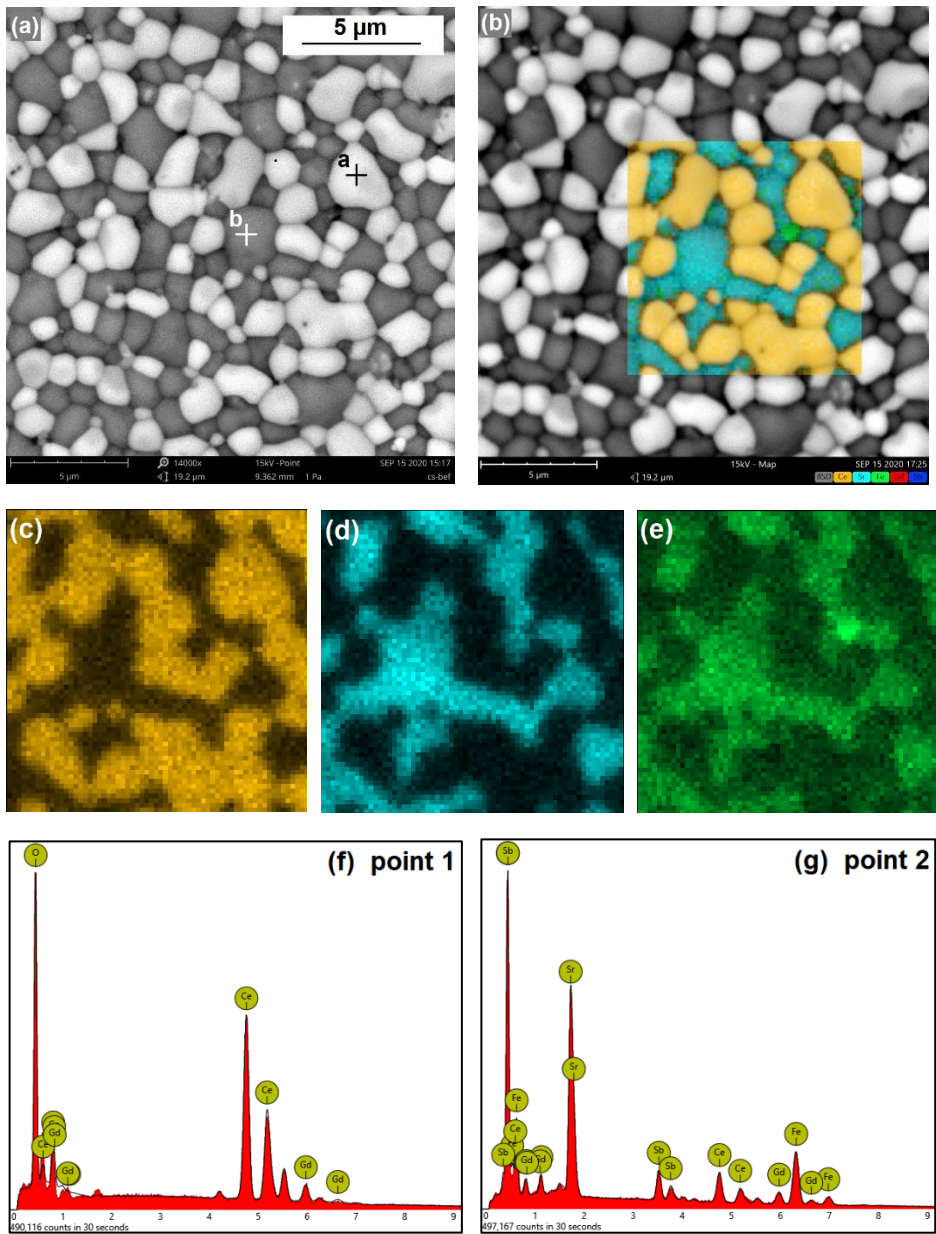
proved the thermal instability of the material for long-term operation.

### 5.3.2 Comparison between the SFSb and CGO-SFSb dual-phase membranes



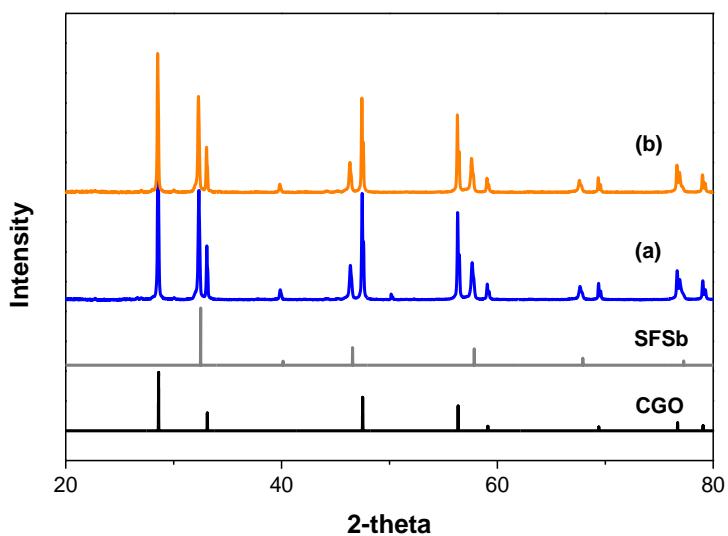
**Figure 5.5.** SED microscopy of (a) SFSb membrane and (b) CGO-SFSb dual-phase membrane.

Considering the thermal instability of the SFSb membrane and the reaction of the material with the alumina plate during the sintering process, some CGO powders were mixed into the casting slurry for the fabrication of the CGO-SFSb dual-phase membrane. Microstructure of the SFSb and CGO-SFSb membranes were observed with the assistance of the SED in SEM (Figure 5.5). Although no large leakage was detected, some small holes can be observed on the SFSb single-phase membrane, which means inferior sintering temperature. In comparison, the CGO-SFSb membrane which was sintered at the same condition was found to be free of obvious defects and holes from the SEM images, and this result indicates that the CGO powders can act as sintering aid for the SFSb membrane.



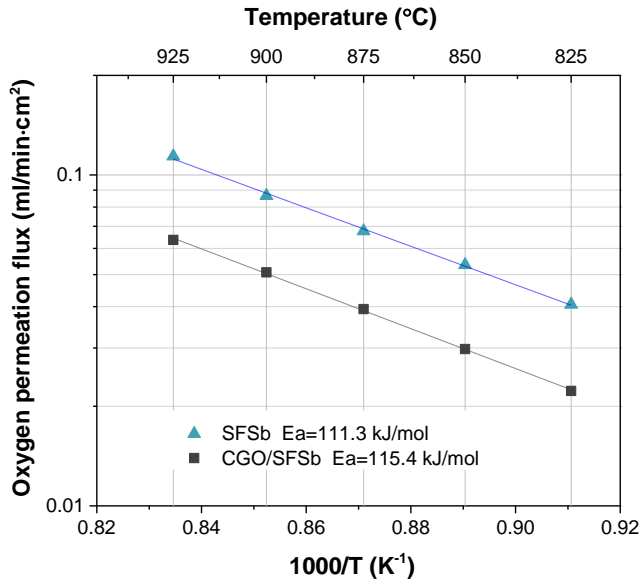
**Figure 5.6.** (a) BSD microscopy of the CGO-SFSb membrane; (b) combined EDS-mapping (c) EDS-mapping of Ce; (d) EDS-mapping of Sr; (e) EDS-mapping of Fe (f, g) EDS analysis of two points on the membrane surface.

Phase composition of the sintered dual-phase membrane was determined with SEM and the EDS analysis. With the BSD of SEM, two phases in light and dark grey, respectively, can be observed. The two phases showed similar grain size of 1-3  $\mu\text{m}$ . According to the EDS analyse, the light grey grains are supposed to be CGO, while the darker ones are SFSb. No new phases were observed for the fresh sintered dual-phase membrane from the SEM and XRD analysis (Figure 5.7), however weak signals of Ce and Gd were detected in the SFSb phase. A similar phenomenon was observed for the triple-phase membranes in Chapter 4.



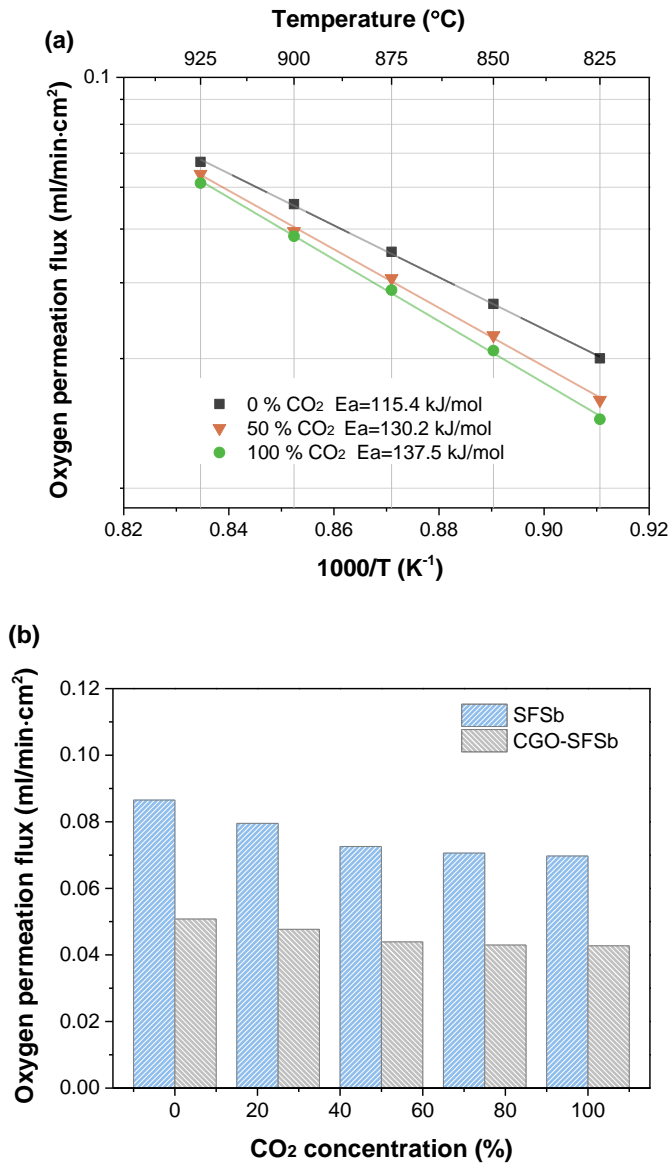
**Figure 5.7.** XRD patterns of (a) fresh CGO-SFSb membrane and (b) CGO-SFSb membrane after permeation test in CO<sub>2</sub>-atmosphere





**Figure 5.8.** Permeation fluxes through SFSb and CGO-SFSb dual-phase membranes at different temperatures.

The oxygen permeation rate through the SFSb and CGO-SFSb dual-phase membranes are compared in Figure 5.8. Over the test temperature range, the SFSb single-phase membrane provided higher permeability together with a slightly lower activation energy compared with the CGO-SFSb membrane. With a He flowrate of 500 ml/min, the oxygen permeation flux through the SFSb membrane is 0.114 ml/min·cm<sup>2</sup> at 925 °C, which is 0.040 ml/min·cm<sup>2</sup> higher than that of the dual-phase composites at the same operation temperature. Adding CGO into the membrane recipe depressed permeability of the SFSb membrane.



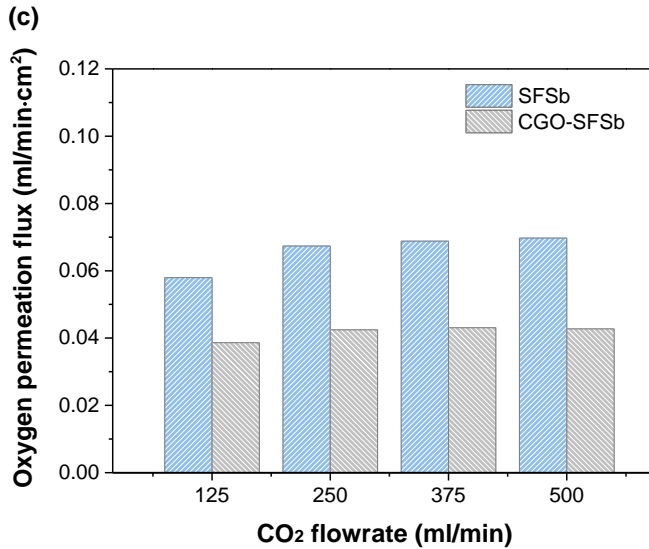


**Figure 5.9.** (a) Permeation fluxes through the CGO-SFSb membrane as a function of temperature with different CO<sub>2</sub> concentrations in the sweep gas; Permeation fluxes comparison between the CGO-SFSb and SFSb membranes with (b) different CO<sub>2</sub> concentration in the sweep gas and (c) different sweep gas flowrates.

Figure 5.9 (a) compares the oxygen permeation evolution trends with temperature when the CGO-SFSb membrane was swept with pure Helium, 50% CO<sub>2</sub> and 100% CO<sub>2</sub>. Similar to the results obtained for the SFSb membrane, increased temperature brought in higher permeation fluxes even with pure CO<sub>2</sub> as sweep gas, and improved CO<sub>2</sub> concentration in the permeate side increased the activation energy for oxygen permeation.

The permeabilities of the CGO-SFSb and SFSb single-phase membranes were compared by feeding 500 ml/min sweep gas of different CO<sub>2</sub> concentrations (Figure 5.9b). The permeation fluxes through SFSb membrane were found to be higher than that of the dual-phase membrane at each CO<sub>2</sub> concentration in the sweep gas. Then the permeability of the SFSb membrane was compared with that

of the CGO-SFSb membrane by feeding pure CO<sub>2</sub> of different flowrates to the permeate side of the membranes. It can be observed from Figure 5.9c that higher CO<sub>2</sub> flowrates led to higher permeation fluxes through both of these two membranes, and adding CGO in the preparation recipe caused lower permeability at each flowrate of CO<sub>2</sub>. However, according to the SEM images (Figure 5.10) and XRD analysis (Figure 5.7) no new phases were formed in the membrane after the permeation test, which suggests better operation stability of the CGO-SFSb membrane compared with that of the SFSb membrane.

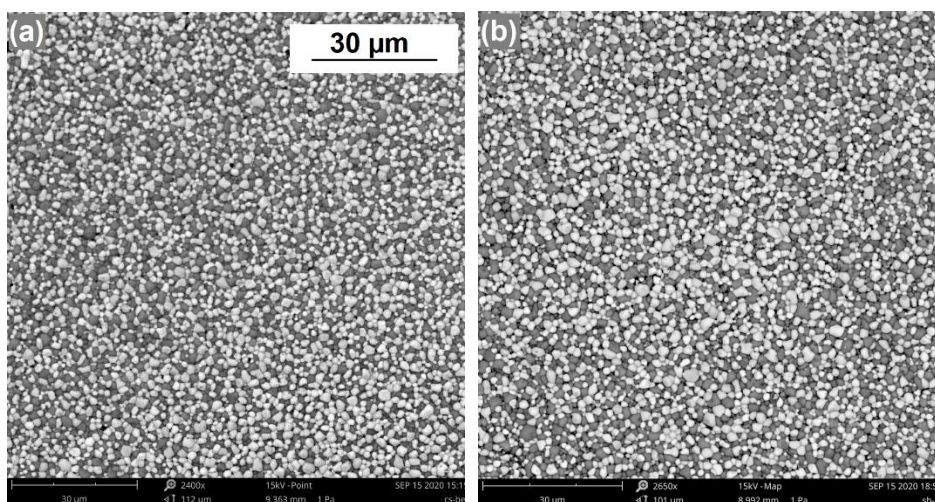


**Figure 5.10.** BSD microscopy of the CGO-SFSb membrane (a) before and (b) after the permeation test.

## 5.4 Conclusions

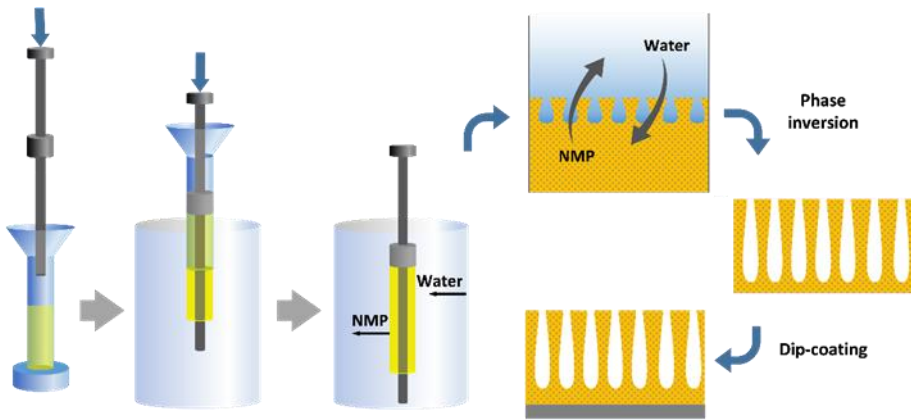
B-site doped  $\text{SrFeO}_{3-\delta}$  material was used for the preparation of oxygen transport membranes. The resulted SFSb membrane showed lower permeability than the CGO-BSCF dual-phase membrane but better performance when swept with pure  $\text{CO}_2$ . An increase in temperature and sweep gas flowrate led to higher permeability of the SFSb membrane when pure  $\text{CO}_2$  was used as the sweep gas. SEM images of the SFSb membrane exhibited new phases formed after operation at high temperature, which indicated a low thermal stability of the material. To solve the problem, CGO was mixed with the SFSb forming a dual-phase membrane. The CGO-SFSb membrane showed lower permeability than the SFSb membrane with either He or  $\text{CO}_2$  as sweep gas, however no phase precipitation was observed on the dual-phase membrane after the permeation test, indicating improved thermal stability of this dual phase CGO-SFSb membrane.

## References

- [1] F. Schulze-Küppers, S. F. P. Ten Donkelaar, S. Baumann, P. Prigorodov, Y. J. Sohn, H. J. M. Bouwmeester, W. A. Meulenber, O. Guillon, Structural and functional properties of SrTi<sub>1-x</sub>Fe<sub>x</sub>O<sub>3-δ</sub> (0 ≤ x ≤ 1) for the use as oxygen transport membrane, *Sep. Purif. Technol.* 147 (2015) 414–421.
- [2] F. Lohne, J. Gurauskis, T. N. Phung, M. A. Einarsrud, T. Grande, H. J. M. Bouwmeester, K. Wiik, Effect of B-site substitution on the stability of La<sub>0.2</sub>Sr<sub>0.8</sub>Fe<sub>0.8</sub>B<sub>0.2</sub>O<sub>3-δ</sub>, B=Al, Ga, Cr, Ti, Ta, Nb, *Solid State Ionics.* 225 (2012) 186–189.
- [3] H. Luo, Y. Wei, H. Jiang, W. Yuan, Y. Lv, J. Caro, H. Wang, Performance of a ceramic membrane reactor with high oxygen flux Ta-containing perovskite for the partial oxidation of methane to syngas, *J. Memb. Sci.* 350 (2010) 154–160.
- [4] K. Partovi, F. Liang, O. Ravkina, J. Caro, High-flux oxygen-transporting membrane Pr<sub>0.6</sub>Sr<sub>0.4</sub>Co<sub>0.5</sub>Fe<sub>0.5</sub>O<sub>3-δ</sub>: CO<sub>2</sub> stability and microstructure, *ACS Appl. Mater. Interfaces.* 6 (2014) 10274–10282.
- [5] T. Klande, O. Ravkina, A. Feldhoff, Effect of A-site lanthanum doping on the CO<sub>2</sub> tolerance of SrCo<sub>0.8</sub>Fe<sub>0.2</sub>O<sub>3-δ</sub> oxygen-transporting membranes, *J. Memb. Sci.* 437 (2013) 122–130.
- [6] W. Chen, C. S. Chen, L. Winnubst, Ta-doped SrCo<sub>0.8</sub>Fe<sub>0.2</sub>O<sub>3-δ</sub> membranes: Phase stability and oxygen permeation in CO<sub>2</sub> atmosphere, *Solid State Ionics.* 196 (2011) 30–33.
- [7] Y. Han, J. Yi, X. Guo, Improving the chemical stability of oxygen permeable SrFeO<sub>3-δ</sub> perovskite in CO<sub>2</sub> by niobium doping, *Solid State Ionics.* 267 (2014) 44–48.
- [8] J. Sunarso, S. Baumann, J. M. Serra, W. A. Meulenber, S. Liu, Y. S. Lin, J. C. Diniz da Costa, Mixed ionic-electronic conducting (MIEC) ceramic-based membranes for oxygen separation, *J. Memb. Sci.* 320 (2008) 13–41.
- [9] J. Yi, T. E. Weirich, M. Schroeder, CO<sub>2</sub> corrosion and recovery of perovskite-type BaCo<sub>1-x-y</sub>Fe<sub>x</sub>Nb<sub>y</sub>O<sub>3-δ</sub> membranes, *J. Memb. Sci.* 437 (2013) 49–56.

- [10] K. Efimov, T. Klande, N. Juditzki, A. Feldhoff, Ca-containing CO<sub>2</sub>-tolerant perovskite materials for oxygen separation, *J. Memb. Sci.* 389 (2012) 205–215.
- [11] M. Arnold, Q. Xu, F. D. Tichelaar, A. Feldhoff, Local charge disproportion in a high-performance perovskite, *Chem. Mater.* 21 (2009) 635–640.
- [12] N. C. Jeong, J. S. Lee, E. L. Tae, Y. J. Lee, K. B. Yoon, Acidity scale for metal oxides and Sanderson's electronegativities of lanthanide elements, *Angew. Chemie - Int. Ed.* 47 (2008) 10128–10132.
- [13] J. Yi, M. Schroeder, M. Martin, CO<sub>2</sub>-tolerant and cobalt-free SrFe<sub>0.8</sub>Nb<sub>0.2</sub>O<sub>3-δ</sub> perovskite membrane for oxygen separation, *Chem. Mater.* 25 (2013) 815–817.
- [14] P. Engineering, C. Zhang, Novel ceramic membranes for gas separation in enabling the clean energy delivery, (2016).

# Chapter 6 Supported membranes fabricated with a combined phase-inversion and dip-coating process



*Conventional preparation methods of membrane supports usually result in highly tortuous channels with relatively high mass transfer resistance. In this chapter, tubular porous MgO and MgO/CGO supports with finger-like channels were fabricated with the phase inversion casting method. These supports were used to produce thin-film supported CGO membranes. Compatible shrinkage behaviours of the two layers was realized and gas-tight membranes were obtained by adjusting the slurry composition for membrane preparation.*

***This chapter is based on the paper: Microstructure control of tubular micro-channelled supports fabricated by the phase inversion casting method. Processes, 2019, 7(6): 322.***



## 6.1. Introduction

The membranes reported in previous chapters showed good chemical stability but comparatively low permeability of oxygen because of the relatively large membrane thickness. As a simple way to achieve high oxygen fluxes, thin-film membranes are preferred for separation processes. Since a reduced membrane thickness is accompanied with lower mechanical stability, the thin-film membrane layers are usually coated onto porous supports resulting in asymmetric membrane structures [1–7].

Thermoplastic extrusion is frequently used to produce tubular substrates for asymmetric membranes. Pores in the support tubes are formed by burning of the sacrificial phases, which are added to the paste prepared before the extrusion process. The resulting support tubes usually show a sponge-like microstructure. Although compared with the single-layer membranes, improved oxygen permeability has been achieved by coating thin-film membrane layers on to porous supports, the highly tortuous channels in the sponge-like support layer (Figure 6.1a) still result in mass transfer resistances that limit the oxygen flux. To further decrease the gas transfer resistance, phase inversion can be used for preparation of membrane substrates showing low tortuosity. In this process, no pore formers need to be introduced into the ceramic paste. Instead of connected pores, finger like channels are formed because of the solvent replacement with water. The channels provide comparatively short path for gas transfer through the membrane support, which is shown in Figure 6.1b.

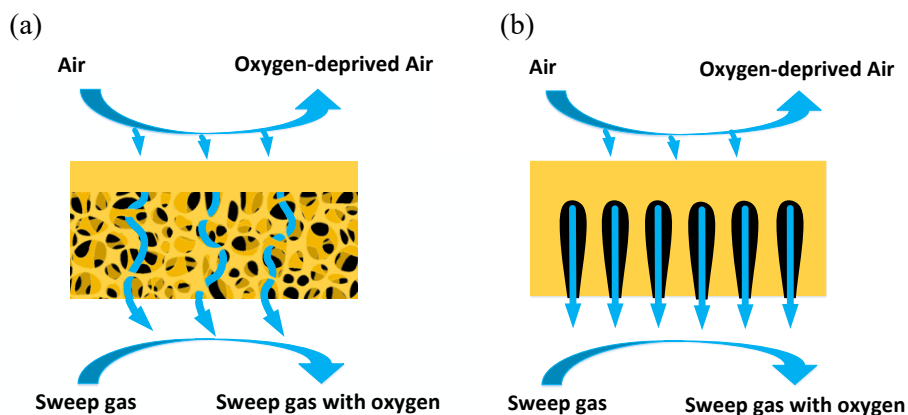


**Figure 6.1.** Schematic illustration of gas transport through porous supports with (a) sponge-like microstructure and (b) micro channels.

In this chapter, the modified phase inversion casting process is applied to fabricate MgO and MgO-CGO dual-phase support tubes. CGO layers were coated onto the substrates with dip-coating method. The effect of ceramic and polymer concentrations, particle size of the ceramic powders and the introduction of ethanol inside the casting slurries on the micro-channel size and tube shrinkage speed during sintering process were investigated to obtain MgO-CGO supports with a low mass transfer resistance and to achieve compatible shrinkage behaviour of the membrane layers and supports.

## 6.2. Materials and Methods

### 6.2.1. Materials

MgO powders purchased from VWR were used as the support tube material. CGO powders supplied from Ningbo Sofcman Energy were used as the second phase in the support tube, after milling for 1 h in a planetary ball mill. The influence of particle surface area on the channel growth was studied by applying two other kinds of CGO powders provided by Solvay and Marion Technologies, respectively, which were also ball milled for 1 h before adding them into the slurries.

The milled CGO powders from Ningbo Sofcman Energy were used for the membrane layer fabrication. PVP and PVB purchased from Sigma-Aldrich were used as the dispersant and binder in the suspensions for the dip-coating process, while ethanol (absolute, VWR, Pennsylvania, USA) was employed as the solvent.

### 6.2.2. Phase inversion casting for support tube preparation

For preparing the casting slurries, first, PES and PVP were fully dissolved into NMP to form polymer solutions in the mixer reported in Chapter 3. MgO and CGO powders (or only MgO powders) were mixed successively with the solutions to form the slurry. The PVP concentration (weight ratio of PVP over PVP+NMP) was fixed at 3.2 wt%, while the ceramic loadings (the weight ratio of CGO+MgO to CGO+MgO+NMP) were varied from 43 wt% to 60 wt% and a range of polymer concentrations (weight ratio of PES to PES+NMP) from 11 wt% to 25 wt% was selected to investigate their influence on the microstructure and shrinkage of the support tubes.

The phase-inversion casting process employed for the preparation of the micro-

channelled support tubes is schematically depicted in Figure 6.2. The same casting device as in the previous chapters was used for preparation of the support tubes. An appropriate amount of the de-foamed slurry was used in the mould and pushed inside the device with a piston for driving air out. Then the slurry was pushed out into water with the piston at a controlled speed. The slurry was kept inside water for 12 h at a temperature of 20 °C. Afterward, the green tube was taken off from the piston and dried at room temperature for 48 h before deposition of the membrane layer, because wet surfaces of the porous supports would result in non-uniform membrane layer formation. Outer and inner diameters of the obtained green support tubes were ~12 mm and ~8 mm, respectively.

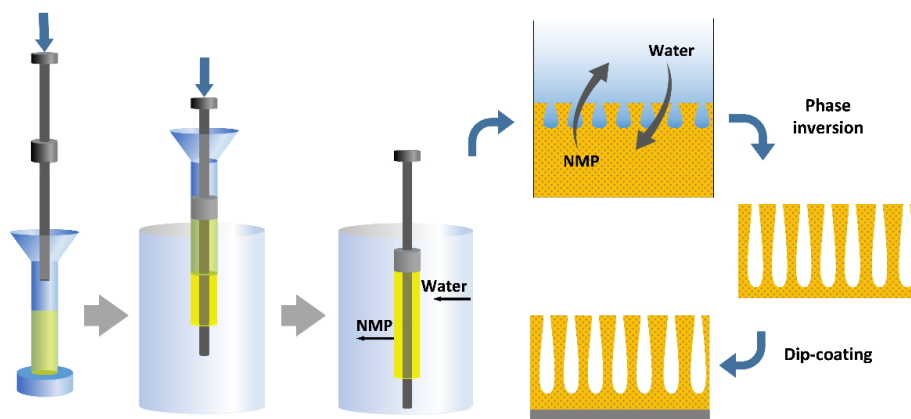


**Figure 6.2.** Schematic representation of the supported membrane preparation process by combined phase-inversion casting and dip-coating method.

### **6.2.3. Fabrication of membrane layer**

CGO membrane layers were coated onto the green tubular supports by a dip-coating method. Because the micro-channels grew from outside surface of the porous supports in the water bath, CGO membrane layers were coated inside, while the external surface of the tubes was covered with plastic films during the

dip-coating process. Before the dip-coating process, an ethanol-based suspension with a concentration of 23.9 wt% CGO, 2.4 wt% PVP and 1.9 wt% PVB was prepared with the planetary centrifugal mixer. Similar as for the preparation of the casting slurries, PVP and PVB were firstly added into ethanol to make a solution and subsequently the CGO powders were mixed with the solution at a speed of 1850 rpm for 30 min. An automatic dip-coater was employed to dip-coat membrane layers onto the green support tubes. The thickness of the membranes could be precisely controlled by programming the dip-coating speed and times with the dip-coater. The tubes were coated three times to achieve desirable gas-tightness by increasing the thickness of the coating.

The sintering process is of great importance for the fabrication of asymmetric membranes. After drying at room temperature, the membrane layers were sintered together with the green support tubes at 1350 °C for 2 h to form ceramic membranes with good mechanical strength. A heating rate of 30 °C/h was employed to increase the oven temperature to 1350 °C. The low heating rate is required because of two reasons. Firstly, uneven heating could break the ceramic supports and lower heating rate provides enough time for each part of the tubes to reach a uniform temperature. Besides, faster heating rate could result in a larger difference in strain rate between the membrane layers and the support tubes, which would cause cracks on the membrane layers. After sintering, the samples were cooled down inside the oven with a speed of 60 °C/h.

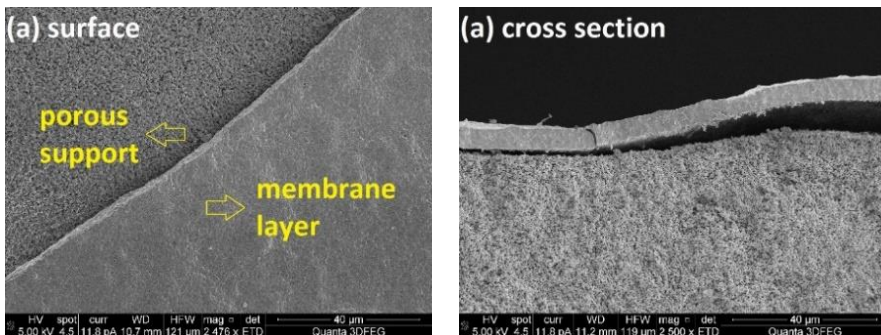
#### ***6.2.4. Analysis of the membranes***

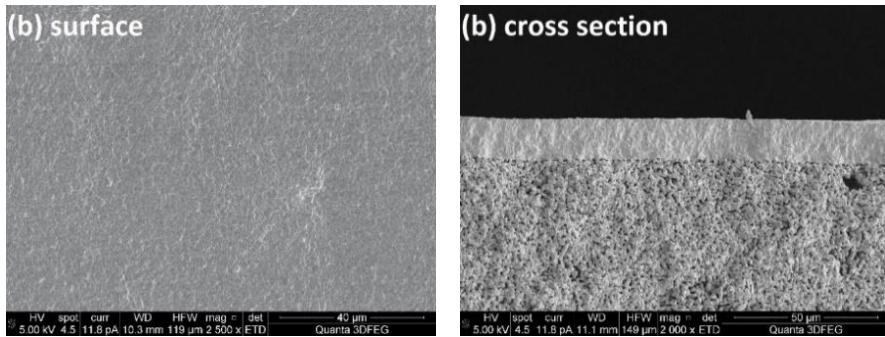
The microstructure of the tubular asymmetric membranes was observed with SEM (Quanta). The element distribution of the CGO-MgO dual-phase supported CGO membrane was obtained using the EDX mapping (Phenom). The specific surface area of the ceramic powders was measured with BET nitrogen adsorption

isotherm (TriStar II, Micromeritics) and the slurry viscosity was determined with the same rheometer reported in Chapter 3. Nitrogen permeation measurements were conducted to test the mass transfer resistance of the support tubes. The setup for the permeability test mainly consisted of a chamber, a gas supply unit and a film flow meter (STEC SF, Horiba). The membranes were introduced into the chamber after being sealed with some metal tubes. Nitrogen was fed into the membranes through the tubes using a mass flow controller and the nitrogen permeated through the porous supports was collected at the shell side and sent to the flow meter for the flow rate measurement. In this work, we are only interested in the gas tightness of the membranes, thus no perm-selectivities and oxygen fluxes have been measured. The chemical stability of the dual-phase supported membrane was tested in pure CO<sub>2</sub> atmosphere at 850 °C for 500 min. The flowrate of CO<sub>2</sub> was set at 480 ml/min. For better contact of the membrane material with the feeding gas, the membrane was crashed into small pieces. The XRD patterns of the samples before and after the stability test were obtained.

### 6.3. Results and discussion

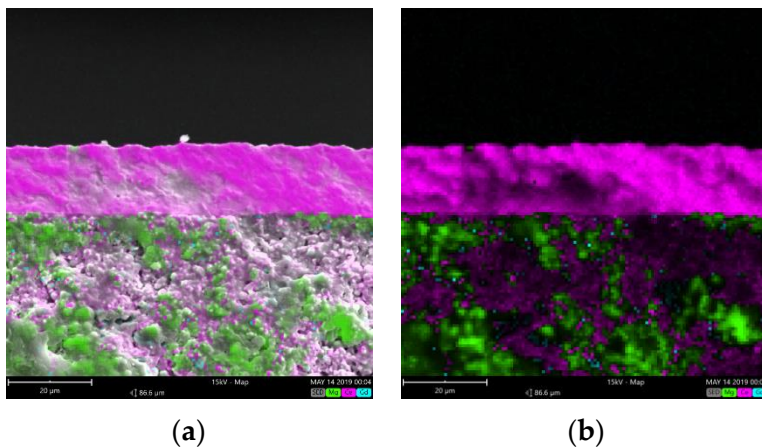
SEM images of the prepared porous MgO-supported CGO membrane are presented in Figure 6.3a. Partial delamination of the sintered CGO layer from the support tube can be observed from surface and cross section of the asymmetric membrane. This result was reproducible for several membranes and is mainly caused by differences in shrinkage behaviour of the membrane support and the selective layer. To increase attachment of the membrane layer onto the substrate and to improve gas tightness of the supported membrane, a mixture of 60 wt% MgO and 40 wt% CGO powders was used instead of the pure MgO powders for the preparation of the casting slurries for phase inversion. A defect-free CGO membrane layer with a thickness of  $\sim 20\ \mu\text{m}$  was obtained on the dual-phase support and strong attachment was achieved between the two layers (Figure 6.3b). This result was again quite reproducible for several membranes. However, the figure also shows a very homogeneous membrane support, which would result in pronounced mass transfer resistances. Thus, the next step is to create a porous structure in the supports before coating the selective layers. The composition of the casting slurry was varied to investigate the effect on the microstructure and performance of the dual-phase ceramic support.





**Figure 6.3.** Scanning electron microscopy (SEM) images of CGO layers fabricated on (a) MgO and (b) MgO-CGO dual-phase support tubes.

The element distribution on the cross section of the CGO-MgO dual-phase supported membrane is presented in Figure 6.4. It can be observed that in the membrane support both the element of Ce and Mg were detected, while only Ce was found in the membrane layer and the distribution of Ce in the membrane layer is denser than that in the support, suggesting that the CGO concentration is higher in the membrane layer than inside the support.





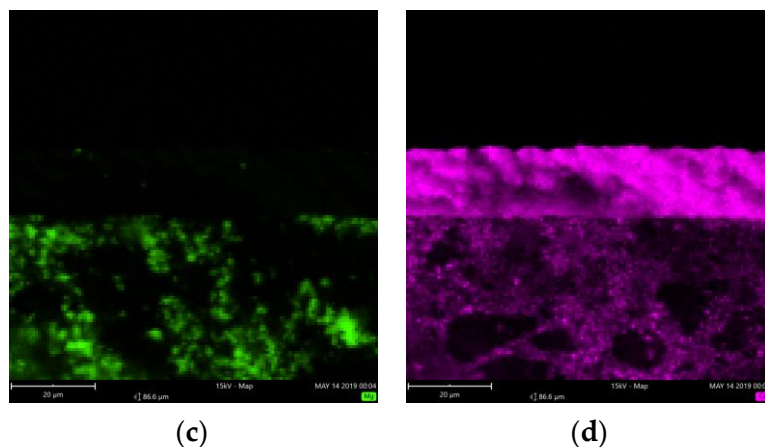
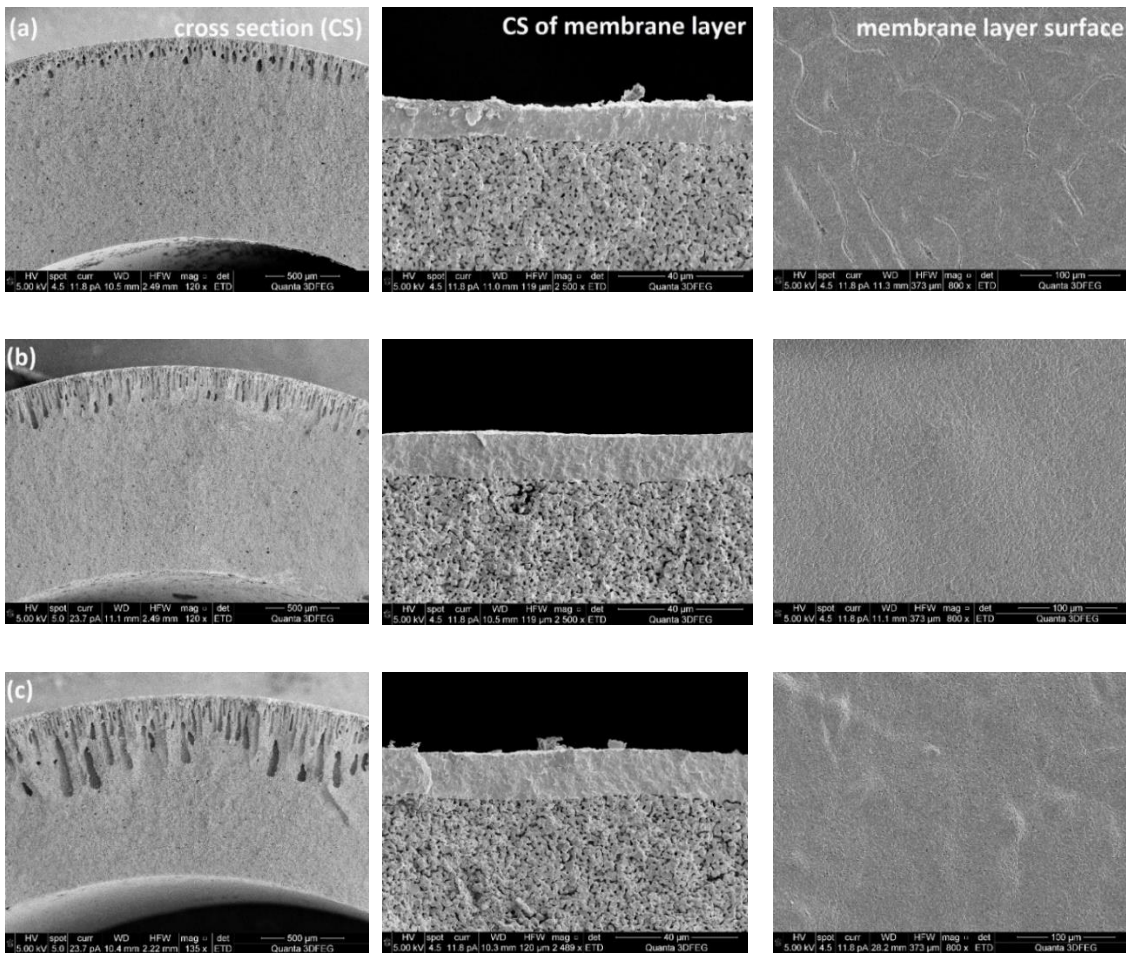


**Figure 6.4.** Element distribution on the cross section of the CGO-MgO dual-phase supported membrane: (a) Combined mapping and SEM image; (b) Combined element mapping; (c) Mg mapping; (d) Ce mapping.

### 6.3.1. Influence of ceramic loading

The polymer concentration in the solution is the key factor that can influence the channel length in the polymer membranes by affecting the resistance for water transfer into the solution. In addition to the polymer concentration, also the ceramic loading in the slurry is an important parameter that can influence the length of the micro-channels in the ceramic tubes. Moreover, the ceramic concentration also influences the shrinkage behaviour of the support tubes during the sintering process and thereby the adherence of the membrane layers on the supports. When the ceramic loading was lower than 43 wt%, the slurry exhibited inadequate plasticity to maintain the tubular shape during the casting process, while a ceramic loading above 60 wt% caused cracks on the sintered support tube because the chosen PES concentration in the solution was insufficient to handle this ceramic loading. According to this, the ceramic loading was varied from 43 wt% to 60 wt% to investigate its influence on quality of CGO coatings and growth

of the micro-channels, while the polymer concentration was fixed at 18 wt%. For each 20 g of NMP, 15 g, 17.5 g, 20 g, 25 g and 30 g PES were added, respectively, in the polymer solution, resulting in ceramic loadings of 43 wt%, 47 wt%, 50 wt%, 56 wt% and 60 wt%. Bigger step was applied for the change of ceramic loading from 50 wt% to 60 wt%, because the ceramic content in the slurry shows smaller influence on the slurry viscosity and microstructure of the support at high ceramic loading than at the range from 43 wt% to 50 wt%.



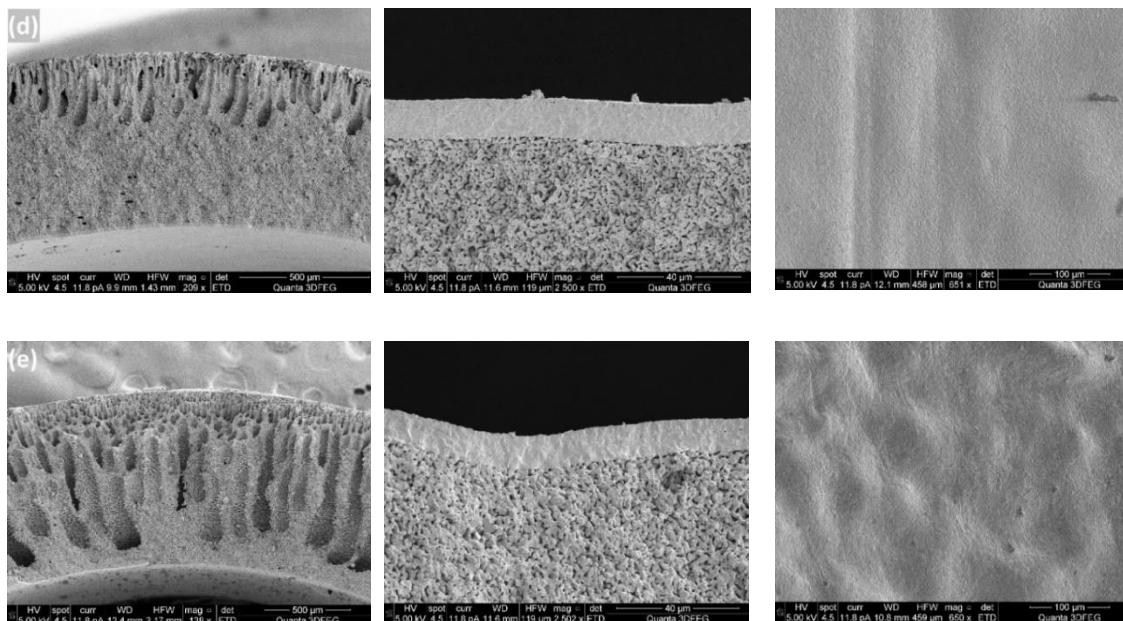


**Figure 6.5.** SEM images of MgO-CGO porous supports fabricated from slurries with (a) 60 wt%, (b) 56 wt%, (c) 50 wt%, (d) 47 wt% and (e) 43 wt% ceramic loadings together with the CGO layers coated inside.

Figure 6.5 shows SEM images of porous supports prepared with different ceramic loadings and the membrane layers coated on top (in the inner part of the support). It can be observed from cross sections of the membrane supports, that all the support tubes have two layers: one layer with finger-like pores (channels) which provides low mass transfer resistance and the other one with a sponge-like microstructure. It is also clear that the ceramic loading in the preparation recipe has a large effect on the thickness of the layer with channels. Sufficiently long and very homogeneous channels were obtained in the support tube, when the ceramic loading was 43 wt%, while the “pore-size” decreased when adding ceramic powders to the casting slurries, which could be attributed to the improved resistance for the channel growth because of the increased viscosity of the slurries

(Figure 6.6). It should be noted that the slurry with a ceramic concentration of 43 wt% showed a rather high fluidity, which means a high pushing speed was required to keep a tubular shape of the slurry when introducing the piston into water.

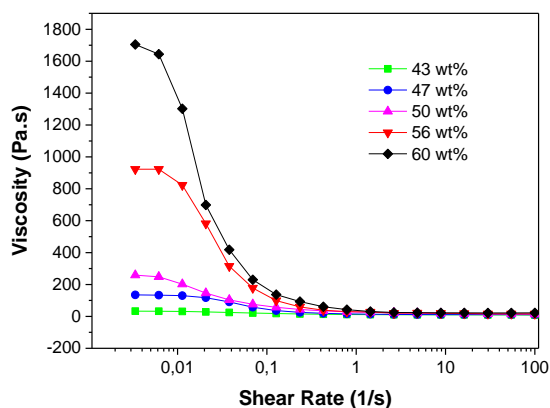


**Figure 6.6.** Rheological behaviour of the slurries with different ceramic loadings.

Large shrinkages of the porous support tubes were observed after the sintering, because of burning of the polymers and sintering of the ceramic particles. The ceramic loading had a great influence on the tube shrinkage. In this work the shrinkage of a support tube was quantified by measuring the tube length before and after the sintering process. Table 6.1 shows the effect of the ceramic loading in the casting slurry on the shrinkage of the porous supports. The results can be explained by the decrease in the weight ratio of polymers to ceramic powders, where the smaller shrinkage of the support is attributed to reduced polymer burning during the sintering process. Dense membrane layers can be achieved only when the porous supports and membrane layers exhibit uniform shrinkage behaviours. From SEM images of the surfaces of the membrane layers (Figure 6.5), it is clear that with a ceramic loading of 60 wt%, several cracks were formed

on the membrane layer which indicates that the shrinkage of the membrane was faster than that of the support tube. However, when the ceramic loading was below 47 wt%, the MgO-CGO supports shrank faster than the layers, which caused the membrane layers to be corrugated and thus also fragile. Accordingly, in terms of the shrinkage behaviour compatibility between the membranes and supports, ceramic loadings between 50 wt% and 56 wt% (polymer/ceramic ratios between 0.225 and 0.180) were the best choice for preparing the casting slurries, which resulted in selective layers with no connected pores or cracks but some closed pores and surface defects with a pore size of 0.2-1 $\mu$ m. No obvious effect of the closed pores and surface defects was observed on the gas-tightness of the selective layers.

**Table 6.1.** Shrinkage comparison of the coated support tubes fabricated from slurries with different ceramic loadings.

<b>Ceramic loading (wt%)</b>	<b>Polymer/ceramic ratio</b>	<b>Shrinkage of support tube (%)</b>	<b>Microstructure of CGO layer</b>
60	0.150	33.6	Cracked
56	0.180	35.6	Smooth
50	0.225	36.7	Smooth
47	0.257	37.1	Corrugated
43	0.300	38.6	Corrugated

Nitrogen permeation measurements were conducted for the porous supports fabricated with different ceramic loadings. Pressure differences ( $\Delta P$ ) from 10 kPa to 50 kPa were applied across the support tubes and the gas permeation through the supports are plotted as a function of  $\Delta P$  in Figure 6.7. A small increase in the nitrogen permeability with  $\Delta P$  was observed for all the test membranes, because

of viscous flow through the small pores [8]. Figure 6.7 also reveals that the effect of reducing ceramic loading inside the slurry is an increase in gas permeability through the support tubes. Especially when the ceramic loading was decreased from 47 wt% to 43 wt%, a very significant increase in the gas permeation flux was observed, which could be attributed to a decrease in the tortuosity of the micro-channels.

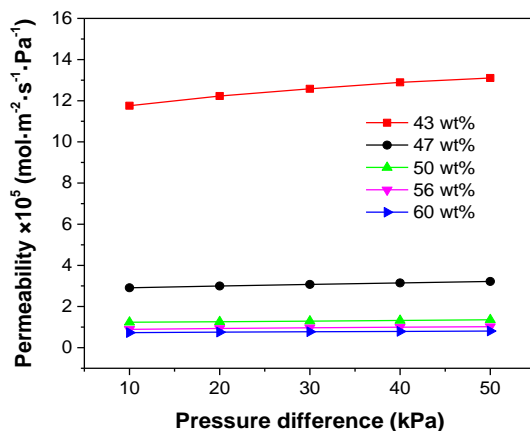


**Figure 6.7.** Nitrogen permeability through MgO-CGO supports fabricated from slurries with different ceramic loadings.

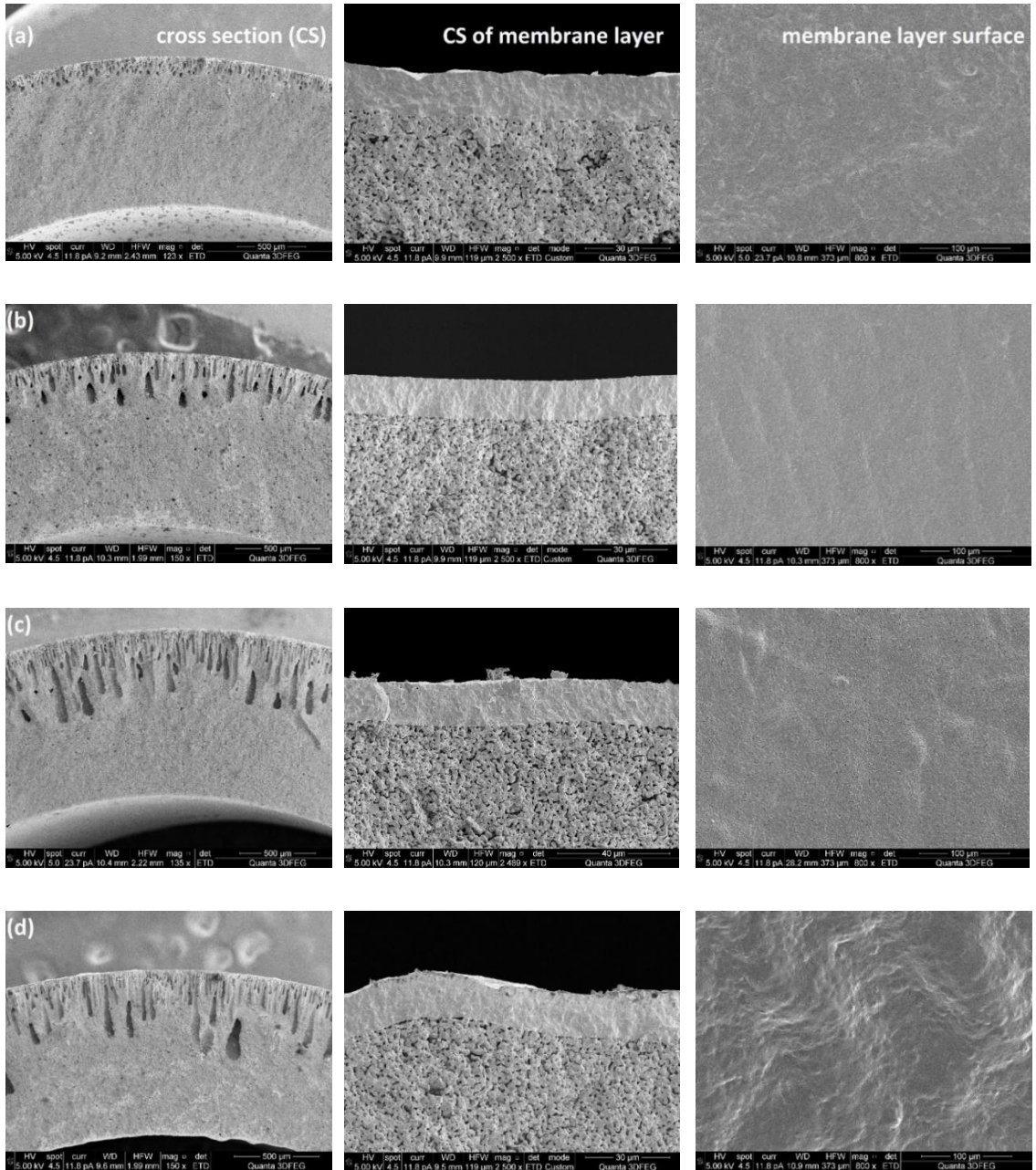
### **6.3.2. Influence of polymer concentration**

A high water-solvent exchange rate promotes the growth of micro-channels during the phase inversion. For polymer membranes, the number and size of finger-like channels formed in the water bath tend to decrease when the PES concentration in the solution was increased, which indicates that a high polymer concentration would frustrate the conversion between water and solvent [9]. Based on the research of polymer membranes, in this work the effect of the PES

concentration on the channel growth in the ceramic membrane supports was investigated. As with excessive ceramic loadings inside the slurries, when the polymer concentrations were below 11 wt%, the supports generally broke during the sintering process, because the polymer was insufficient to handle the ceramic powders. As a result, a range of polymer concentrations from 11 wt% to 25 wt% was selected to investigate its influence on the microstructure of the supports and membrane layers while the ceramic loading was kept at 50 wt%. For each 20 g of NMP, 2.5 g, 3.5 g, 4.5 g, 5.5 g and 6.5 g PES was added, respectively, in the polymer solution.

As shown in Figure 6.8, for the chosen ceramic loading, the channel length increases when increasing the polymer concentration in the recipe, which is opposite to the result obtained for polymer membranes. Adding ceramic powders to the polymer solutions caused a large increase in the resistance for water exchange with the solvent, while PES in the suspension performed as a surfactant for the ceramic powders by adsorbing on the surface of the particles [10]. Aggregation of the ceramic particles could be avoided due to the presence of the polymers, so increased PES contents resulted in a reduced resistance for channel growth. In addition, the finger-like pores were found to disappear gradually with increasing the phase inversion time [11] but a higher content of PES, which also performed as binder of the particles, would result in stronger walls of the channels. The rheological behaviour of the slurries with different PES concentrations at a fixed ceramic loading of 50 wt% is shown in Figure 6.9a. It is evident that all the slurries exhibited shear thinning behaviour (viscosities decreased with increased shear rate) and this behaviour became more pronounced when the polymer concentration was decreased. As a result, at low shear rate the viscosities of the ceramic slurries decreased with increased PES concentrations, while at high shear rate the slurries with low PES concentrations were less viscous than the ones with more PES. The rheological behaviours in the zero-shear viscosity plateau region

were consistent with the decrease of water transfer resistances when increasing the PES concentrations.





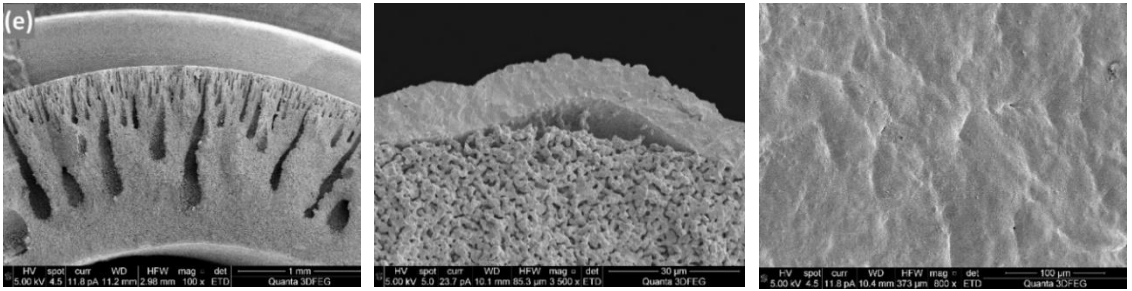
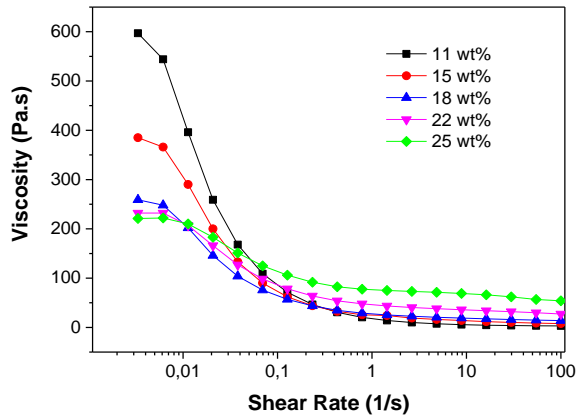


**Figure 6.8.** SEM images of MgO-CGO porous supports fabricated from slurries with (a) 11 wt%, (b) 15 wt%, (c) 18 wt%, (d) 22 wt% and (e) 25 wt% polymer concentrations together with the CGO layers coated inside.

(a)



(b)

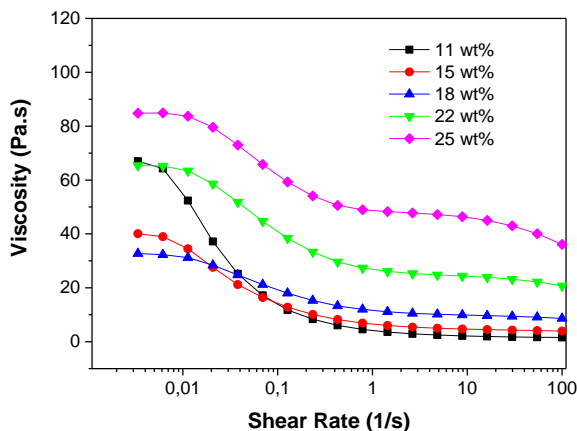


**Figure 6.9.** Rheological behaviour of the slurries with different polymer concentrations when the ceramic loadings fixed at (a) 50 wt% and (b) 43 wt%.

Table 6.2 presents how the shrinkages of the porous supports after the sintering process are affected by the polymer concentrations in the slurries. It is clear that increased polymer concentrations result in larger length shrinkages of the support tubes. During sintering, shrinkage of the ceramic substrate can be divided into two stages: the initial stage starts at relatively low temperature, which is caused by the release of the organic polymers, while the second and more significant shrinkage occurs at a much higher temperature due to sintering of the ceramic particles and the reduction of the residual porosity formed by the burning of the polymers. Increase of the polymer content in the green substrates caused larger initial shrinkages during release of the polymers and larger pore volumes, which also resulted in increased shrinkages during the second stage. Microstructures of membrane layers formed on substrates with different polymer concentrations are shown in Figure 6.8. Good membrane layers were obtained with polymer concentrations between 15 wt% and 18 wt% (polymer/ceramic ratios between

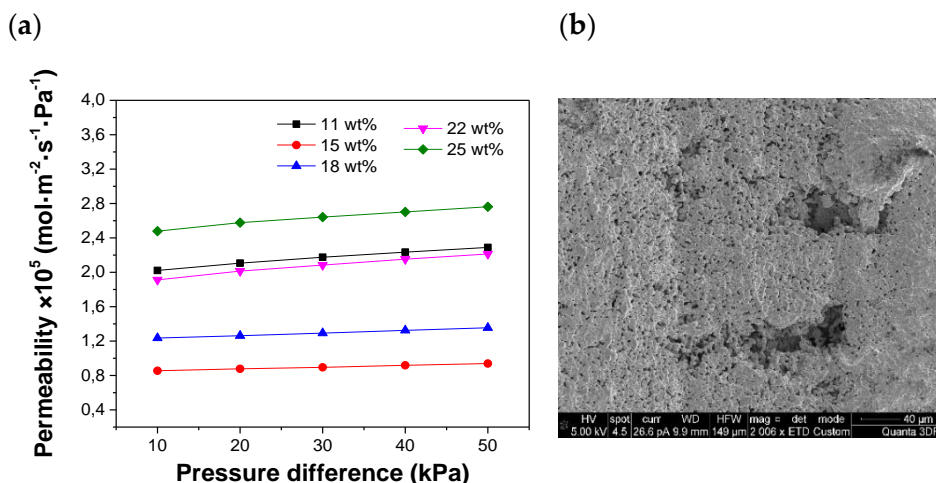
0.175 and 0.225), which is because of the compatible shrinkage behaviour of the substrates and the inside films. No connected pores or cracks but some surface defects and closed pores with a pore size of 0.2-1 $\mu$ m were observed in these selective layers. However, these closed pores and surface defects did not show obvious effect on the gas-tightness of the selective layers. Detachment and cracks of the membrane were formed with a polymer concentration of 25 wt% in the casting slurry, because of over-shrinkage of the support tube.

**Table 6.2.** Shrinkage comparison of the support tubes fabricated from slurries with different polymer concentrations.

Polymer concentration (wt%)	Polymer/ceramic ratio	Shrinkage of support tube (%)	Microstructure of CGO layer
11	0.125	31.8	Cracked
15	0.175	35.3	Smooth
18	0.225	36.7	Smooth
22	0.275	38.3	Corrugated
25	0.325	38.7	Corrugated

Figure 6.10a shows the gas permeation as a function of  $\Delta P$  for the support tubes prepared with different polymer concentrations, when ceramic loadings fixed at 50 wt%. The slurry with 25 wt% PES resulted in a porous support with the highest permeability and a declined permeation flux was observed when the polymer concentration was reduced to 15 wt%, which is attributed to the reduced channel length and the decreased porosity formed by burning of the polymers. However, decreasing the polymer concentration to 11 wt% did not further reduce the gas permeability, because some micro-cracks were formed on the support tubes (Figure 6.10b), which could be expected from the insufficient polymer

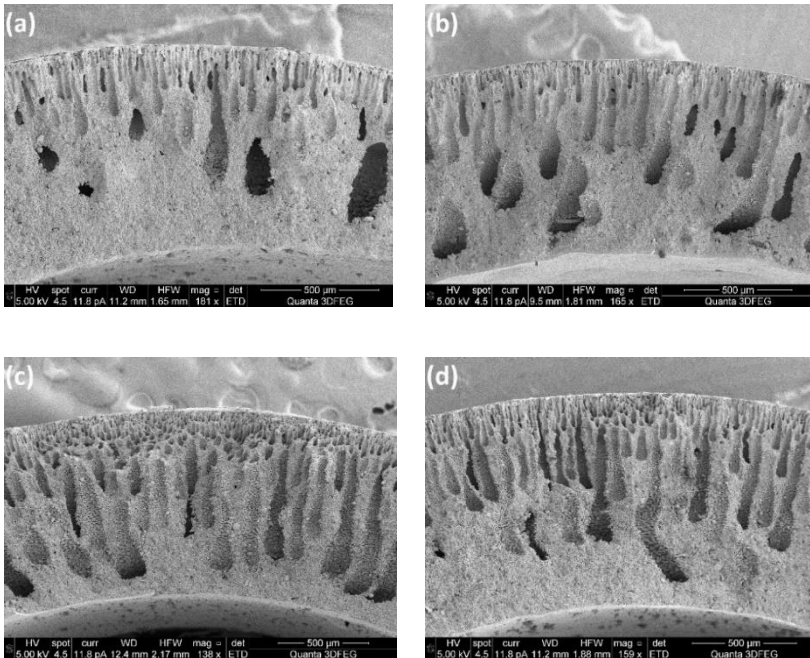
concentration for handling the ceramic loading.



**Figure 6.10.** (a) Nitrogen permeability through MgO-CGO supports fabricated from slurries with different polymer concentrations; (b) SEM image of cracks on the support tube made from a slurry with 11 wt% polymer concentration.

To further examine the role of PES in the phase inversion process for ceramic support fabrication, another group of slurries with a ceramic loading of 43 wt% was prepared and the polymer concentration was increased from 11 wt% to 25 wt% to investigate the growth of micro-channels inside the tubular supports. From the SEM images of the support tube cross sections (Figure 6.11), it is observed that the longest and most homogeneous channels were achieved when the polymer concentration was 18 wt%, which means that this slurry provided the lowest resistance for water-solvent exchange. Below the polymer concentration of 18 wt%, the channel length increased with the PES content, which could be attributed to the dispersing effect of PES. However, a reduced channel size was observed when more PES was added into the slurry with polymer concentration of 18 wt% and this can be understood by considering that, when the surfaces of

the particles were fully covered with polymer, excess polymer increases the resistance for phase inversion, as for the polymer membranes. Consistent results were also observed for the rheological behaviour of the slurries at the zero-shear viscosity plateau region (Figure 6.9b), which means that the lowest viscosity of the slurries (lowest channel growth resistance) was obtained at the polymer concentration of 18 wt%. Dong et al. [10] reported similar rheological behaviour for NiO/YSZ ceramic slurries by adjusting the dispersant concentration in the suspension. By comparing the results of these two sets of experiments with the ceramic loadings fixed at 50 wt% and 43 wt%, it is evident that an increased ceramic loading requires more polymer as surfactant to achieve sufficiently long channels in the ceramic supports because of the improved specific surface areas of the powders.



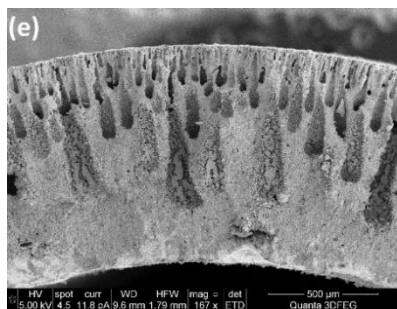


**Figure 6.11.** SEM images of MgO-CGO supports fabricated from slurries with (a) 11 wt%, (b) 15 wt%, (c) 18 wt%, (d) 22 wt% and (e) 25 wt% polymer concentration with a fixed ceramic loading of 43 wt%.

### **6.3.3. Influence of particle surface area**

Three kinds of ceramic powders with BET specific surface areas (SSA) of 12.53 m<sup>2</sup>/g, 24.11 m<sup>2</sup>/g and 26.33 m<sup>2</sup>/g, respectively, were applied to the preparation of ceramic casting slurries for phase inversion. The PES concentration was fixed at 25 wt%, while the ceramic loading was 50 wt%. The microstructures of the support tubes fabricated with these three slurries are shown in Figure 6.12. The channel length decreased significantly when the SSA of the ceramic particles was increased from 12.53 m<sup>2</sup>/g to 24.11 m<sup>2</sup>/g, leading to an abrupt decrease in the gas permeability through the porous support (Figure 6.13). This result further confirms the surfactant role of PES by coating on the surface of the ceramic particles. Larger SSA of the powders requires more surfactant to reduce the resistance for the water-solvent conversion. Accordingly, for a specific polymer concentration, the slurry with the lower SSA might have a lower resistance for channel growth.

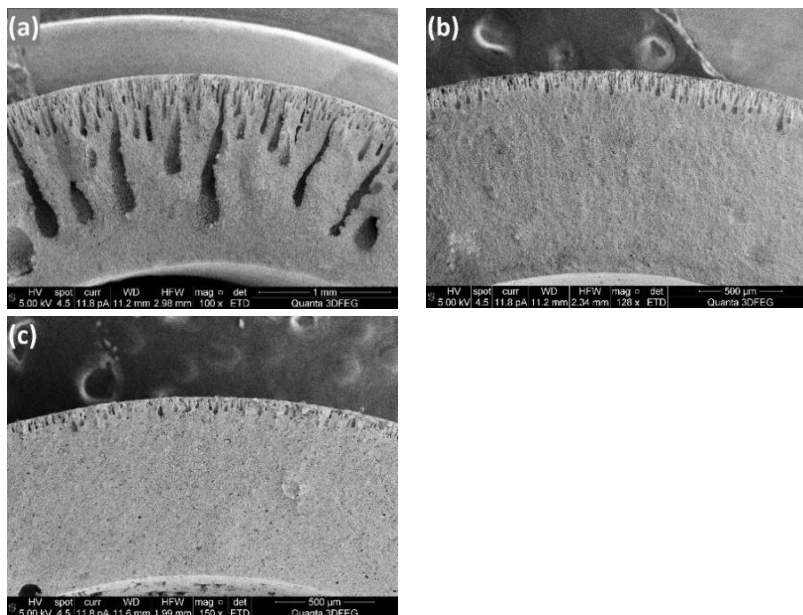


**Figure 6.12.** SEM images of MgO-CGO porous supports fabricated using ceramic powders with specific surface areas of (a) 12.53 m<sup>2</sup>/g, (b) 24.11 m<sup>2</sup>/g and (c) 26.33 m<sup>2</sup>/g.

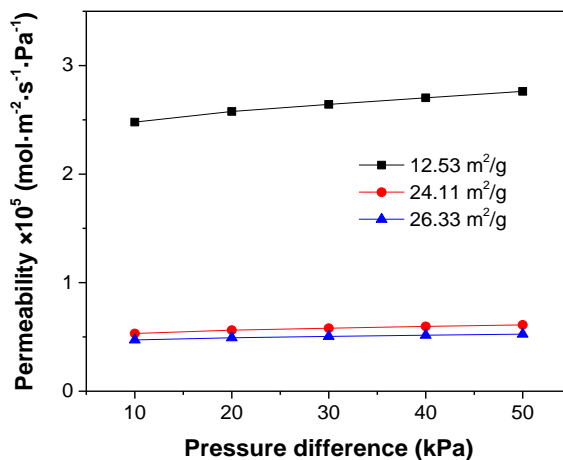


**Figure 6.13.** Nitrogen permeability through MgO-CGO supports fabricated with ceramic powders of different specific surface areas.

Figure 6.14 reports the effect of the ceramic powder SSA on the slurry viscosities. At low shear rate, the CGO powders with an SSA of 12.53 m<sup>2</sup>/g resulted in a much lower slurry viscosity than the ones with an SSA of 24.11 m<sup>2</sup>/g and 26.33 m<sup>2</sup>/g.

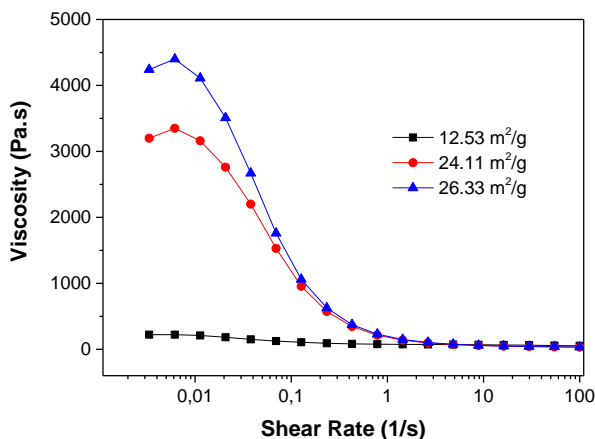


**Figure 6.14.** Rheological behaviour of the slurries prepared with ceramic powders of different specific surface areas.

#### **6.3.4. Addition of ethanol to the ceramic slurry**

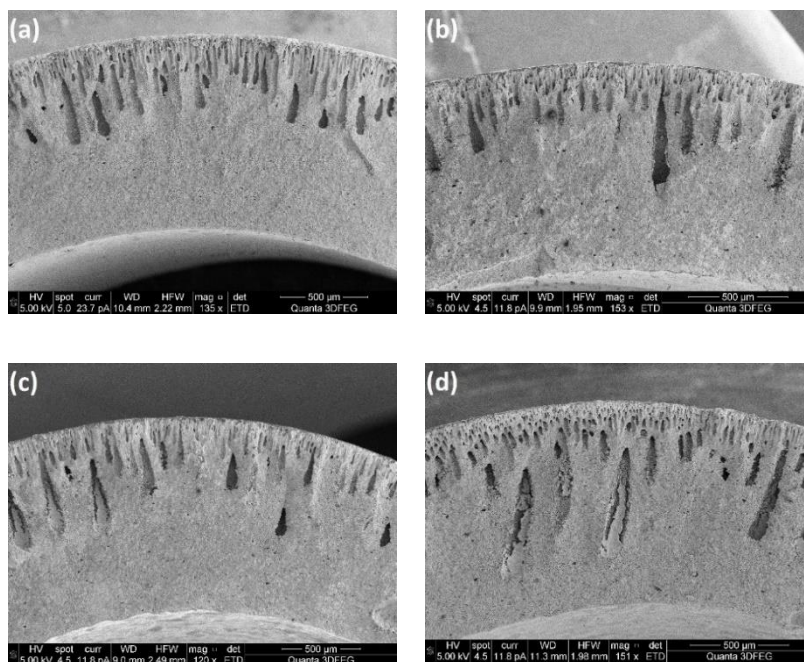
Smolders et al. [12] proposed a mechanism for the formation of macrovoids (channels), by attributing the occurrence of the channels inside polymer membranes to the instantaneous liquid-liquid demixing and the formation of membranes without channels to the delayed demixing. They also concluded that the low non-solvent (water) concentration in the diffusion front would cause delayed demixing, which would hinder growth of the channels, while adding a certain amount of water to the polymer solution could change delayed demixing to instantaneous demixing and increase the channel length.



In this work, also the effect of adding a non-solvent to the casting slurries on the microstructures of the ceramic membrane supports was also investigated. Ethanol was applied instead of water as the non-solvent additive because of the low solubility of PES in water, which would cause precipitation of the PES before the phase inversion casting process when adding a small amount of water into the polymer solutions. Excess ethanol in the mixture would also cause precipitation of the polymers, which means that the amount of ethanol added to the solution should be precisely controlled. Various NMP-ethanol-PES-PVP solutions with ethanol contents (weight ratios of ethanol to ethanol+NMP) ranging from 0 wt% to 27 wt% were prepared. Precipitation of PES occurred at the surface of the polymer solution when ethanol was dripped into the mixture because of the lower density of ethanol compared to NMP. However, the solution tended to become pellucid after mixing for 5 min in the centrifugal mixer, when ethanol mixed thoroughly with the solution. Then, the ceramic powders were added into the solution to obtain the ceramic casting slurries. The PES concentration (weight ratio of PES to PES+ethanol+NMP) was fixed at 18 wt%, while the ceramic loading (weight ratio of ceramic powders to CGO+MgO+ethanol+NMP) was 50 wt% in this set of experiments.

From the cross sections of the obtained ceramic supports (Figure 6.15), it can be observed that the length of the channels tended to increase when the ethanol contents were increased from 0 wt% to 27 wt%. Jin et al. [11] employed the solubility difference parameter ( $|\Delta\delta|$ ) for the evaluation of the driving force to form finger-like channels. By applying liquids with different solubilities as the coagulants to adjust the driving force, they verified that the figure-like channels are easier to form when  $|\Delta\delta|$  between NMP and the coagulant is improved. The solubility parameters for NMP, water and ethanol are 22.9, 47.9 and 26.0 respectively. In the channel growth front, the water concentration is lower (NMP concentration is higher) than at the initial interface between the slurry and water

bath, which may result in a declined solubility of the coagulant and the resulting  $|\Delta\delta|$  is insufficient for the formation of long enough channels. Since the solubility parameter of ethanol is higher than that of NMP, adding a certain amount of ethanol to the casting slurry can help increasing the solubility in the diffusion front and improve the driving force for channel growth. Moreover, in Figure 6.16 it is shown that the slurry viscosity at the zero-shear viscosity plateau region declined when the ethanol concentration was increased. According to the former results, a decreased low shear rate viscosity would promote channel growth inside the ceramic membrane supports.



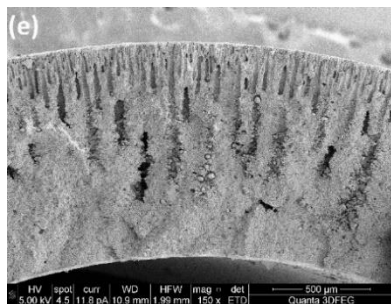


**Figure 6.15.** SEM images of MgO-CGO porous supports fabricated from slurries with (a) 0 wt%, (b) 7 wt%, (c) 13 wt%, (d) 20 wt% and (e) 27 wt% ethanol concentrations.

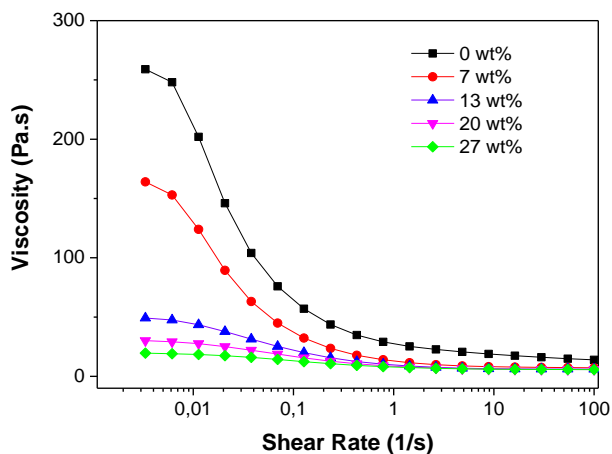


**Figure 6.16.** Rheological behaviour of the slurries prepared with different ethanol concentrations.

### 6.3.5. Chemical stability of the membrane

The XRD patterns of the dual-phase supported CGO membrane pieces before and after the chemical stability test in  $\text{CO}_2$  atmosphere, together with the XRD patterns of MgO and CGO powders are presented in Figure 6.17. It indicated that CGO and MgO remain unchanged in the CGO-MgO dual-phase material after

the heat treatment during the membrane preparation process. Moreover, it can also be observed that after the stability test, the membrane pieces completely kept their dual phases (CGO and MgO). No carbonate was formed. The chemical stability of the membrane in CO<sub>2</sub> atmosphere was confirmed to be good during the testing period (500min).

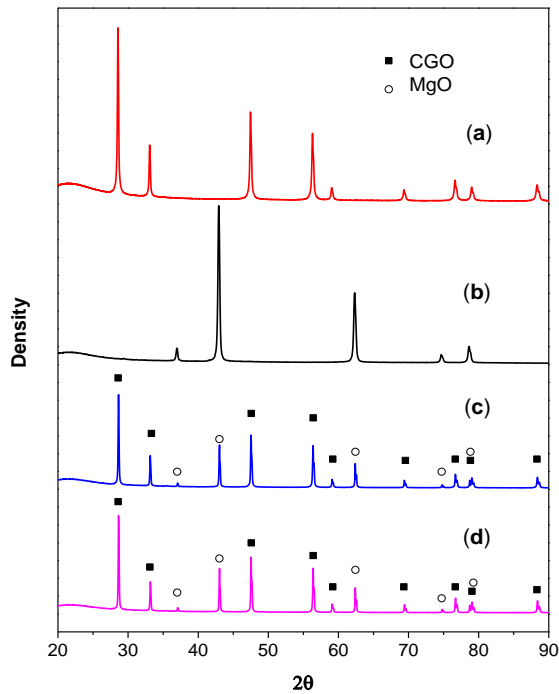


**Figure 6.17.** X-ray diffraction (XRD) patterns of (a) CGO powders, (b) MgO powders, (c) CGO-MgO dual-phase supported CGO membrane before the chemical stability test, (d) CGO-MgO dual-phase supported CGO membrane after the chemical stability test.

## 6.4. Conclusions

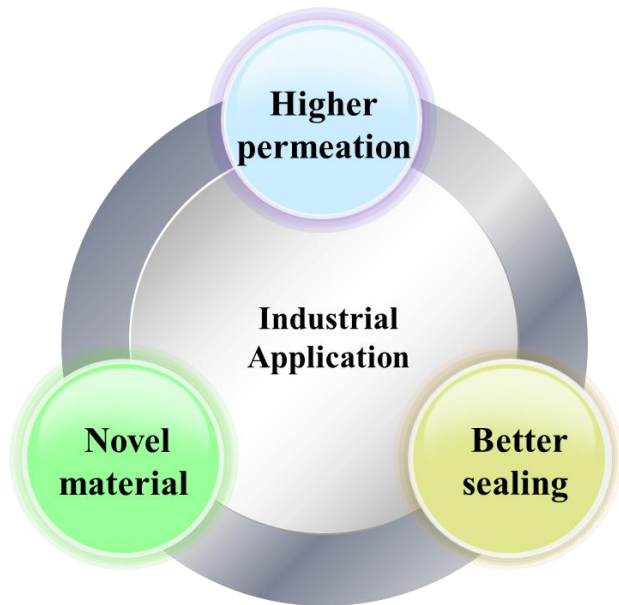
Micro-channelled MgO and MgO-CGO dual-phase support tubes were fabricated with a low-cost phase inversion casting method. Gas-tight CGO membrane layers were obtained on the dual-phase supports, while the layers tended to peel off from the MgO tubes after sintering. The composition of the casting slurries was a key factor that influenced channel length and shrinkage of the MgO-CGO supports. Increased ceramic loading frustrated the channel growth, causing decreased gas permeability through the support tubes. PES performed as surfactant of the ceramic powders, which means that addition of a certain amount of PES to the casting slurry or a decrease in the specific surface area of the ceramic particles can help reducing the channel-growth resistances. However, saturated adsorption of polymers onto the ceramic powders resulted in a lower water-solvent conversion speed and reduced channel length. Moreover, addition of ethanol to the casting slurry was found to be an effective way to increase the channel length in the casted support tubes. Slurries that provided lower channel-growth resistances exhibited lower viscosities at the zero-shear plateau region. An increase in the PES/ceramic ratio caused larger shrinkage of the tubes during the sintering process and compatible shrinkage behaviours between the dense membranes and substrates were achieved when PES/ceramic ratios were between 0.175 and 0.225. The chemical stability of the dual-phase supported membrane in CO<sub>2</sub> atmosphere was confirmed to be good during a testing period of 500 min.

## References

- [1] D. F. Souza, E. H. M. Nunes, W. L. Vasconcelos, Preparation of  $\text{Ba}_{0.5}\text{Sr}_{0.5}\text{Co}_{0.8}\text{Fe}_{0.2}\text{O}_{3-\delta}$  asymmetric structures by freeze-casting and dip-coating, *Ceram. Int.* 44 (2018) 1002–1006.
- [2] P. L. Rachadel, D. F. Souza, E. H. M. Nunes, J. C. D. da Costa, W. L. Vasconcelos, D. Hotza, A novel route for manufacturing asymmetric BSCF-based perovskite structures by a combined tape and freeze casting method, *J. Eur. Ceram. Soc.* 37 (2017) 5249–5257.
- [3] W. Xing, M. L. Fontaine, Z. Li, J. M. Polfus, Y. Larring, C. Denonville, E. Nonnet, A. Stevenson, P. P. Henriksen, R. Bredesen, Asymmetric tubular  $\text{CaTi}_{0.6}\text{Fe}_{0.15}\text{Mn}_{0.25}\text{O}_{3-\delta}$  membranes: Membrane architecture and long-term stability, *J. Memb. Sci.* 548 (2018) 372–379.
- [4] T. Liu, Y. Chen, S. Fang, L. Lei, Y. Wang, C. Ren, F. Chen, A dual-phase bilayer oxygen permeable membrane with hierarchically porous structure fabricated by freeze-drying tape-casting method, *J. Memb. Sci.* 520 (2016) 354–363.
- [5] Z. Liu, G. Zhang, X. Dong, W. Jiang, W. Jin, N. Xu, Fabrication of asymmetric tubular mixed-conducting dense membranes by a combined spin-spraying and co-sintering process, *J. Memb. Sci.* 415–416 (2012) 313–319.
- [6] X. Yin, L. Hong, Z. Liu, Oxygen permeation through the LSCO-80/ $\text{CeO}_2$  asymmetric tubular membrane reactor, 268 (2006) 2–12.
- [7] N. Y. Teraoka, T. Fukuda, N. Miura, Development of oxygen semipermeable membrane using mixed conductive perovskite-type oxides (part 2): preparation of dense film of perovskite-type oxide on porous substrate, *J. Ceram. Soc. Japan.* 97 (1989) 533–538.
- [8] D. K. Ramachandran, M. Sjøgaard, F. Clemens, B. R. Sudireddy, A. Kaiser, Low cost porous MgO substrates for oxygen transport membranes, *Mater. Lett.* 169 (2016) 254–256.
- [9] J. Barzin, S. S. Madaeni, H. Mirzadeh, M. Mehrabzadeh, Effect of polyvinylpyrrolidone on morphology and performance of hemodialysis membranes prepared from polyether sulfone, *J. Appl. Polym. Sci.* 92 (2004) 3804–3813.
- [10] D. Dong, J. Gao, X. Liu, G. Meng, Fabrication of tubular NiO/YSZ anode-support of solid oxide fuel cell by gelcasting, *J. Power Sources.* 165 (2007) 217–223.
- [11] C. Jin, C. Yang, F. Chen, Effects on microstructure of NiO-YSZ anode support fabricated by phase-inversion method, *J. Memb. Sci.* 363 (2010) 250–255.

- [12] C. A. Smolders, A. J. Reuvers, R. M. Boom, I. M. Wienk, Microstructures in phase-inversion membranes. part 1. formation of macrovoids, *J. Memb. Sci.* 73 (1992) 259–275.

# Chapter 7 Conclusions and outlook





## 7.1 Conclusions

The MIEC membrane opens the possibility of the oxygen production for industrial application. Great efforts have been made in last few decades to improve the membrane performance by development of robust materials. Many perovskite oxides show favourable permeability, but the low chemical/thermal stability restricts their application, while many fluorite-type compounds show a better performance under harsh conditions, but their oxygen permeation is hindered by the insufficient electronic-conductivity as summarised in Chapter 2.

In order to develop oxygen transport membranes suitable for the industrial applications at various conditions, the material, micro-structure, geometry and preparation method of the membranes have been studied in detail in this thesis. Considering the dilemma of single-phase material, the preparation of an oxygen membrane from a composite material is considered to be a promising alternative strategy. Several dual-phase and triple-phase membranes have been fabricated from various materials in Chapter 3 and Chapter 4, and their performance have been compared. A modified phase-inversion casting method was used to shape the membrane into dead-end tubular geometry, which simplifies the sealing process and is preferred for integration of the membranes in membrane reactors. The phase inversion process was initially developed for the polymer membrane fabrication. However, in recent years this technique has found its application in the formation of asymmetric ceramic membranes. Ceramic-based slurries need to be prepared and casted into desired geometries before introduced into water for phase inversion. In the water bath, the solvent in the slurry exchanges with water, and since the dissolved polymer exhibits low solubility in water, the solution solidifies due to polymer precipitation. Although many researchers reported the fabrication of ceramic oxygen transport membranes with phase inversion technique, most works were focused on flat membranes or hollow fibres.

Application of this technique to the fabrication of tubular membranes and especially dead-end tubes is rather limited.

The CGO-BSCF dual-phase membranes fabricated with different ceramic loadings and CGO/BSCF ratios have been investigated in Chapter 3, and it was found that higher CO<sub>2</sub> concentration in the sweep gas caused lower oxygen permeation rate through the membranes, while the permeation flux increased with temperature when pure CO<sub>2</sub> fed as sweep gas. Channel length inside the CGO-BSCF membranes and oxygen permeation fluxes were observed to be promoted by the reduced ceramic loading in the casting slurry, but the ceramic loading showed little influence on membrane mechanical strength. The composites with higher BSCF concentration showed higher permeability but lower CO<sub>2</sub> resistance. Moreover, adding CGO into the preparation recipe for the CGO-BSCF membranes facilitated better mechanical strength of the dual-phase membranes. The three-point bending strength of the CGO/BSCF50 membrane is 181.6 N, which is more than two times the strength of CGO/BSCF60 membrane (81.0 N)

When the CGO-BSCF was compared with the CGO-NFO and CGO-LNO membranes, it was clear that the CGO-BSCF membrane provides the highest permeability among the three type of membranes, both when using He or pure CO<sub>2</sub> as sweep gas. Taking the data at 950 °C as a reference, the permeation flux through the C6B4 was 0.29 ml/min·cm<sup>2</sup>, which is more than 6 times the value obtained for the C6N4 and 12 times the value achieved for the C6L4 when swept with He. Two tripe-phase membranes were prepared with CGO, BSCF and NFO powders with the purposed to further improve the CO<sub>2</sub>-resistance of the membranes. Permeabilities of both triple-phase membranes were higher than the CGO-NFO but lower than the CGO-BSCF membranes. However. performance of the triple-phase membrane with 60 wt% CGO was found to be the best among the dual-phase and triple-phase membranes investigated in this work, in high

CO<sub>2</sub>-containing atmosphere.

B-site doped SrFeO<sub>3-δ</sub> material was used for the preparation of oxygen transport membranes in Chapter 5. SEM images of the SFSb membrane exhibited new phases formed after operation at high temperature, which suggested low thermal stability of the material. To solve the problem, CGO was mixed with the SFSb forming a dual-phase membrane. No phase precipitation was observed on the dual-phase membrane after the permeation test.

The modified phase inversion casting process applied in this work is a rather flexible technique, which can be applied to the formation of membranes with not only different materials but also varied structures and geometries. Some MgO and MgO-CGO porous supports were prepared with this method in Chapter 6, and CGO membrane layers were deposited onto the support with dip-coating method. Better compatibility of the CGO layer was observed with the dual-phase support than with the MgO support. The channel growth in the support and the shrinkage of the support after sintering were investigated at different slurry concentrations. As a surfactant of the ceramic powders, a certain amount of PES added to the casting slurry helps promoting the channel growth in the support, but a lower water-solvent conversion speed and reduced channel length was observed when adsorption of polymers onto the ceramic powders was saturated. Similar shrinkage rate of different layers during sintering process is crucial for the successful fabrication of multi-layer membranes. Compatible shrinkage and leakage free membranes were obtained with the PES/ceramics ratio from 0.175 to 0.225.

## **7.2 Future work**

The main purpose of Chapter 3-5 was to select robust material for oxygen production, so a single-layer membrane structure with a relatively high membrane thickness was applied. This membrane structure allows an easier fabrication process but results in a higher resistance for oxygen permeation through the membranes. In future work, some dual-phase porous support with similar material as the selective layer can be prepared with the same phase-inversion casting method. Sacrificial phases, e.g. graphite, can be added into the slurry for the formation of the porous structure after sintering. Then, the dual-phase membrane layers can be coated onto the support with dip-coating method. With this strategy supported dual-phase membrane with improved permeability, good thermal and chemical stability and sufficient mechanical strength can be manufactured. Phase ratios in the supports and membrane layers can be adjusted to achieve compatibility of the shrinkage behaviours and good performance of the membranes.

An Ag-CuO braze paste was used to seal the membranes to the metallic cells. Gas-tight sealing was obtained for the membranes studied in this work under the test conditions. However, for the membranes containing BSCF, reactions were observed on the interface between the sealant and the membrane after the permeation test at high temperature for several days. Although no leakage was observed from the sealing area, it reflects that this sealing method is not favourable for the long-term operation of the membranes in the industrial process. Accordingly, better sealant or protective layers needs to be developed to join the membranes to the gas-tight cells.

The multi-layer membrane structure is gaining increased popularity. The special preparation condition of the ceramic oxygen transport membranes with ultra-high

sintering temperature bring difficulties for producing the multi-layer membranes. Shrinkage was observed for the ceramic powders when heated up and only compatible shrinkage behaviours of the different layers can result in gas-tight membranes. Selection of cost-effective and compatible material for the multi-layer membrane preparation remains an important topic.

## List of Publications

### *Papers related to this thesis*

1. Liu Y., van Sint Annaland M., Gallucci F.

*Performance control of dead-end tubular membranes fabricated with a modified phase inversion casting method*

Ceramics International, 2020, 46(14): 22429-22437

2. Liu Y., Rahimalimamaghani A., van Sint Annaland M., Gallucci F.

*Microstructure control of tubular micro-channelled supports fabricated by the phase inversion casting method*

Processes, 2019, 7(6): 322

3. Arratibel Plazaola A., Cruellas Labella A., Liu Y., Badiola Porras N., Pacheco Tanaka D. A., Sint Annaland M. V., Gallucci F.

*Mixed ionic-electronic conducting membranes (MIEC) for their application in membrane reactors: a review*

Processes, 2019, 7(3): 128

4. Liu Y., Rahimalimamaghani A., van Sint Annaland M., Gallucci F.

*Ce<sub>0.9</sub>Gd<sub>0.1</sub>O<sub>2-δ</sub>-based multi-phase membranes with high CO<sub>2</sub> resistance, Journal of Materials Chemistry A*

ACS Applied Material & Interface, under review

5. Liu Y., Rahimalimamaghani A., van Sint Annaland M., Gallucci F.

*Cobalt-free dual-phase membrane of SrFe<sub>0.8</sub>Nb<sub>0.2</sub>O<sub>3-δ</sub>-Ce<sub>0.9</sub>Gd<sub>0.1</sub>O<sub>2-δ</sub> for oxygen separation*

In preparation

***Papers beyond the scope of this thesis***

1. Liu Y., Zhai J., Li L., Sun L., Zhai C.

*Heat pump assisted reactive and azeotropic distillations in dividing wall columns*  
Chemical Engineering and Processing: Process Intensification, 2015, 95: 289-301

2. Zhai J., Liu Y., Li L., Zhu Y., Zhong W., Sun L.

*Applications of dividing wall column technology to industrial-scale cumene production*  
Chemical Engineering Research and Design, 2015, 102: 138-149

3. Zhai J., Liu Y., Sun L., Wang R.

*A novel thermally coupled reactive distillation column for the hydrolysis of methyl acetate*  
China Petroleum Processing and Petro-chemical Technology, 2015, 17(2): 101-108

4. Li L., Liu Y., Zhai J., Sun L.

*Design and control of self-heat recuperative distillation process for separation of close-boiling mixtures: n-butanol and iso-butanol*  
China Petroleum Processing and Petro-chemical Technology, 2015, 17: 111-120

5. Li L., Sun L., Wang J., Zhai J., Liu Y., Zhong W., Tian Y.

*Design and control of different pressure thermally coupled reactive distillation for methyl acetate hydrolysis*  
Industrial & Engineering Chemistry Research, 2015, 54(49), 12342-12353

6. Sun L., Wang Q., Li L., Zhai J., Liu Y.

*Design and control of extractive dividing wall column for separating benzene/cyclohexane mixtures*  
Industrial & Engineering Chemistry Research, 2014, 53(19): 8120-8131

***Conference presentations***

1. Liu Y., van Sint Annaland M., Gallucci F.

*Tubular oxygen transport membranes fabricated with phase inversion casting method*

14th International Conference on Catalysis in Membrane Reactors (Best Oral Presentation Award)

2. Liu Y., Rahimalimamaghani A., van Sint Annaland M., Gallucci F.

*Fabrication of asymmetric membranes for selective oxygen transportation.*

15th International Conference on Inorganic Membranes (Oral Presentation)

3. Liu Y., van Sint Annaland M., Gallucci F.

*Micro-channelled support tubes for asymmetric oxygen transport membranes*

15th Netherlands Process Technology Symposium (Poster)



## **Acknowledgements**

The four years' PhD study in TU/e provided me the chances to study in an amazing Country, to experience a totally different lifestyle and to work with lots of wonderful people. This thesis could not be completed without the help and support from them. I would like to thank all of them in the last pages of my thesis.

Firstly, I would like to acknowledge my first and second promoters, prof. Fausto Gallucci and prof. Martin van Sint Annaland. Thanks a lot for all the help you provided me in the four years. Fausto, every time I come across problems, I immediately look for you. Your office door is always opening for us. Even when we were working from home, I often bothered you with emails. I am grateful that you can reply the emails in a super-fast speed, even though you are actually very busy. The start of the PhD study was not easy, thanks for the support, patience and encouragement you give to me. Martin is my second promotor but also the first promoter in the 1<sup>st</sup> and 2<sup>nd</sup> year of my PhD. I was extremally excited when you sent me the offer. Thanks for accepting me as a PhD student in TU/e and thanks for the trust you provided to the student that you have never met. It was always a pleasure to have progress meetings with you and I really appreciate your supervision and instruction of my research.

Then I hope to acknowledge all of the committee members of my defence, prof. D. C. Nijmeijer, prof. J. Serra, prof. E. Curcio, dr. Z. Borneman, prof. T. Noël, and dr. A. Arratibel. Thanks for joining my defence. Your comments to my thesis are really appreciated. Special gratitude goes to Alba, who gave me a lot of help when she was in TU/e. Thanks for teaching me to operate many experiment setups and I will never forget your passion for the work and your kindness to each of your colleagues and friends.

I would very much like to thank our technicians. Joris, Erik, Marlies, Carlo and Peter from SPE and Joost, Thijs from SMR. Thanks a lot for helping us with building and fixing the setups, ordering chemicals, doing safety checks, and analysing the samples. Without your help, the ideas would never realise. Moreover, I'd like to thank Ingeborg from SPC, who gave me the guidance about the SEM (Phenom and Quanta). You are so patient with my questions. No matter when I look for you, you can always come immediately with me to the lab and can solve no matter what kind of problems in a short time. You are my superwoman! It is also such a happy thing to talk with you. Thanks for the great warmth you bring to me. Gratitude also goes to Marco who helped me a lot with the rheometer and Pim from PTG who guide me to test mechanical strength of my samples.

There would never be too many thanks to our secretaries, Saskia, Denise and Judith. Judith helped to start up my PhD, to know each colleague and to get used to the life here, while Saskia helped me to prepare everything to finish my PhD study. Thanks for everything you did for me.

I would also like to thank each colleague I meet in our groups. My first officemates were Kai and Vincenzo. It was a great pleasure to be officemates with such kind, humorous, smart and hard-working people like you, who motivates me to be a better PhD student. You gave me many nice advices when I start up in TU/e, and they are proved to be quite useful. My first experience in the lab was following the experiment of Aitor. I really appreciate your kindness, enthusiasm and generosity. My English was not good in the beginning and I sometimes needs you to repeat a sentence for several times, thanks that you never lost your patience with me. There are so many colleagues from SPE and SMR groups that I would like to thank. Maria, Guilia, Carin, Arash H., Jose, Niek, Stefan, Michela, Marian, Xintong, Arash R., Wout, Camilla, Serena, Sirui and Thijs thanks for the

accompany and help from all of you.

I was lucky to have super-nice students during my PhD. Arash, Honglei and Emina, thanks for the wonderful work you have done. Arash I am so happy to become colleague with you now, and it was a pleasure to work with you.

I usually enjoy the lunch that I had in Helix, because of the accompany of friends. Jiangtao, Yali, Lizzy, Lei, Gaopan, Tianwei, Kun, Xiao, Feifei and Lijing, every lunch could become a party thanks to your presence.

Haijing, Xianhong, Zhan, Wei, Ting and Yue, we come to TU/e in the same year. I would always remember the hot-pots we eat and each city we visit together. Wish you all can find good jobs and realise your dreams.

最后，我要感谢我的家人。谢谢我的爸爸妈妈。爸爸虽然您已不能再和我分享许多人生的重要时刻，但我想告诉您，您的女儿已经长大，并实现了自己的欧洲求学梦想。妈妈，谢谢您无论何时都能带给我温暖和支持。谢谢我的姥姥、姥爷对我的关怀和付出。姥爷虽然忘记了许多事，却总是惦念我何时回家。还有许多给予我关心和爱的家人，谢谢你们带给我的大家庭，是你们的支持使我有了解决一切困难的勇气，有你们的陪伴是我最大的幸福。

## Curriculum Vitae



Yuliang (Wendy) Liu was born on 26-01-1991 in Shandong, China. After finishing her bachelor degree in Chemical Engineering and Processing at China University of Petroleum (East China) in 2013, she continued her study as a master student within the group of prof. Lanyi Sun on the design and control of distillation columns in the same university. She joined several projects for the industrial applications of dividing-wall columns, heat-pump assisted columns and some other energy-efficient distillation processes. She was the co-author of the book “*Process Simulation with Aspen Plus (2ed edition, Chinese version)*”, and in 2015 she won the China Nation Scholarship”. She got her master degree in 2016, and in the same year, he joined the group of Chemical Process Intensification for the PhD study with the scholarship from China Scholarship Council. Her PhD research was about the development, characterization and test of oxygen transport membranes under the supervision of prof. Martin van Sint Annaland and prof. Fausto Gallucci. Then she continued her PhD study on the same topic in a new group of Inorganic Membranes and Membrane Reactors chaired by prof. Fausto Gallucci. She presented her work in conferences and won the Best Oral Presentation in 2019. Important results of her PhD study are reported in this thesis.